



1994

Diagenetic controls of reservoir quality in the Mississippian Wayne Beds in the Williston Basin, Bottineau County, North Dakota

Michael M. Wetmore
University of North Dakota

Follow this and additional works at: <https://commons.und.edu/theses>

 Part of the [Geology Commons](#)

Recommended Citation

Wetmore, Michael M., "Diagenetic controls of reservoir quality in the Mississippian Wayne Beds in the Williston Basin, Bottineau County, North Dakota" (1994). *Theses and Dissertations*. 320.
<https://commons.und.edu/theses/320>

This Thesis is brought to you for free and open access by the Theses, Dissertations, and Senior Projects at UND Scholarly Commons. It has been accepted for inclusion in Theses and Dissertations by an authorized administrator of UND Scholarly Commons. For more information, please contact zeinebyousif@library.und.edu.

DIAGENETIC CONTROLS OF RESERVOIR QUALITY IN THE
MISSISSIPPIAN WAYNE BEDS IN THE WILLISTON BASIN,
BOTTINEAU COUNTY, NORTH DAKOTA

by

Michael James Wetmore

Bachelor of Science

South Dakota School of Mines & Technology, 1983

A Thesis

Submitted to the Graduate Faculty

of the

University of North Dakota

in partial fulfillment of the requirements

for the degree of

Master of Science

Grand Forks, North Dakota

May

1994

GEOLOGICAL
T1994
W534

This thesis, submitted by Michael James Wetmore in partial fulfillment of the requirements for the degree of Master of Science from the University of North Dakota, has been read by the Faculty Advisory Committee under whom the work has been done and is hereby approved.

Patricia E. Videtich
(Chairperson)

Richard D. L. Linn

Ronald W. Mathewson

This thesis meets the standards for appearance, conforms to the style and format requirements of the Graduate School of the University of North Dakota, and is hereby approved.

Dean of the Graduate School

PERMISSION

Title: Diagenetic Controls of Reservoir Quality
in the Mississippian Wayne Beds in the
Williston Basin, Bottineau County, North
Dakota.

Department: Geology and Geological Engineering

Degree: Master of Science

In presenting this thesis in partial fulfillment of the requirements for a graduate degree from the University of North Dakota, I agree that the library of this University shall make it freely available for inspection. I further agree that permission for extensive copying for scholarly purposes may be granted by the professor who supervised my thesis work, or in her absence, by the Chairperson of the Department or the Dean of the Graduate School. It is understood that any copying or publication or other use of this thesis or part thereof for financial gain shall not be allowed without my written permission. It is also understood that due recognition shall be given to me and to the University of North Dakota in any scholarly use which may be made of any material in my thesis.

Signature Michael J. Weln

Date 4/22/94

TABLE OF CONTENTS

LIST OF FIGURES..... viii

LIST OF TABLES..... xi

ACKNOWLEDGMENTS..... xii

ABSTRACT..... xv

INTRODUCTION..... 1

REGIONAL GEOLOGY..... 3

STUDY AREA..... 9

METHODS..... 12

 Geophysical Log Analysis..... 12

 Production Statistics..... 12

 Core Examination..... 13

 Core Porosity and Permeability..... 13

 Petrography..... 17

 X-Ray Diffraction..... 17

 Carbon and Oxygen Stable Isotope Analysis..... 18

 Sulfur Stable Isotopes..... 19

PETROLEUM PRODUCTION STATISTICS..... 20

 Ultimate Recoverable Reserves Per Field..... 20

 Ultimate Recoverable Reserves Per Well..... 20

 Petroleum Production Anomalies..... 25

| | |
|--|----|
| STUDY AREA STRATIGRAPHY..... | 32 |
| Previous Work..... | 32 |
| Type Log..... | 35 |
| Pre-Mesozoic Subcrop..... | 38 |
| STUDY AREA STRUCTURAL EVOLUTION..... | 41 |
| Previous Work..... | 41 |
| Structural Genesis in the Study Area..... | 42 |
| Tilston Argillaceous Marker Structure..... | 44 |
| Wayne Argillaceous Marker Structure..... | 44 |
| Pre-Mesozoic Unconformity Structure..... | 47 |
| Spearfish Formation Structure..... | 52 |
| Structural Growth During Wayne and | |
| Landa Beds Deposition..... | 52 |
| Paleotopography During Spearfish | |
| Deposition..... | 55 |
| STUDY AREA LITHOLOGIES..... | 60 |
| Previous Work..... | 60 |
| Lithofacies of the Wayne Beds..... | 63 |
| Packstone Sublithofacies..... | 64 |
| Wackestone Sublithofacies..... | 71 |
| Mudstone Sublithofacies..... | 71 |
| Anhydrite Sublithofacies..... | 82 |
| DEPOSITIONAL ENVIRONMENTS..... | 88 |
| Previous Work..... | 88 |
| Wayne Beds Depositional Model..... | 91 |

| | |
|--|-----|
| DISCUSSION: OIL PRODUCTION ANOMALIES..... | 95 |
| Structure..... | 95 |
| Depositional Environments and Lithofacies..... | 103 |
| DIAGENESIS..... | 104 |
| Previous Work..... | 104 |
| Marine Phreatic Diagenesis..... | 105 |
| Cementation..... | 105 |
| Micritization..... | 110 |
| Dolomitization..... | 110 |
| Hypersaline Phreatic Diagenesis..... | 111 |
| Dolomitization..... | 111 |
| Dissolution and Replacement by Anhydrite..... | 114 |
| Freshwater Vadose Diagenesis..... | 118 |
| Dissolution of Grains and Cement..... | 118 |
| Cementation..... | 118 |
| Freshwater Phreatic Diagenesis..... | 121 |
| Mineralogical Stabilization..... | 121 |
| Cementation..... | 122 |
| Burial Diagenesis..... | 123 |
| Compaction..... | 123 |
| Pressure Solution..... | 126 |
| Dolomite and Calcite Cementation..... | 129 |
| Anhydritization..... | 132 |
| Summary of Diagenetic History..... | 135 |

| | |
|--|-----|
| STABLE-ISOTOPE DATA..... | 139 |
| Carbon- and Oxygen-Isotope Geochemistry..... | 139 |
| Sulfur-Isotope Geochemistry..... | 143 |
| POROSITY AND PERMEABILITY..... | 154 |
| Porosity Formation and Preservation..... | 154 |
| Porosity Occlusion..... | 158 |
| Permeability Reduction..... | 167 |
| PETROLEUM EXPLORATION MODELS..... | 174 |
| Previous Work..... | 174 |
| Paleoisland Model..... | 175 |
| Eroded Paleohigh Model..... | 177 |
| SUMMARY AND CONCLUSIONS..... | 187 |
| APPENDIX A: Petrographic Descriptions..... | 191 |
| REFERENCES..... | 227 |

LIST OF FIGURES

| Figure | Page |
|---|------|
| 1. Study area location map..... | 5 |
| 2. Bottineau County, North Dakota, stratigraphic column..... | 7 |
| 3. Boundaries of oil fields in the study area..... | 11 |
| 4. Wayne beds core location map..... | 16 |
| 5. Map showing ultimate recoverable oil reserves per field..... | 23 |
| 6. Cimbel field map showing ultimate recoverable oil reserves per well..... | 27 |
| 7. Leonard field map showing ultimate recoverable oil reserves per well..... | 29 |
| 8. Roth field map showing ultimate recoverable oil reserves per well..... | 31 |
| 9. Evolution of Mississippian stratigraphic terminology..... | 34 |
| 10. Study area type geophysical log..... | 37 |
| 11. Pre-Mesozoic subcrop map..... | 40 |
| 12. Tilston argillaceous marker (TAM) structure map..... | 46 |
| 13. Wayne argillaceous marker (WAM) structure map..... | 49 |
| 14. Pre-Mesozoic unconformity surface structure map..... | 51 |
| 15. Spearfish Formation structure map..... | 54 |

| | | |
|-----|--|-----|
| 16. | Wayne and Landa beds isopach map..... | 57 |
| 17. | Spearfish Formation isopach map..... | 59 |
| 18. | Photomicrograph and core photograph of pisolitic packstones..... | 68 |
| 19. | Photomicrograph and core photograph of peloidal packstones..... | 70 |
| 20. | Photomicrograph and core photograph of skeletal packstones..... | 73 |
| 21. | Photomicrograph and core photograph of pisolitic wackestones..... | 76 |
| 22. | Photomicrograph of a skeletal wackestone..... | 78 |
| 23. | Photomicrograph and core photograph of massive mudstones..... | 81 |
| 24. | Photomicrograph and core photograph of stromatolitic mudstones..... | 84 |
| 25. | Photomicrograph and core photograph of bedded anhydrites..... | 87 |
| 26. | Wayne beds depositional environments model..... | 93 |
| 27. | Cimbel field Tilston argillaceous marker (TAM) structure map with ultimate recoverable oil reserves per well..... | 97 |
| 28. | Leonard field Tilston argillaceous marker (TAM) structure map with ultimate recoverable oil reserves per well..... | 99 |
| 29. | Roth field Tilston argillaceous marker (TAM) structure map with ultimate recoverable oil reserves per well..... | 101 |
| 30. | Paragenetic sequence for the Wayne beds..... | 107 |
| 31. | Photomicrographs of marine phreatic cements..... | 109 |
| 32. | Photomicrographs of possible hypersaline phreatic dolomite..... | 113 |
| 33. | Photomicrographs of interpreted hypersaline phreatic anhydrite..... | 117 |

| | | |
|-----|---|-----|
| 34. | Photomicrographs of freshwater vadose features..... | 120 |
| 35. | Photomicrograph of freshwater phreatic cement..... | 125 |
| 36. | Photomicrographs showing pressure solution features..... | 128 |
| 37. | Photomicrographs of burial dolomite and calcite cements..... | 131 |
| 38. | Photomicrographs of dolomite and anhydrite age relationships..... | 134 |
| 39. | Photomicrographs of pore-bridging anhydrite cements..... | 137 |
| 40. | $\delta^{13}\text{C}$ versus $\delta^{18}\text{O}$ | 141 |
| 41. | Stable-isotope sample-location map..... | 146 |
| 42. | Sulfur isotope age curve..... | 148 |
| 43. | Expanded sulfur isotope age curve..... | 152 |
| 44. | Whole rock $\delta^{13}\text{C}$ versus depth for NDIC-12357..... | 157 |
| 45. | Core porosity versus dolomite weight percent for well NDIC-12357..... | 163 |
| 46. | $\delta^{18}\text{O}$ versus dolomite weight percent for well NDIC-12357..... | 166 |
| 47. | Core permeability versus pore-bridging anhydrite percent for well NDIC-12357..... | 171 |
| 48. | Paleoisland and eroded-paleohigh model for Cimbel field..... | 179 |
| 49. | Paleoisland and eroded-paleohigh model for Leonard field..... | 181 |
| 50. | Paleoisland and eroded-paleohigh model for Roth field..... | 183 |

LIST OF TABLES

| Table | Page |
|---|------|
| 1. NDIC number, well location, and cored intervals for examined core..... | 14 |
| 2. Recoverable petroleum reserves per field..... | 21 |
| 3. Recoverable petroleum reserves per well..... | 24 |
| 4. Lithofacies classification schemes..... | 61 |
| 5. Wayne beds lithofacies, allochems, and modifiers..... | 65 |
| 6. Wayne beds packstone sublithofacies in decreasing order of abundance..... | 66 |
| 7. Wayne beds wackestone sublithofacies in decreasing order of abundance..... | 74 |
| 8. Wayne beds mudstone sublithofacies in decreasing order of abundance..... | 79 |
| 9. Wayne beds anhydrite sublithofacies in decreasing order of abundance..... | 85 |
| 10. Frobisher-Alida depositional environments..... | 89 |
| 11. Carbon and oxygen isotopic composition..... | 144 |
| 12. Sulfur isotopic composition..... | 150 |
| 13. Example of reserves lost due to porosity reduction..... | 159 |
| 14. Core porosity and dolomite weight percent (well NDIC-12357)..... | 161 |
| 15. Permeability and point count data (well NDIC-12357)..... | 168 |

ACKNOWLEDGMENTS

The completion of this thesis is the result of the assistance of so many people that I hardly know where to begin. The fairest way to acknowledge everyone's help would be to do so in more or less chronological order.

In the spring of 1990, I called my father to discuss giving up a secure oil company geologist position to venture into the unknowns of graduate school. After I expressed doubts about my own abilities my father said, "Don't start anything thinking about how many different ways there are to fail. If you're going to do it, do it with the attitude that you're going to succeed." That attitude has served me well.

To my wife Stephanie I give thanks for her love, support, and gentle understanding. Her acceptance into the UND School of Physical Therapy is one of the reasons I decided to go to graduate school. I like to tease her that I gave up my job, my house, my boat, my motorcycle, and my dog for her.

I would like to thank GeoResources, Inc. for giving me a shot at the oil business and for having faith in my prospects. Because of them I can say that I survived the

oil bust of '86. This thesis has benefited immensely from the many stimulating conversations that I had with Jeff Vickers, president of GeoResources.

This thesis was well funded and I would like to thank the following entities for generously providing that financial support:

GeoResources, Inc.

Beard Oil Company

Citation Oil Company

Balcron Oil Company

Axem Resources, Inc.

UND Department of Geology

UND Carbonate Fund

My thanks to Dr. Patricia Videtich, Dr. Richard LeFever and Dr. Ronald Matheney for their guidance and assistance in the completion of this thesis. Special thanks go to Gloria Pederson, the department secretary, for calmly and rationally explaining the UND bureaucracy to me.

In Memory of
James H. Wetmore
1932-1992

"We must sail, sometimes with the wind and sometimes
against, but we must sail and not drift."

- Oliver Wendell Holmes

"Even if you are on the right track, you will get run over
if you just sit there."

- Will Rogers

"Ah, how my heart doth ache for faraway kingdoms in faraway
lands."

- Opus, Bloom County

ABSTRACT

The carbonate Wayne beds of the Frobisher-Alida interval (Mississippian Mission Canyon Formation) in the Williston Basin, North Dakota, are capable of producing as much as 400,000 barrels of oil per well at depths of only 3,100 feet. Wayne production is from structural traps in the intertidal packstone-wackestone lithofacies; however, the ultimate recoverable reserves of oil per well is controlled neither by structure, nor by depositional environments.

The Wayne beds underwent cementation and micritization in the marine phreatic diagenetic environment. Hypersaline diagenesis caused minor dolomitization and anhydritization. Dissolution and minor cementation occurred in the freshwater vadose zone. Freshwater phreatic diagenesis resulted in mineralogical stabilization and minor cementation. Compaction, pressure solution, dolomite and calcite cementation, and anhydritization occurred in the burial diagenetic environment.

Depleted $\delta^{13}\text{C}$ in the carbonates immediately below the pre-Mesozoic unconformity surface suggests that vugular and

solution-enlarged porosity formed in the freshwater vadose zone. Beneath paleoislands, mineralogical stabilization in the freshwater phreatic zone prevented later porosity reduction by compaction or cementation. On the flanks of the paleoislands and in paleolows, porosity was occluded by dolomite and calcite cement. The dolomite cement has $\delta^{18}\text{O}$ consistent with a burial diagenesis origin. Permeability reduction by pore-bridging anhydrite cements post-date the pore-occluding dolomites. Wayne beds contain much less pore-bridging anhydrite beneath paleohighs where the overlying Glenburn evaporites were removed due to erosion than beneath paleolows where the Glenburn is still present. Sulfur stable-isotope data suggest that the sulfur in these pore-bridging anhydrites originated in the Glenburn evaporites.

The amount of Wayne oil production from structural traps in the study area is controlled by diagenetic rather than depositional features. Porosity was occluded by burial dolomite and calcite cements in paleolows. Permeability was reduced by burial anhydrite cements in localities where the Glenburn has not been eroded. Thus, the best production within a field comes from those portions of the reservoir which were once beneath islands and/or eroded highs.

INTRODUCTION

Numerous new oil field discoveries in the Bluell and Sherwood carbonate beds of the Frobisher-Alida interval along the Mississippian shoreline in North Dakota have sparked renewed interest in the Mission Canyon Formation in the Williston Basin (Montana Oil Journal, 1991, 1992). This new exploration and development effort has extended Bluell and Sherwood production from north-central North Dakota southward into central North Dakota. The combination of substantial petroleum reserves per well and low drilling costs due to shallow depths has led at least one worker to describe the shallow Mississippian play as having the best economics in the Williston Basin (Jennings, 1987).

The Wayne carbonate beds of the Frobisher-Alida interval are also productive at shallow depths in north-central North Dakota. The Hanson No. 1 in the Roth field is expected to produce over 400,000 barrels of oil (discussed below) at a depth of only 3,100 feet. Despite good production history in Bottineau County, the Wayne beds in central North Dakota have not received very much attention.

Focusing exploration efforts on extending Wayne oil production from north-central North Dakota to central North Dakota could be very rewarding. The purpose of this thesis is to investigate structural, depositional, and diagenetic controls of petroleum production from the Wayne beds in Bottineau County, North Dakota. Hopefully, this study will prove useful for the exploration and development of new petroleum reserves in the Wayne beds.

REGIONAL GEOLOGY

The Williston Basin covers portions of the provinces of Saskatchewan and Manitoba in Canada and the states of North Dakota, Montana, and South Dakota in the U.S.A. (Figure 1). The basin developed on a relatively stable continental or cratonic platform (Sloss, 1956). The zero elevation of the Cretaceous Inyan Kara Formation is regarded as the edge of the Williston Basin (Laird, 1956).

A stratigraphic nomenclature chart representative of the rock column in Bottineau County, North Dakota, is presented in Figure 2 (modified after Bluemle et al., 1981, 1986). The stratigraphic column shows eras, periods, and unconformities. The formations of interest to this thesis are the Prairie evaporites, the Mission Canyon carbonates, and the Spearfish sandstone-siltstone-shale complex.

The Paleozoic was generally a time of marine carbonate and clastic deposition in the Williston Basin. Notable exceptions to this are the evaporitic potassium and sodium salt deposits of the Devonian Prairie Formation. These evaporites have been removed locally due to multistage, differential salt dissolution (Baillie, 1953; Milner, 1956;

Figure 1.- Study area location map. The study area is located on the eastern flank of the Williston Basin in Bottineau County, North Dakota, within the Superior Geologic Province.

STUDY AREA LOCATION MAP

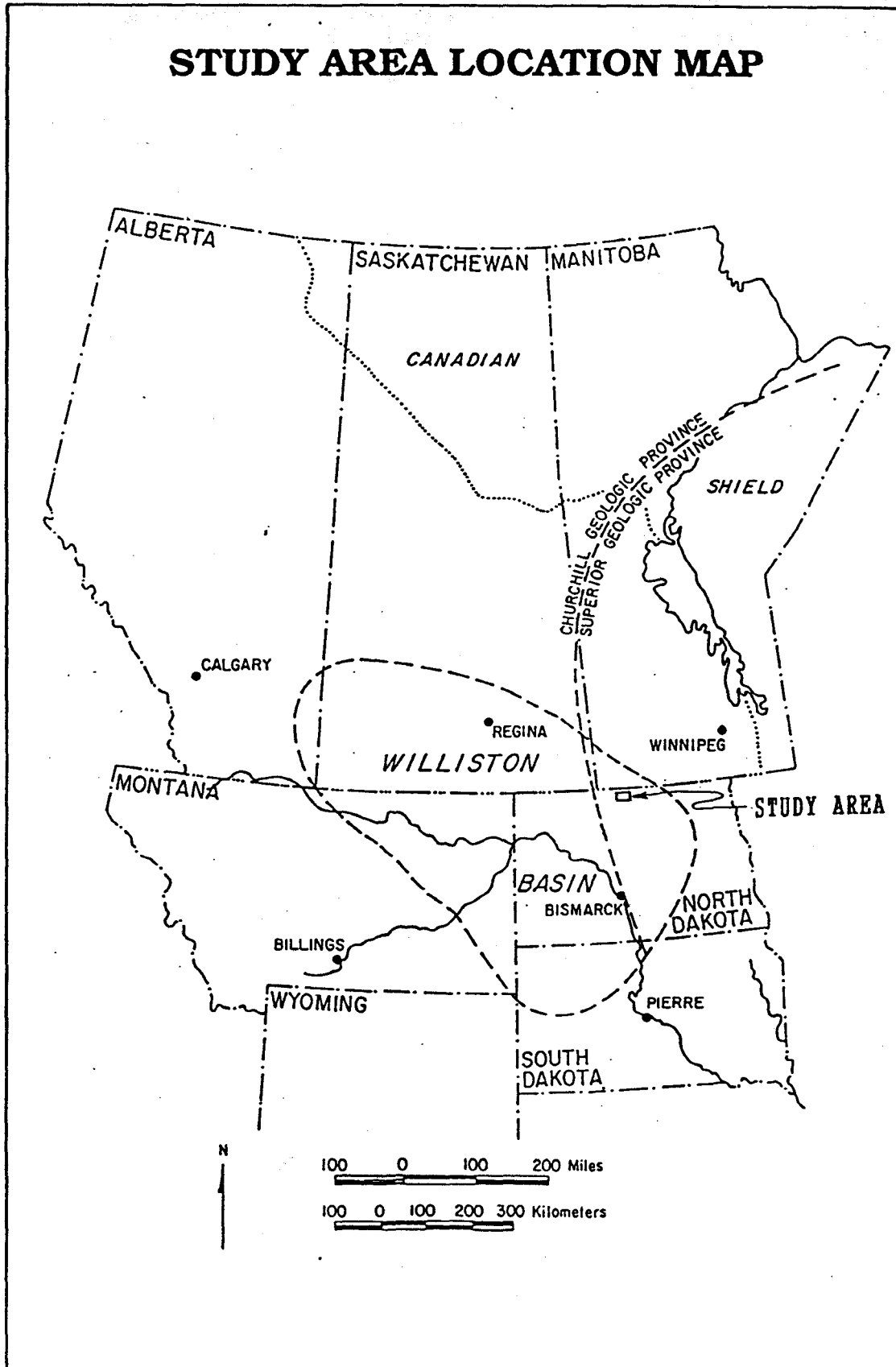


Figure 2.- Bottineau County, North Dakota, stratigraphic column (modified after Bluemle et al., 1981, 1986). Formations of interest to this thesis are the evaporites of the Prairie, the carbonates of the Mission Canyon, and the sandstone-siltstone-shale complex of the Spearfish.

| BOTTINEAU COUNTY, ND STRATIGRAPHIC COLUMN | | | |
|---|-----------|---------------|------------------------|
| YEARS (MILL) | ERA | PERIOD | FORMATIONS OF INTEREST |
| 67 | CENOZOIC | QUATERNARY | |
| | | TERTIARY | |
| 250 | MESOZOIC | CRETACEOUS | |
| | | JURASSIC | |
| | | TRIASSIC | SPEARFISH |
| | | PERMIAN | |
| | | PENNSYLVANIAN | |
| | PALEOZOIC | MISSISSIPPIAN | MISSION CANYON |
| | | DEVONIAN | PRAIRIE |
| | | SILURIAN | |
| | | ORDOVICIAN | |
| | | CAMBRIAN | |
| 570 | | PRECAMBRIAN | |

Kupsch, 1958; Anderson and Hunt, 1964; De Mille et al., 1964; Christiansen, 1967; McTavish and Vigrass, 1987; Oglesby, 1987; McTavish, 1991). Carbonate deposition in the Mississippian epeiric sea followed Devonian sedimentation.

The Pennsylvanian and Permian are missing in Bottineau County. This pre-Mesozoic unconformity was due to non-deposition and erosion before the Spearfish Formation was deposited. The Mesozoic and Cenozoic were mostly a time of both terrestrial and marine clastic sedimentation in the Williston Basin.

STUDY AREA

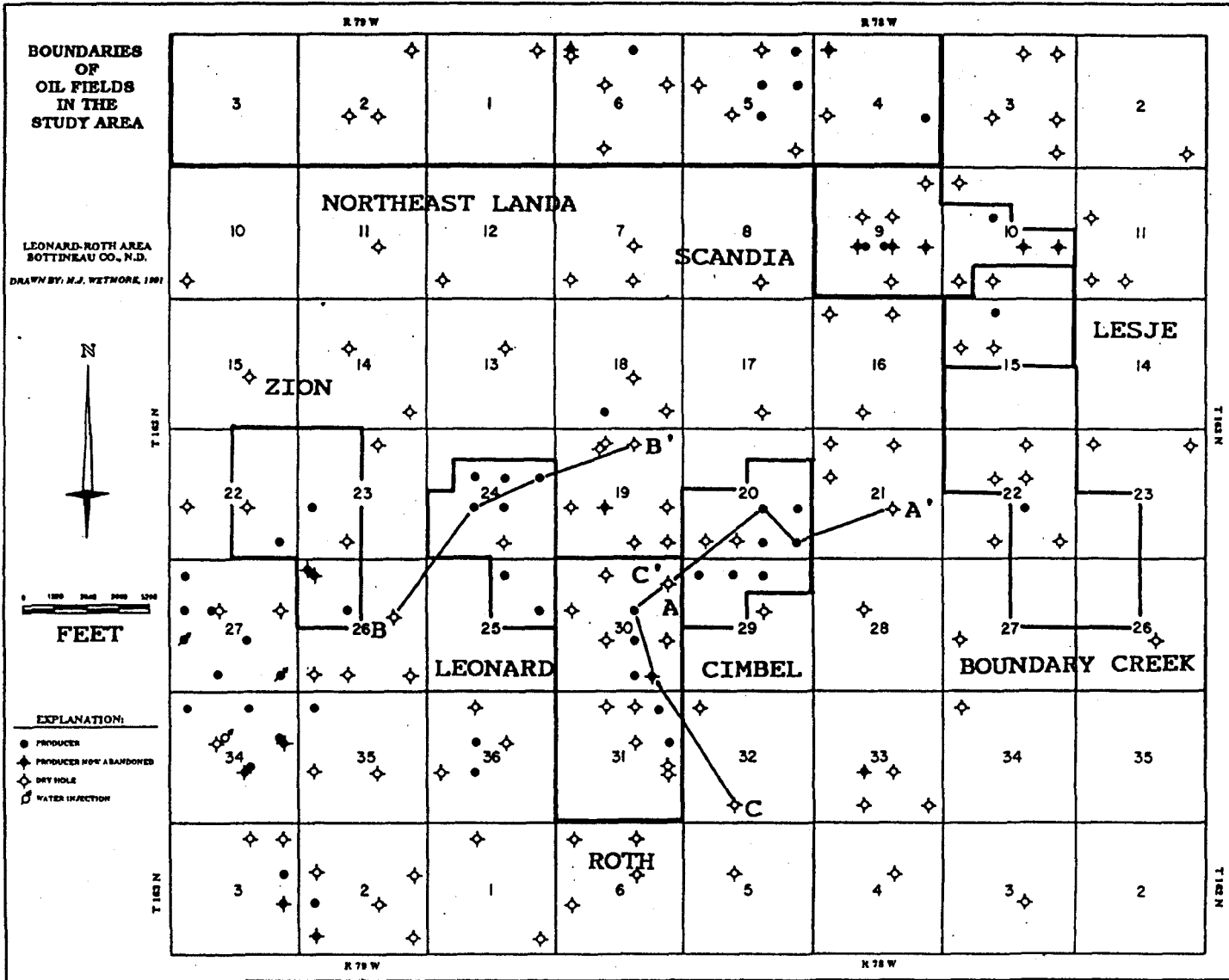
The study area is on the eastern flank of the Williston Basin in Bottineau County, North Dakota. Geographic and geologic boundary relationships are shown in Figure 1. The study area lies within the Superior Geologic Province near the North Dakota-Canada boundary.

A detailed study area location plate showing sections, townships, ranges, producing oil wells, abandoned oil wells, dry holes, and waterflood injection wells is presented in Figure 3. The study area includes portions of Townships 162-163 North and Ranges 78-79 West.

The Wayne beds produce hydrocarbons from numerous oil fields. Production from the Wayne occurs in the Boundary Creek, Cimbøl, Leonard, Lesje, Northeast Landa, Roth, Scandia and Zion fields. Locations and boundaries of these fields, as determined by the North Dakota Industrial Commission (NDIC), are also shown in Figure 3.

Figure 3.- Boundaries of oil fields in the study area.

Shown are sections, townships, ranges, producing oil wells, abandoned oil wells, dry holes, and waterflood injection wells. The legal boundaries for Mission Canyon Formation oil fields, as determined by the North Dakota Industrial Commission (NDIC), are delineated. The locations of the cross-sections in Figures 48, 49, and 50, are shown as A-A', B-B', and C-C', respectively.



METHODS

Geophysical Log Analysis

All available wireline geophysical logs were examined from approximately 190 wells in the study area. The logs were obtained from the North Dakota Geological Survey Wilson M. Laird Core and Sample Library located at the University of North Dakota. Stratigraphic correlations for each borehole were made using the logs. Using sea level as the datum, subsea structural elevations were calculated for each stratigraphic interval of interest.

Production Statistics

The ultimate recoverable petroleum reserves were calculated for 39 wells in the eight oil fields which produce from the Wayne beds in the study area. The production data were obtained from the production statistics files of the North Dakota Industrial Commission. These reserves were calculated using the exponential decline curve analysis method (Thompson and Wright, 1983).

Core Examination

Approximately 700 feet of core from 16 wells were retrieved from the North Dakota Geological Survey Wilson M. Laird Core and Sample Library located at the University of North Dakota. The North Dakota Industrial Commission (NDIC) well file numbers, well locations, and cored intervals are presented in Table 1. The location of these cores within the study area are shown in Figure 4. The core was slabbed and treated for 30 seconds with a 10% hydrochloric acid wash before being megascopically examined and photographed.

Core Porosity and Permeability

Commercial whole-core or core-plug porosity and permeability analyses were obtained from the NDIC well files.

TABLE 1: NDIC NUMBER, WELL LOCATION,
AND CORED INTERVALS FOR EXAMINED CORE

| <u>NDIC No.</u> | <u>Section, Township, and Range</u> | <u>Cored Interval (ft) Sea Level Datum</u> |
|-----------------|---|--|
| 1159 | 2-162-79 | 3164-3246 |
| 1977 | 31-163-78 | 3164-3199 |
| 2038 | 23-163-78 | 3078-3107 |
| 2176 | 30-163-78 | 3114-3163 |
| 2776 | 15-163-79 | 3240-3271 |
| 2902 | 30-163-78 | 3123-3153 |
| 3238 | 2-163-78 | 3053-3076 |
| 3375 | 23-163-78 | 3054-3131 |
| 3451 | 22-163-78 | 3086-3134 |
| 3472 | 22-163-78 | 3114-3151 |
| 3527 | 22-163-78 | 3110-3128 |
| 3577 | 22-163-78 | 3094-3129 |
| 3933 | 10-163-78 | 3053-3085 |
| 11889 | 24-163-79 | 3116-3212 |
| 12357 | 29-163-78 | 3102-3163 |
| 12358 | 20-163-78 | 3116-3164 |

Figure 4.- Wayne beds core location map. Well symbols enclosed by diamonds indicate those wells from which Wayne core was examined, sampled, and analyzed.

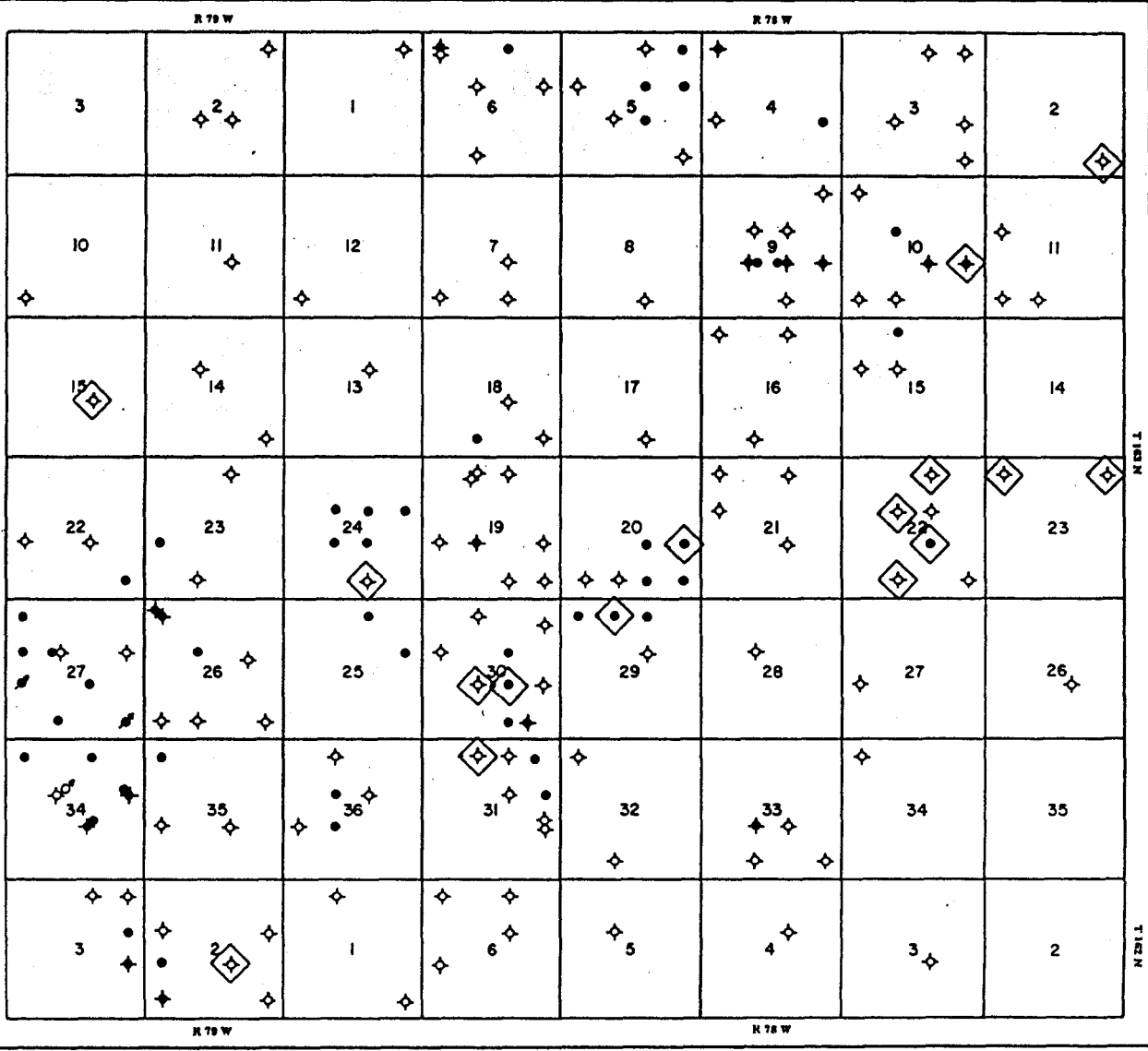
WAYNE CORE LOCATION MAP

LEONARD-ROTH AREA
BOTTINEAU CO., N.D.
DRAWN BY: H.J. WETMORE, 1991



EXPLANATION:

- PRODUCER
- ◆ PRODUCER NOW ABANDONED
- ◇ DRY HOLE
- ◊ WATER INJECTION



Petrography

Approximately 260 rock slabs were cut from the core using a rock saw. These slabs were impregnated with epoxy and made into slide-mounted, 27 x 46 mm, 30 micron-thick petrographic thin sections (uncovered and unpolished) by Quality Thin Sections. The thin sections were examined using a Leitz petrographic microscope. Four hundred point counts of allochems and cements were performed on each of 16 thin sections from well NDIC-12357. Pores were counted as being either open, bridged by anhydrite, or plugged by anhydrite.

X-Ray Diffraction

Twenty-eight carbonate and anhydrite whole rock samples were analyzed by x-ray diffraction. Samples were collected using either a dental drill or a rock saw and were crushed, sieved to pass 63 microns, split, and packed into side-drift mounts. Analysis was performed using a Phillips x-ray diffractometer with a theta-compensating slit and monochromator, and a copper, long fine-focus x-ray tube. Peaks were matched using JCPDS mineral powder-diffraction file data book (Bayliss et al., 1980). The x-ray diffraction analysis was conducted to estimate the relative

amounts of calcite, dolomite, and anhydrite present in the samples. The weight percent dolomite and calcite content of the samples were determined by the peak-height-ratio method (Carver, 1971, p. 558-560). No internal standards were used.

Carbon and Oxygen Stable Isotope Analysis

All ten powder sample splits from well NDIC-12357 were sent to the University of Michigan Department of Geological Sciences stable-isotope laboratory for analysis using a Finnigan-MAT 251 mass spectrometer. The mixed calcite and dolomite samples were treated as dolomite and completely reacted at 73°C with 100% phosphoric acid. The carbonate- CO_2 oxygen isotopic fractionation was assumed 1.008652. The analyzed carbon dioxide was compared against three National Bureau of Standards (NBS) standards: NBS-18, NBS-19, and NBS-20. The analytical error (one standard deviation) of the analyses, using the largest error reported for any of the three standards (NBS-18), was reported by the lab to be $\pm 0.09\text{‰}$ for $\delta^{13}\text{C}$ and $\pm 0.32\text{‰}$ for $\delta^{18}\text{O}$. All results are reported in the conventional delta (δ) nomenclature relative to the PDB standard (Craig, 1957).

Sulfur Stable Isotopes

Seven bedded anhydrites, nine pore-occluding anhydrites, and two replacement anhydrites were taken from selected core using a dental drill. These samples were crushed using a ceramic mortar and pestle and passed through a 63 micrometer sieve. The samples were sent to Krueger Enterprises, Inc., Geochron Laboratories Division, for sulfur stable isotope analysis. Sulfate samples were reduced to silver sulfide and then combusted at 850°C for 15 minutes. $\delta^{34}\text{S}$ was measured using a VG Isogas stable-isotope-ratio mass spectrometer. Sulfur values are reported in the conventional $\delta^{34}\text{S}$ nomenclature relative to Canon Diablo troilite (MacNamara and Thode, 1950). Analytical precision of the analyses (one standard deviation) was reported by the lab to be +/- 0.1‰.

PETROLEUM PRODUCTION STATISTICS

Ultimate Recoverable Reserves Per Field

The ultimate recoverable petroleum reserves in barrels of oil per field for the Wayne beds in the study area are shown in Table 2 and in Figure 5. The number of wells per field ranges from 1 to 7 with a mean of 4.6 wells per field. Petroleum reserves per field range from 69,000 to 869,000 barrels (bbls) of oil with a mean of 330,000 bbls of oil per field.

Ultimate Recoverable Reserves Per Well

The mean recoverable oil reserves per well for each Mission Canyon field within the study area are shown in Table 3. The mean reserves per well per field range from 19,000 to 124,000 barrels of oil. Due to the size of their oil reserves, the three oil pools of greatest interest to this thesis are the Cimbel, Leonard, and Roth fields. The ultimate recoverable petroleum reserves from the Wayne beds for each well in the Cimbel, Leonard, and Roth fields

TABLE 2: RECOVERABLE PETROLEUM RESERVES PER FIELD

| <u>OIL FIELD</u> | <u>RECOVERABLE RESERVES (bbls) ⁽¹⁾</u> | <u>No. WELLS</u> |
|------------------|---|------------------|
| Boundary Creek | 69,000 | 1 |
| Cimbel | 869,000 | 7 |
| Leonard | 395,000 | 7 |
| Lesje | 106,000 | 1 |
| Northeast Landa | 299,000 | 5 |
| Roth | 679,000 | 6 |
| Scandia | 136,000 | 7 |
| Zion | <u>89,000</u> | <u>3</u> |
| Mean | 330,000 | 4.6 |

(1)- decline curve analysis

Figure 5.- Map showing ultimate recoverable oil reserves per field. Production data for each field based on exponential decline curve analysis for every well within that field. The approximate outline of the Wayne beds producing oil pool is shown for each field. Dashed lines connect oil pools which are within the same field boundaries.

**ULTIMATE
RECOVERABLE
OIL RESERVES
PER
FIELD MAP**

LEONARD-ROTH AREA
BOTTINEAU CO., N.D.

DRAWN BY: N.J. WETMORE, 1991



0 1000 2000 3000 4000
FEET

EXPLANATION:

- PRODUCER
- ◆ PRODUCER NOW ABANDONED
- ◇ DRY HOLE
- ◻ WATER INJECTION

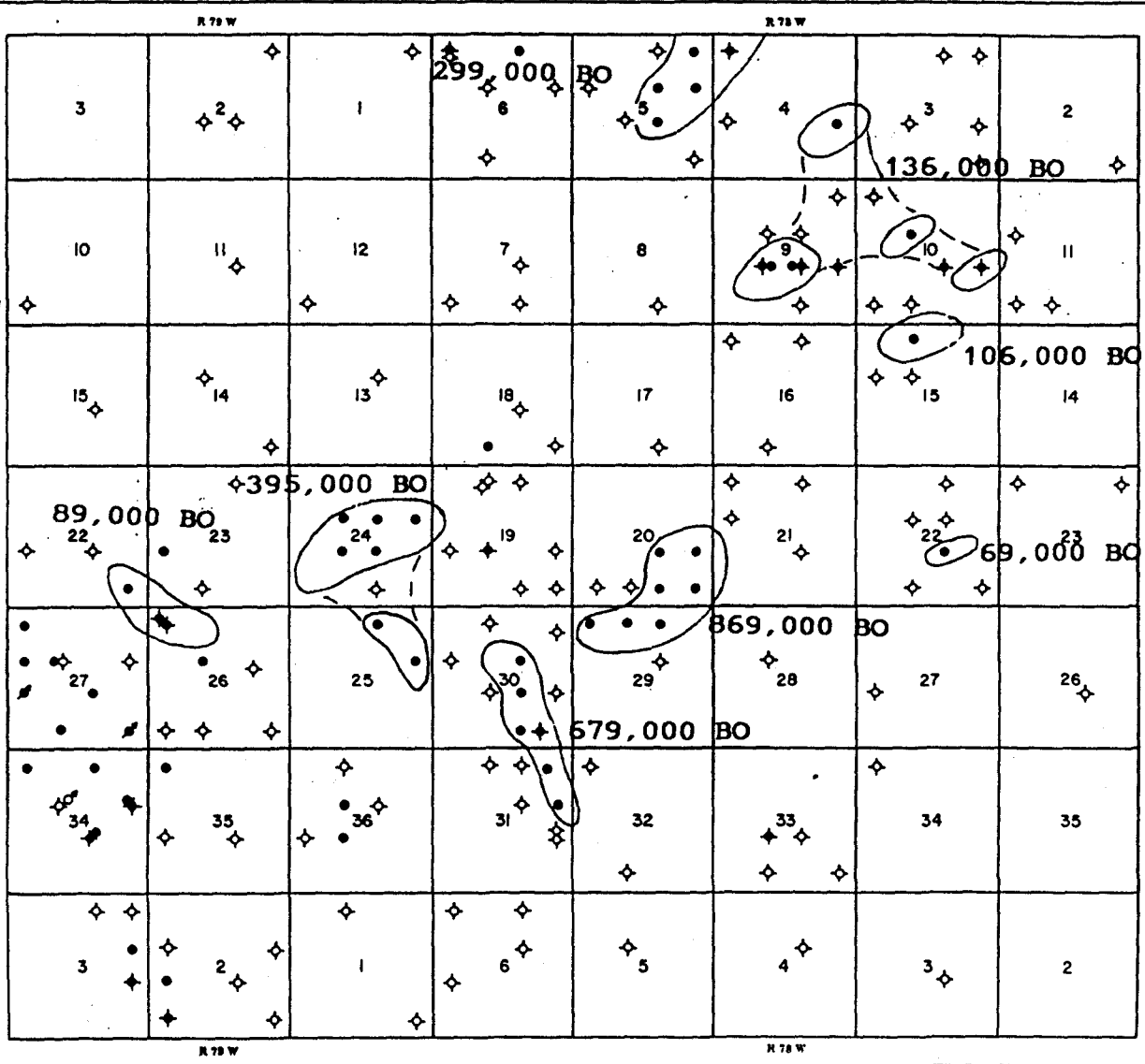


TABLE 3: RECOVERABLE PETROLEUM RESERVES PER WELL

| <u>OIL FIELD</u> | <u>MEAN RESERVES PER WELL (bbls)</u> |
|------------------|--|
| Boundary Creek | 69,000 |
| Cimbel | 124,000 |
| Leonard | 56,000 |
| Lesje | 106,000 |
| Northeast Landa | 60,000 |
| Roth | 113,000 |
| Scandia | 19,000 |
| Zion | <u>30,000</u> |
| Mean | 72,000 |

vary considerably, as shown in Figures 6, 7, and 8, respectively. Within the field boundaries of these three pools (Figure 3), petroleum reserves for each well vary widely, from 0 to 406,000 bbls of oil.

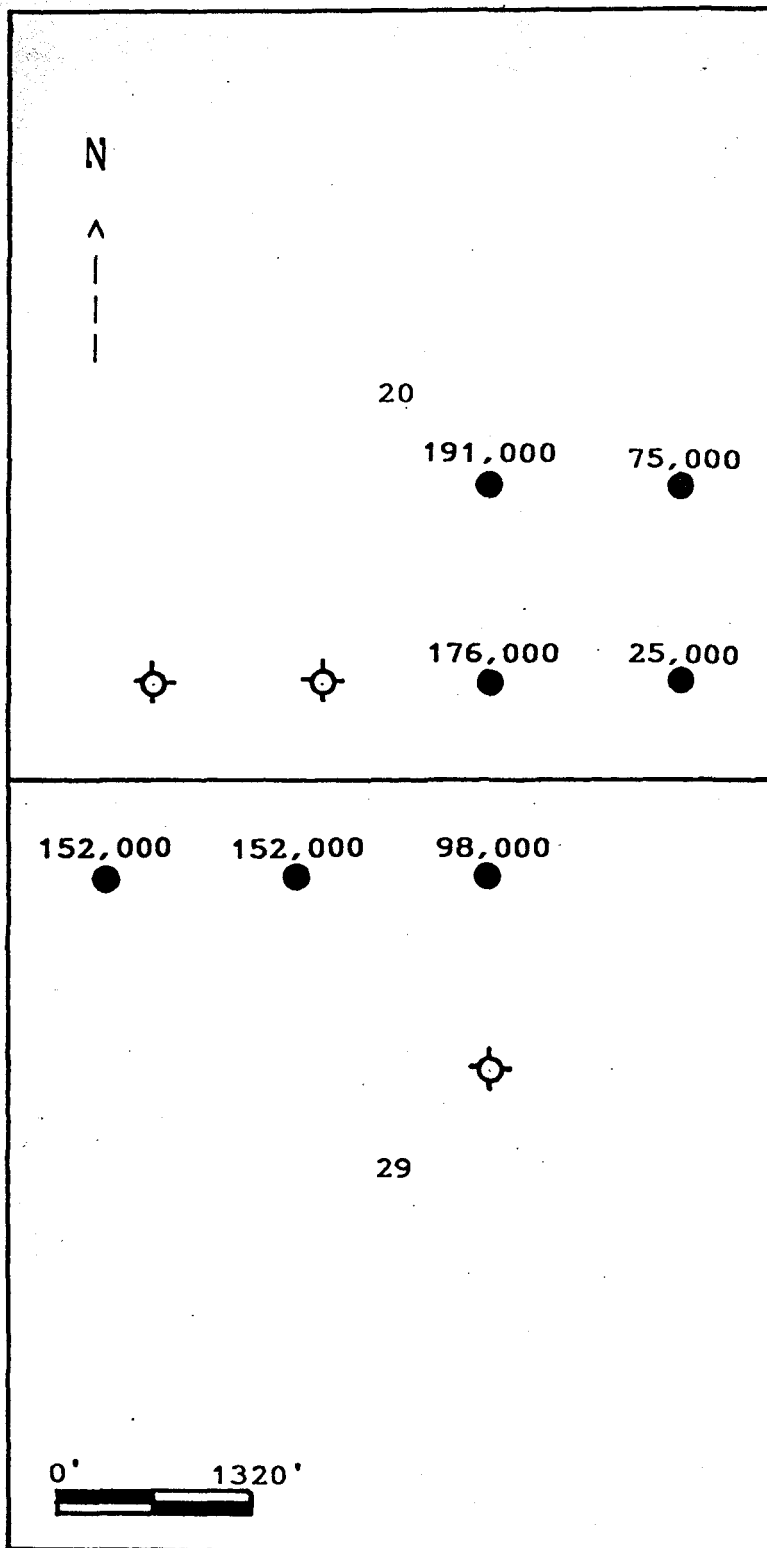
Petroleum Production Anomalies

Petroleum production from individual wells varies greatly from field to field and within each field (Tables 2 and 3; Figures 5, 6, 7, and 8). For example, two wells in the Cimbel field (Figure 6), which are approximately 1,867 feet apart, will produce 191,000 barrels of oil and 25,000 barrels, respectively. Similarly, in the Leonard field (Figure 7) two wells which are about 1,867 feet apart, will produce 7,000 barrels of oil and 121,000 barrels, respectively.

In some cases the amount of production in wells located within the same field differs by over two orders of magnitude. For example, the Roth field contains a prolific producer which is expected to produce over 400,000 barrels of oil and another well which only produced 2,000 barrels before being abandoned.

Figure 6.- Cimbel field map showing ultimate recoverable oil reserves per well. Production data based on exponential decline curve analysis for each well.

27



T 163 N

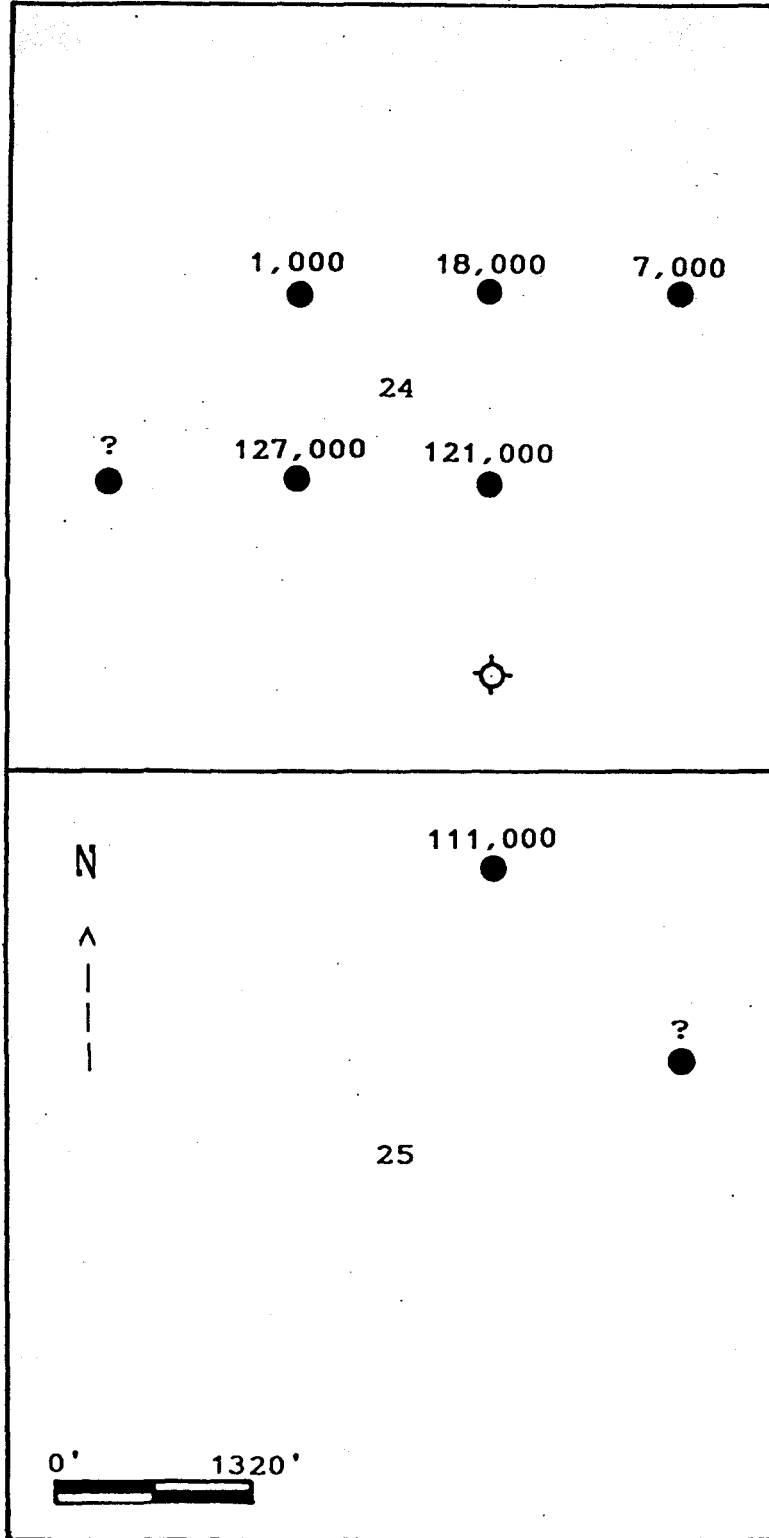
R 78 W

CIMBEL FIELD

RECOVERABLE RESERVES (BBLs)

Figure 7.- Leonard field map showing ultimate recoverable oil reserves per well. Production data based on exponential decline curve analysis. The production data for wells which were not available at the time of this thesis are depicted as question marks (?).

29



T 163 N

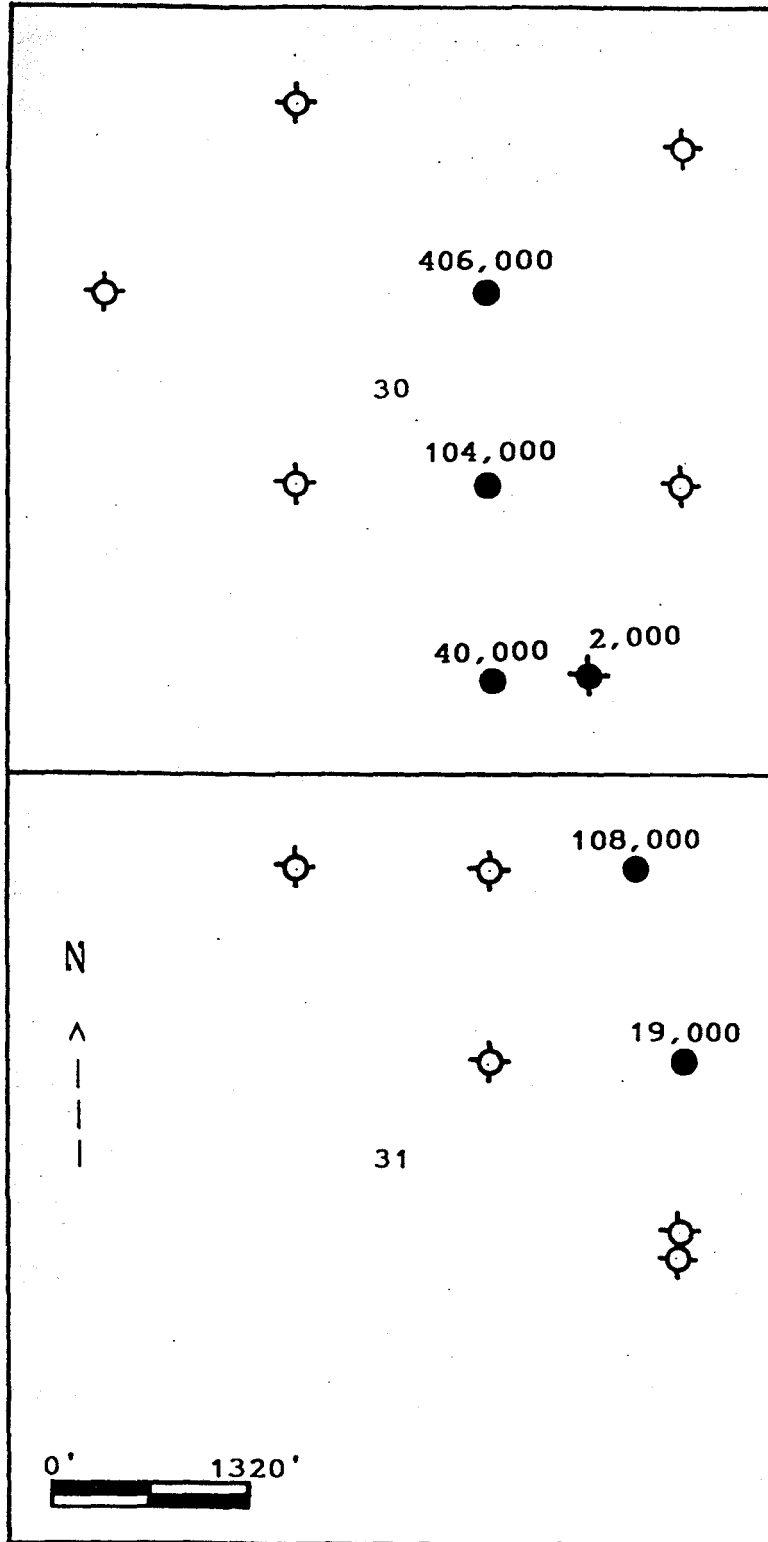
R 79 W

LEONARD FIELD

RECOVERABLE RESERVES (BBLs)

Figure 8.- Roth field map showing ultimate recoverable oil reserves per well. Production data based on exponential decline curve analysis for each well.

31



T 163 N

N
^
|
|
|

0' 1320'

R 78 W

ROTH FIELD

RECOVERABLE RESERVES (BBLs)

STUDY AREA STRATIGRAPHY

Previous Work

The evolution of stratigraphic terminology concerning the Wayne beds of the Mission Canyon Formation is shown in Figure 9. Based on outcrop studies in southwestern Montana, the Mississippian was first divided into the Lodgepole, Mission Canyon, and Charles Formations (Sloss and Moritz, 1951). The Mission Canyon Formation was subsequently subdivided into five members designated M.C.-1 through M.C.-5 (Thomas, 1954). The Saskatchewan Geological Society (1956) proposed using the Tilston beds in place of the M.C.-1 and M.C.-2 members, and the Frobisher-Alida beds in place of the M.C.-3 through M.C.-5 members.

The Madison Group stratigraphic terminology most widely used today incorporates the use of argillaceous geophysical-log markers at the top of shoaling upward cycles within the Tilston and Frobisher-Alida intervals to help delineate discrete beds. The Tilston and Frobisher-Alida intervals are most commonly subdivided into the LMC, Landa, Wayne, Glenburn, Mohall, Sherwood, and Bluell beds with the M.C.-2,

Figure 9.- Evolution of Mississippian stratigraphic terminology.

| PERIOD | GROUP | SLOSS & MORITZ (1951) | THOMAS (1954) | SGS (1956) | HARRIS ET AL (1966) | THIS REPORT |
|---------------|---------|--------------------------|--------------------------------------|-----------------|------------------------|--------------|
| MISSISSIPPIAN | MADISON | CHARLES FM | CHARLES FM | CHARLES FM | MIDALE | MIDALE |
| | | MISSION CANYON FM | MC-5 MC-4 MC-3 MC-2 MC-1 | FROBISHER-ALIDA | RIVAL | RIVAL |
| | | | | | FROB EVAP | FROB EVAP |
| | | | | | STATE A | STATE A |
| | | | | | BLUELL | BLUELL |
| | | | | | SAM | SAM |
| | | | | | K-1 | MAM |
| | | | | | K-2 | GAM |
| | | | | | K-3 | WAM |
| | | | | | LAM | LAM |
| | | | | | MC-2 | TAM |
| | | TILSTON | TILSTON LS | | | |
| | | LODGEPOLE FM | LODGEPOLE FM | LODGEPOLE FM | LODGEPOLE FM | LODGEPOLE FM |

Landa argillaceous (LAM), K-3, K-2, K-1, Sherwood argillaceous (SAM), and State A markers at the top of each bed, respectively (Harris et al., 1966) (Figure 9).

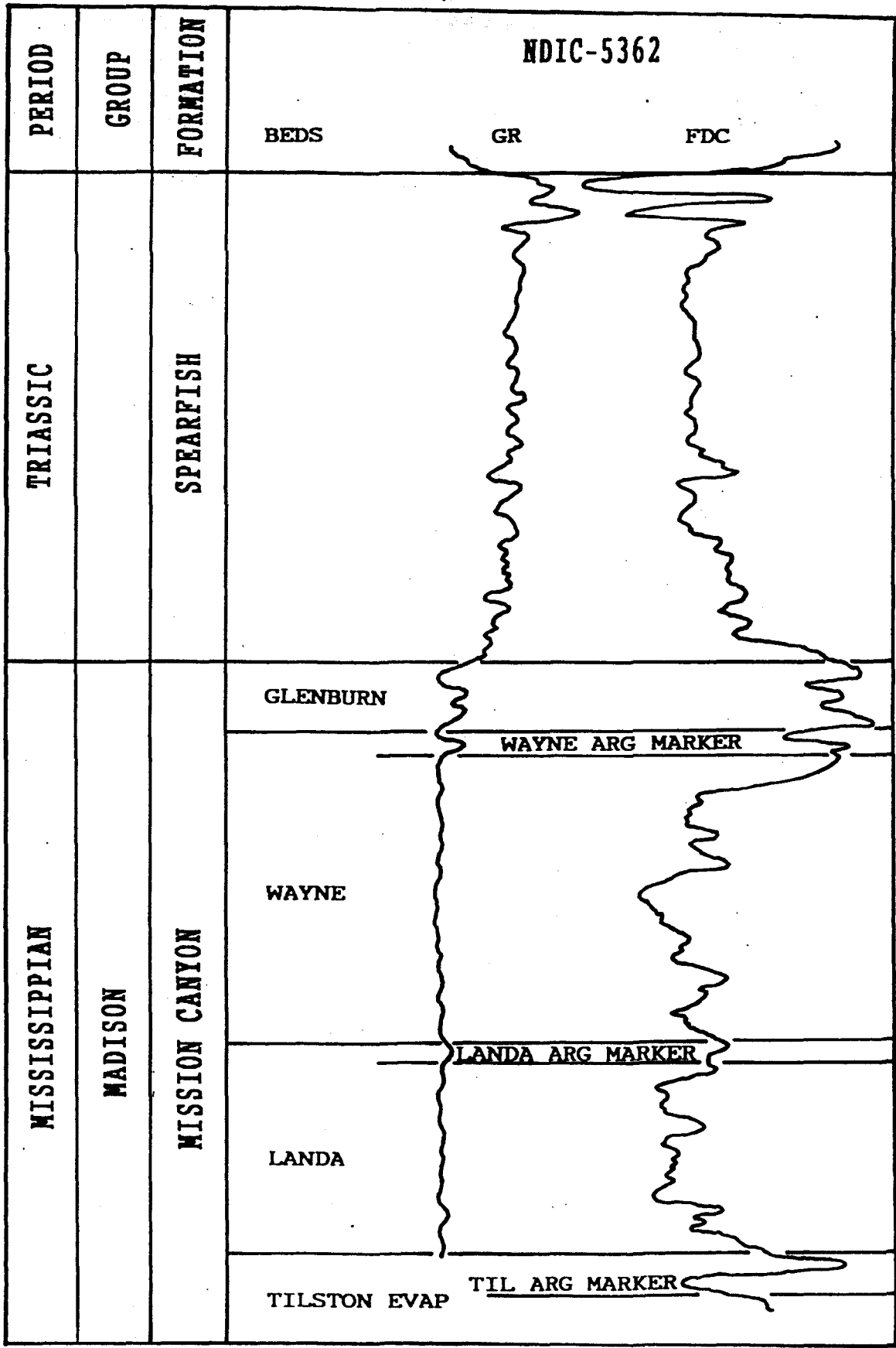
However, the M.C.-2, K-3, K-2, and K-1 marker bed identification scheme is often confused with the M.C.-1 through M.C.-5 stratigraphic terminology of Thomas (1954).

Except for the use of marker bed terminology, the Mississippian stratigraphic terminology used in this thesis conforms with the terminology as it has been previously published (Sloss and Moritz, 1951; Saskatchewan Geological Society, 1956; Harris et al., 1966). This thesis designates the argillaceous markers at the top of each unit according to the name of the underlying interval. Thus, the K-3 marker becomes the Wayne argillaceous marker (WAM), and the M.C.-2 marker becomes the Tilston argillaceous marker (TAM), and so on. This system of stratigraphic terminology for the Mission Canyon Formation is simpler to use and is already in general usage.

Type Log

A gamma-ray and compensated-formation-density type log from the NDIC-5362 Borgen 1, located in the S1/2NE1/4, Section 26, T163N, R79W, is shown in Figure 10. This type log illustrates typical geophysical log responses to the

Figure 10.- Study area type geophysical log. The gamma ray (GR) and compensated formation density (FDC) logs shown are from well NDIC-5362. The Spearfish Formation unconformably overlies the Mission Canyon Formation. Evaporites of the Glenburn beds conformably overlie the Wayne beds which overlie the Landa beds. Carbonates of the Wayne and Landa beds are delineated by the Wayne argillaceous (WAM), Landa argillaceous (LAM), and Tilston argillaceous (TAM) markers.



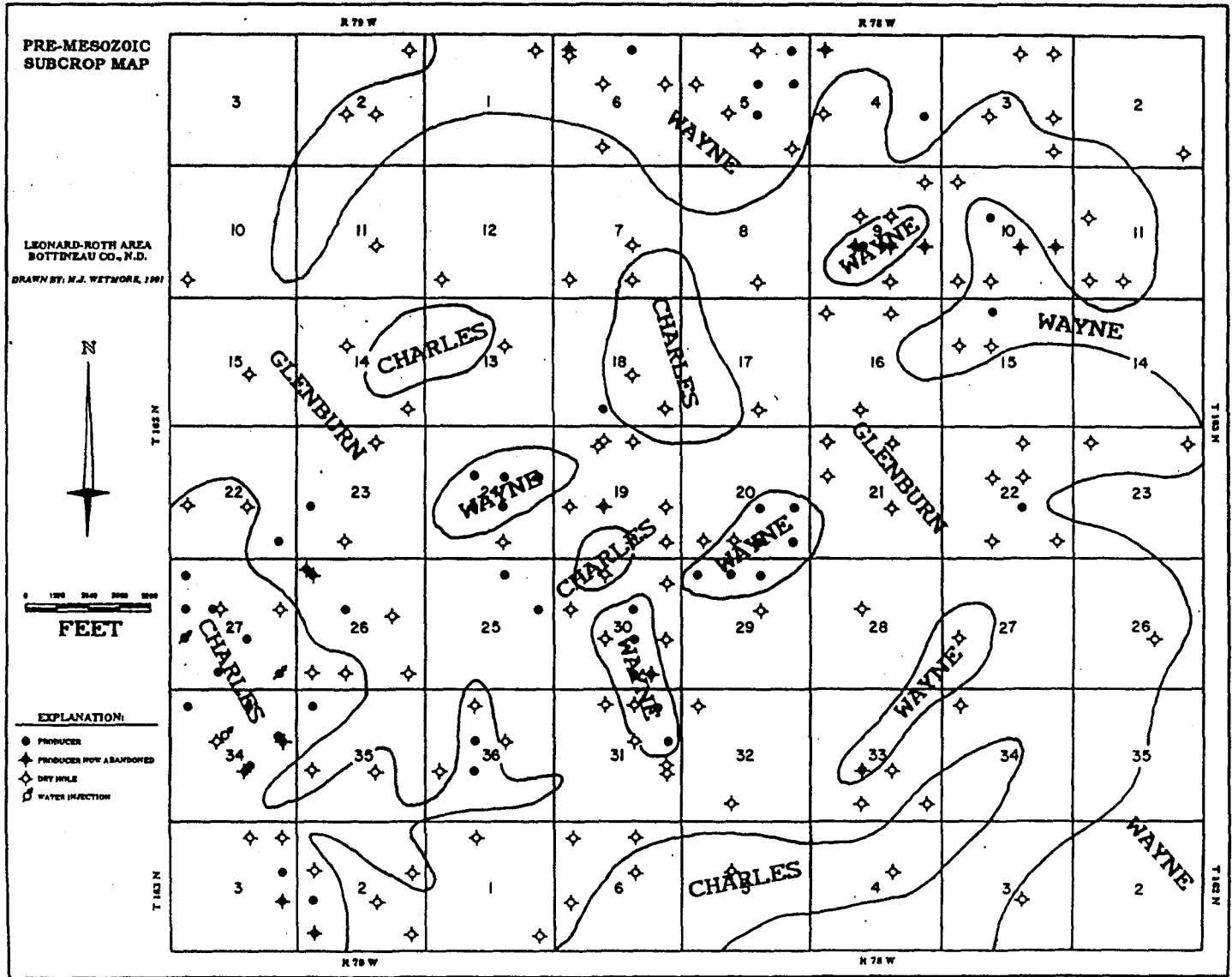
Tilston evaporite beds, Tilston argillaceous marker (TAM), Landa beds, Landa argillaceous marker (LAM), Wayne beds, Wayne argillaceous marker (WAM), Glenburn beds, pre-Mesozoic unconformity, and Spearfish Formation. For the most part, these stratigraphic units are easily recognized on geophysical logs throughout the study area.

Pre-Mesozoic Subcrop

The period of erosion and nondeposition between the Mississippian and the Triassic is marked by an angular unconformity. From west to east across the study area, progressively older stratigraphic units are truncated by this angular unconformity and exposed on the pre-Mesozoic subcrop.

Based on well log interpretations, the subcrop pattern of this erosional exposure is shown in Figure 11. In some areas paleohighs have been eroded exposing older rocks below. Paleolows expose younger rocks which have not been eroded away.

Figure 11.- Pre-Mesozoic subcrop map. Erosion exposed progressively older intervals (Figures 9 and 10) on the pre-Mesozoic unconformity surface from west to east across the study area. Paleohighs were eroded to expose older units and paleolows contain uneroded younger units.



STUDY AREA STRUCTURAL EVOLUTION

Previous Work

Mississippian structures on the eastern flank of the Williston Basin are believed to be the result of multistage, differential salt dissolution of the underlying Devonian Prairie Formation. Baillie (1953) noted that the Devonian Winnipegosis Formation, which is directly beneath the Prairie, is sometimes overlain by up to 100 feet of breccia, which he attributed to salt dissolution and collapse. A number of examples of downwarped Mississippian blocks, which have been related to Prairie salt solution, have been described in the Williston Basin (Milner, 1956; Anderson and Hunt, 1964; McTavish, 1991).

The formation of large structures due to salt dissolution may have been associated with deep-seated faults (Kupsch, 1958; Christiansen, 1967). Anderson and Hunt (1964) concluded that geologic structures in north-central North Dakota were the result of differential salt dissolution and that similar, potentially oil-productive structures could possibly be found in the study area. The

literature contains many examples of structural petroleum traps formed by Prairie salt solution in the Williston Basin (Oglesby, 1987; McTavish and Vigrass, 1987).

Structural Genesis in the Study Area

The present Mississippian structures found in the study area are probably the result of three separate processes: (1) basin subsidence, (2) differential compaction of sediments, and (3) multistage, differential dissolution of the Prairie. Basin subsidence has resulted in the regional western dip of the beds in the study area, but subsidence seems an improbable mechanism to explain the formation of study area structures. Basin subsidence could have led to thickening of the Wayne beds and the Spearfish Formation basinward to the west (Figures 16 and 17), but subsidence cannot account for the convoluted structures (Figures 12 and 13) observed in the study area.

Compaction of marine sediments was proposed by Beach and Schumacher (1982) to account for Frobisher-Alida interval geologic structures in the Stanley field area, Mountrail County, North Dakota. However, these structures were associated with intertidal to supratidal barrier islands and banks, which have not been recognized in the study area. Because major lithofacies changes do not occur

in the Wayne beds of the study area, isopach variations cannot be attributed to differential compaction. Also, compaction alone probably could not result in the creation of these structures.

Multistage, differential dissolution of the underlying Prairie is the most likely mechanism to account for the nearly 100 feet of structural relief found in some locations in the study area. Dissolution of the Prairie could account for such large structures (Anderson and Hunt, 1964; Christiansen, 1964). Collapse has occurred in other areas of the Williston Basin which have experienced Prairie salt solution (Milner, 1956; Kupsch, 1958; McTavish and Vigrass, 1987; Oglesby, 1987; McTavish, 1991). However, proving conclusively that study area structures formed as a result of salt dissolution is difficult due to the lack of Devonian well penetrations.

The following sections contain interpretations regarding the present day structure, structural growth during specific time intervals, and the location of paleostructures in the area of study. These structural interpretations are based on formation tops and intervals picked from geophysical logs.

Tilston Argillaceous Marker Structure

The Tilston argillaceous marker (TAM) is composed of argillaceous mudstone beds deposited near the top of the Tilston evaporite beds (Figure 9) and commonly displays a characteristic spike on gamma ray and porosity logs (Figure 10). The TAM has not been eroded anywhere in the study area and is therefore a reliable representation of present-day structure.

The present-day TAM structure is shown in Figure 12. Structural development reflected in the TAM is believed to have been caused by multistage, differential dissolution of the underlying Prairie. Structural highs on the TAM are closely associated with oil production from the overlying Wayne beds.

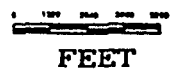
Wayne Argillaceous Marker Structure

The Wayne argillaceous marker (WAM) is an argillaceous mudstone at the top of the Wayne beds near the base of the Glenburn beds (Figure 9). The WAM is a very good geophysical log marker in the study area as it usually exhibits a characteristic spike on gamma ray and porosity logs (Figure 10).

Figure 12.- Tilston argillaceous marker (TAM) structure map. This map shows present Mississippian structure beneath the Wayne beds. Structural highs correlate with oil production in the overlying Wayne beds. Datum is sea level. Contour interval is 100 feet.

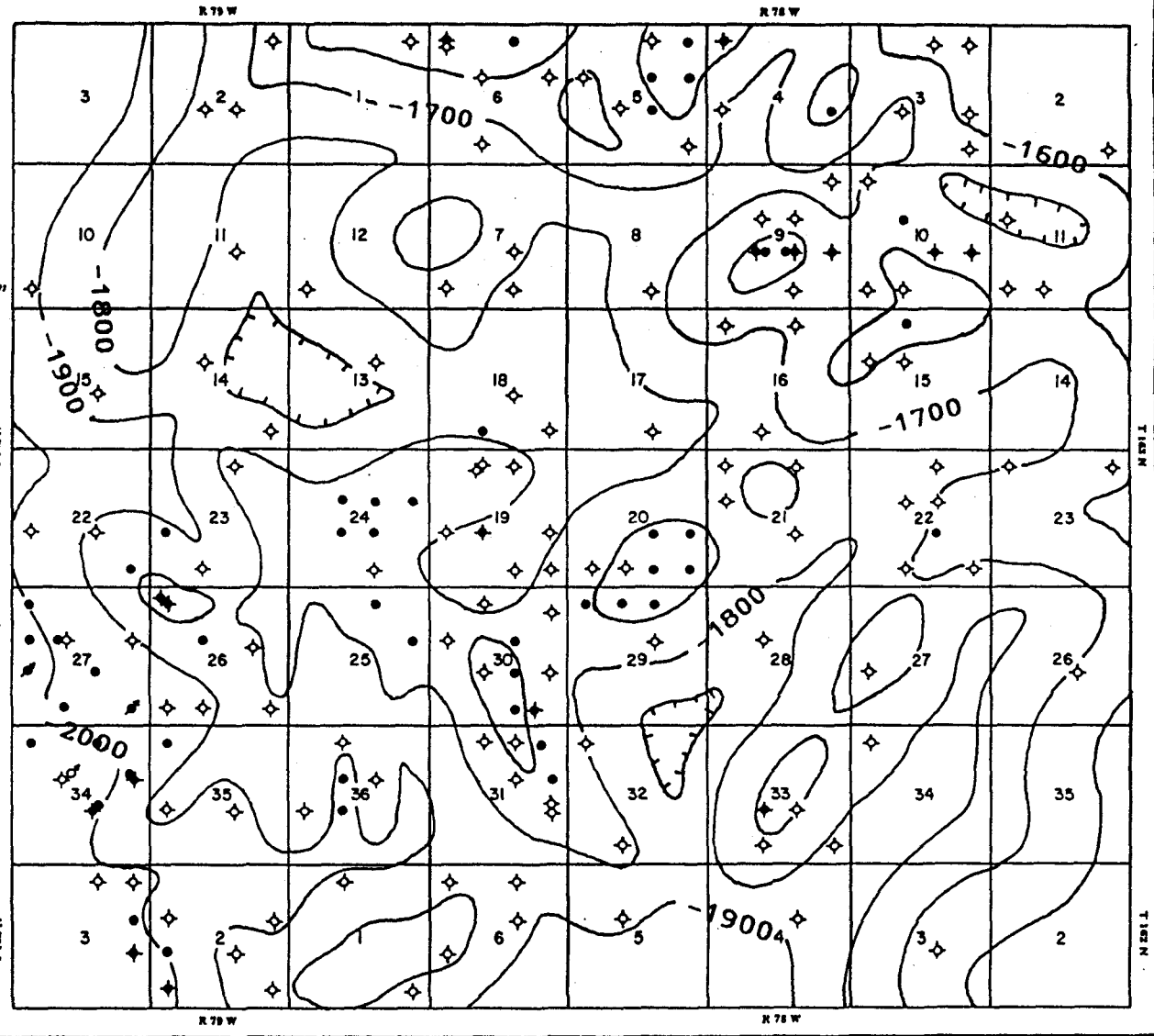
**TILSTON
ARGILLACEOUS
MARKER (TAM)
STRUCTURE
MAP**

LEONARD-ROTH AREA
BOTTINEAU CO., N.D.
DRAWN BY: H.J. WETMORE, 1991



- EXPLANATION:**
- PRODUCER
 - ◆ PRODUCER NOW ABANDONED
 - ◇ DRY HOLE
 - ◊ WATER INFLECTION

CI = 100'



The present WAM structure in the study area is presented in Figure 13. Portions of the WAM and the underlying Wayne beds were eroded away during formation of the pre-Mesozoic unconformity (Figure 11). In these areas of erosion the structural elevation of the WAM has been reconstructed from lower stratigraphic markers. Reconstructed structural contours are represented by dashed lines in Figure 13. Oil fields which produce from the Wayne beds in the study area are closely associated with structural highs on the WAM.

Pre-Mesozoic Unconformity Structure

The Mississippian Charles and Mission Canyon Formations are unconformably overlain by the Triassic Spearfish Formation in the study area (Figure 9). The pre-Mesozoic unconformity usually exhibits a characteristic break on all geophysical logs (Figure 10).

A structure map drawn on the present day pre-Mesozoic unconformity surface is shown in Figure 14. The angular nature of the unconformity can be seen by comparing the dip of the unconformity structure illustrated in Figure 14 to the dip of the underlying TAM and WAM structures presented in Figures 12 and 13, respectively. Both the TAM and the

Figure 13.- Wayne argillaceous marker (WAM) structure map.

This map depicts present Mississippian structure at the top of the Wayne beds. Dashed lines indicate those areas where the WAM was eroded during the time of the pre-Mesozoic unconformity. Note that structural highs correlate with oil production in the underlying Wayne beds. Datum is sea level. Contour interval is 100 feet.

**WAYNE
ARGILLACEOUS
MARKER (WAM)
STRUCTURE MAP**

LEONARD-ROTH AREA
BOTTINEAU CO., N.D.
DRAWN BY: M.J. WETMORE, 1961



0 1000 2000 3000 4000
FEET

EXPLANATION:

- PRODUCER
- ◆ PRODUCER NOW ABANDONED
- ◇ DRY HOLE
- ◻ WATER INJECTION

CI = 100'

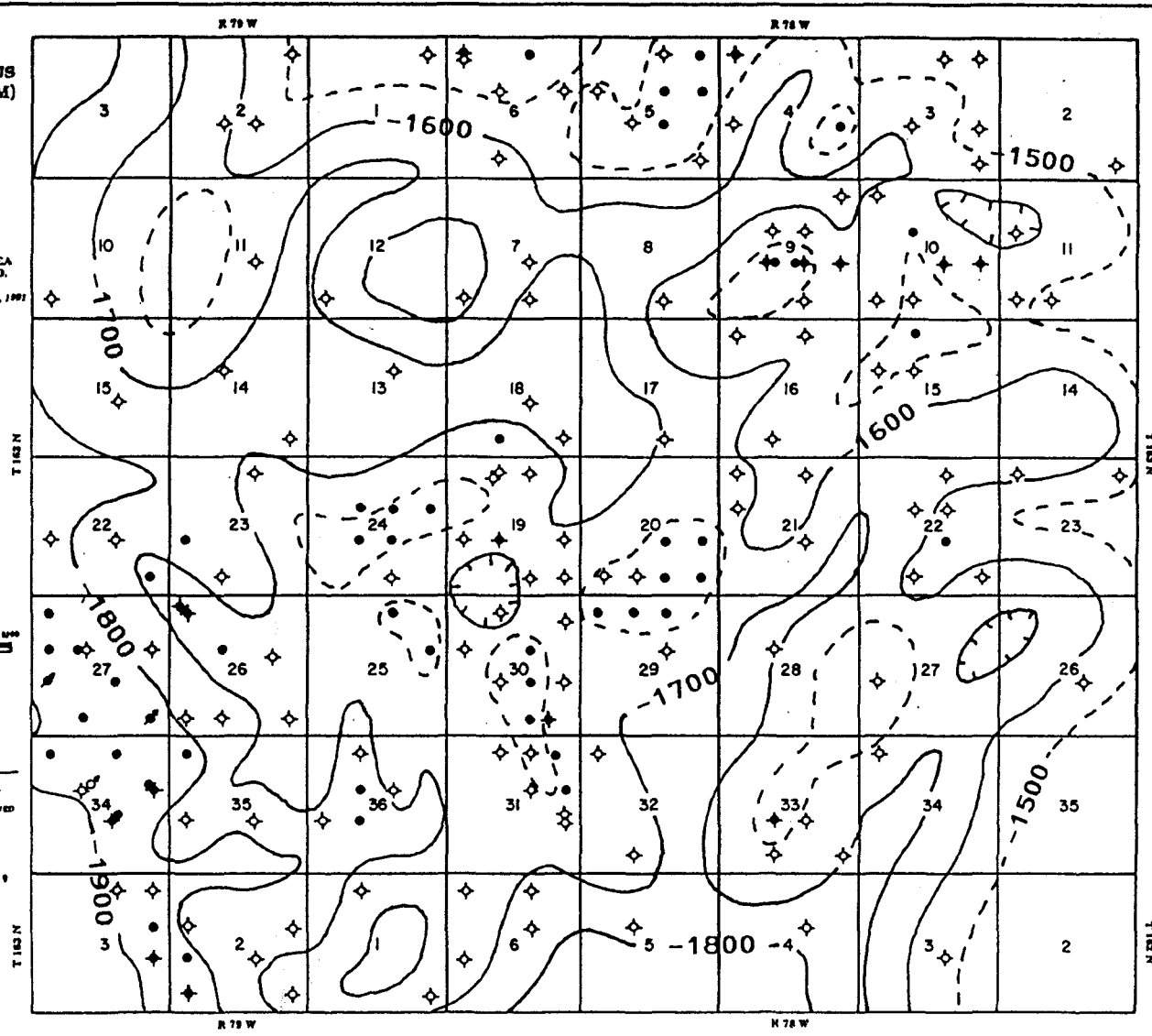


Figure 14.- Pre-Mesozoic unconformity surface structure map. This map displays present structure of the pre-Mesozoic unconformity surface. Datum is sea level. Contour interval is 100 feet.

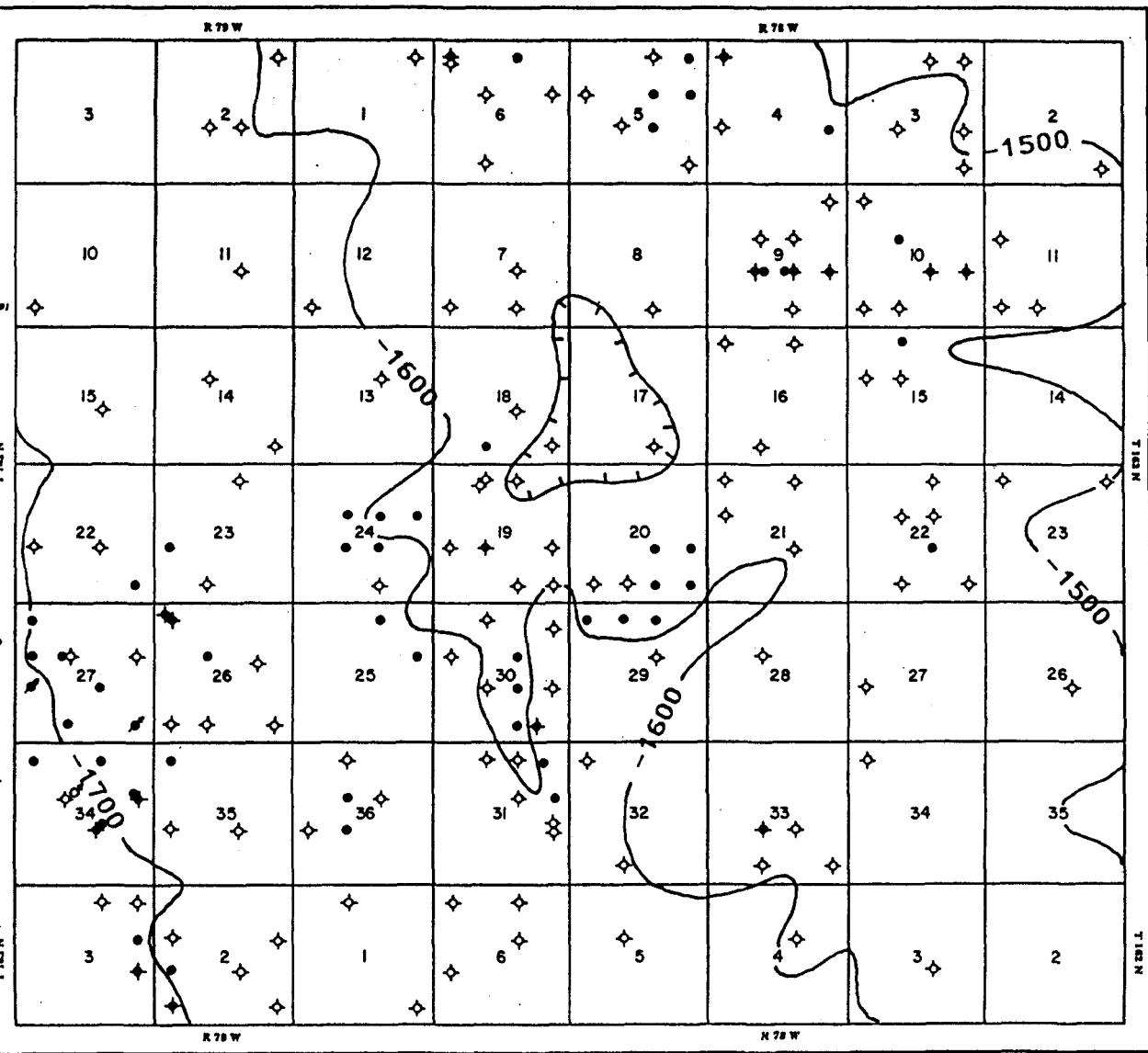
**PRE-MESOZOIC
UNCONFORMITY
SURFACE
STRUCTURE
MAP**

LEONARD-ROTH AREA
BOTTINEAU CO., N.D.
DRAWN BY: W.J. WETMORE, 1991



- EXPLANATION:**
- PRODUCER
 - ◆ PRODUCER NOW ABANDONED
 - ◇ DRY HOLE
 - ◇ WATER INJECTION

CI = 100'



WAM dip more steeply than the overlying pre-Mesozoic unconformity surface.

During the Pennsylvanian and the Permian the study area experienced collapse due to Devonian salt solution. This resulted in the formation of highs and lows on the unconformity surface. Core examination suggests that debris shed from highs accumulated as karst breccias in the lows.

Spearfish Formation Structure

The top of the Spearfish and the base of the overlying Jurassic Piper Formation usually display a characteristic break on all types of geophysical logs (Figure 10). Figure 15 shows the present structure of the Spearfish Formation.

Structural Growth During Wayne and Landa Beds Deposition

Both the TAM and the WAM were originally deposited in a nearly horizontal orientation across the study area. The TAM was deposited over an evaporite unit, and a thin layer of evaporite was deposited over the TAM. The WAM was laid down at the beginning of an evaporite sequence and has evaporite beds both below and above.

Figure 15.- Spearfish Formation structure map. This map shows present structure at the top of the Spearfish Formation. Datum is sea level. Contour interval is 100 feet.

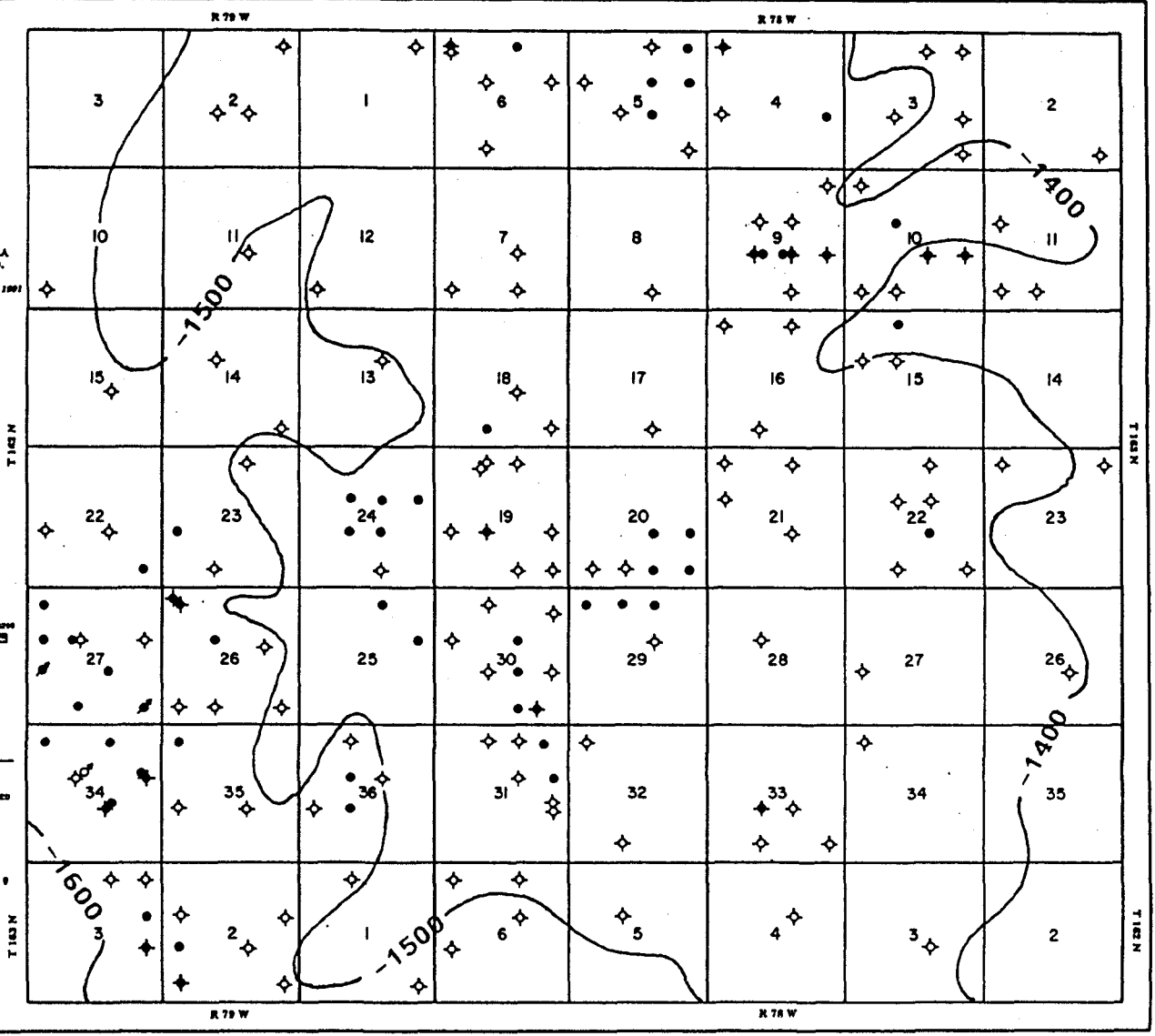
**SPEARFISH
FORMATION
STRUCTURE
MAP**

LEONARD-ROTH AREA
BOTTINEAU CO., N.D.
DRAWN BY: M.J. WETMORE, 1991



- EXPLANATION:**
- PRODUCER
 - ◆ PRODUCER NOW ABANDONED
 - ◇ DRY HOLE
 - WATER INFLECTION

CI = 100'



Positive and negative structures were present during the deposition of the Wayne and Landa beds. This structural growth can be seen in the variable thicknesses of the Wayne and Landa beds, measured from the TAM to the WAM, as shown in Figure 16. The thick areas seen on this isopach map are believed to represent areas of negative structural growth due to the dissolution and collapse of the underlying Prairie, whereas thin areas may be localities in which dissolution had not yet occurred.

Paleotopography During Spearfish Deposition

A Spearfish Formation isopach map is shown in Figure 17. The top of the isopach interval is a shale unit in the Spearfish which was probably deposited in a nearly horizontal position. The bottom of the isopach interval is the pre-Mesozoic unconformity surface. Since this surface exhibits karsted lows and eroded highs, topographic relief probably existed on the unconformity surface before the Spearfish was deposited. Thus, thin areas on the Spearfish isopach probably represent paleohighs and thick areas paleolows.

Figure 16.- Wayne and Landa beds isopach map. Isopach interval measured from the WAM to the TAM. Thick areas on this map depict negative structural growth due to salt dissolution in the underlying Devonian Prairie Formation during Wayne beds deposition. Thin areas represent those localities which had not yet experienced salt collapse. Contour interval is 10 feet.

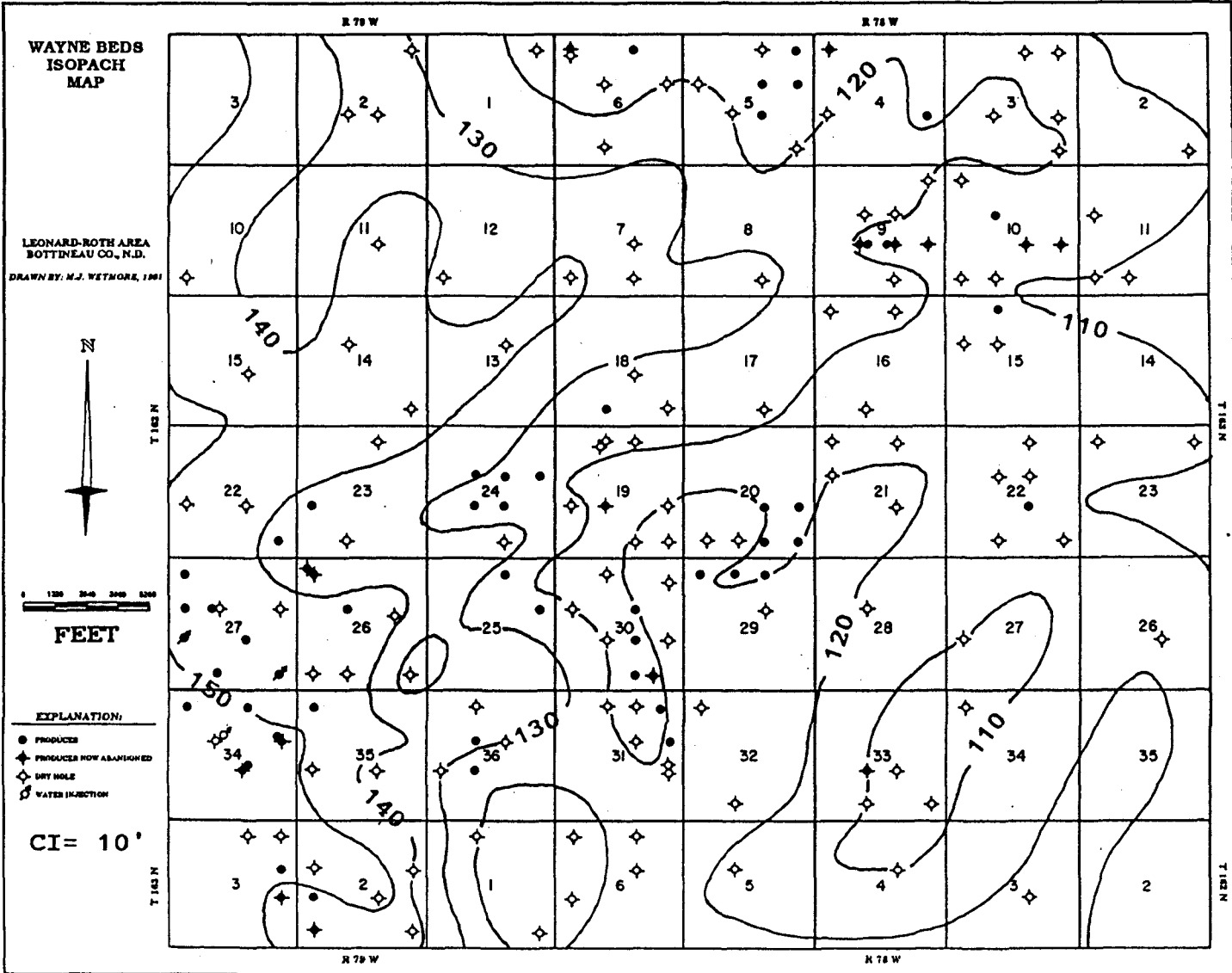
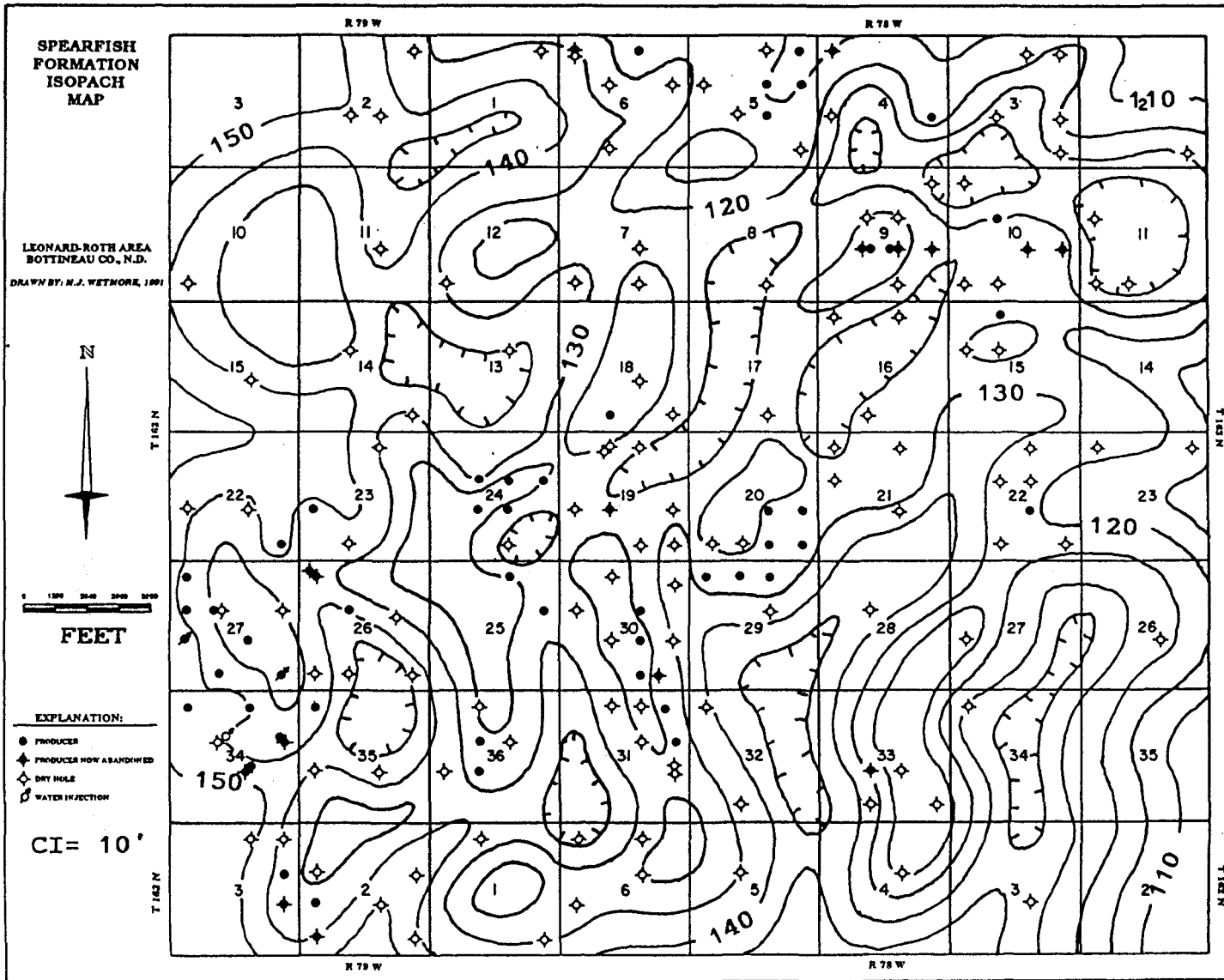


Figure 17.- Spearfish Formation isopach map. Isopach interval measured from the top of the Spearfish Formation to the pre-Mesozoic unconformity surface. Thin areas on this map show highs and thick areas represent lows at the time of Spearfish deposition. Contour interval is 10 feet.



STUDY AREA LITHOLOGIES

Previous Work

The thinly laminated to thickly bedded lithology of the Frobisher-Alida interval has been described by many authors (Shanley, 1983; Obelenus, 1985; Luther, 1988; Ahmed and Last, 1991) as being highly complex. Lithofacies in the Frobisher-Alida can change very rapidly in both the horizontal and vertical directions.

Shanley (1983) identified twelve different lithofacies in the Frobisher-Alida interval, which he described as being a complex mosaic of interfingering lithofacies. The Frobisher-Alida has been divided into eight lithofacies by Obelenus (1985) and into six by Luther (1988). Four lithofacies were recognized by Ahmed and Last (1991), but they described the lithofacies distribution as being highly variable. The lithofacies classification schemes of these authors are shown in Table 4.

These Mission Canyon workers acknowledged the complexity of the Frobisher-Alida on a local scale, yet similarities are observed in their lithofacies

TABLE 4: LITHOFACIES CLASSIFICATION SCHEMES

Shanley (1983)

1. Massive Anhydrite
2. Bedded Anhydrite
3. Bladed Anhydrite
4. Enterolithic Anhydrite
5. Halite
6. Laminated-fenestral mudstone
7. Pisolite
8. Laminated light-dark mudstone
9. Burrowed mudstone-wackestone
10. Coral-brachiopod wackestone-packstone
11. Ooid-peloid packstone
12. Patterned carbonate

Obelenus (1985)

1. Skeletal wackestone and packstone
2. Skeletal grainstone
3. Calcisphere wackestone and packstone
4. Intraclast grainstone
5. Fenestral wackestone and packstone
6. Pisolite ooid wackestone and grainstone
7. Dolomudstone
8. Anhydrite

Luther (1988)

- LF-1: Fossiliferous grainy mudstone-packstone
- LF-2: Coated-grain wackestone-grainstone
- LF-3: Peloidal-intraclastic wackestone-packstone
- LF-4: Dolowackestone-mudstone and anhydrite
- LF-5: Massive anhydrite
- LF-6: Siliciclastic sandstone-siltstone

Ahmed and Last (1991)

1. Stromatolite-cryptalgal laminite-pseudostromata
 2. Bioclastic grainstone
 3. Peloidal grainstone
 4. Vadolite
-

classifications from widely separated study areas. For example, the coral-brachiopod wackestone-packstone of Shanley (1983) is very similar to the skeletal wackestone of Obelenus (1985) and the fossiliferous wackestone of Luther (1988). In addition, other lithofacies similarities exist between these studies. This suggests that while the lithofacies of the Frobisher-Alida are highly complex locally, regionally the lithofacies are relatively consistent.

Lithofacies of the Wayne Beds

Petrographic descriptions of thin sections examined in this study are given in Appendix A. The carbonate classification scheme of Dunham (1962) is used throughout this thesis. Porosity classifications conform to those proposed by Choquette and Pray (1970).

The Wayne beds in the study area are a highly complex, interfingering mosaic of lithofacies and sublithofacies (Appendix A). The thickness of these sublithofacies ranges from thinly laminated to thickly bedded. Based on megascopic and petrographic observations, the lithofacies of the study area can be divided into four main groups: (1) packstones, (2) wackestones, (3) mudstones, and (4) anhydrites.

The non-skeletal and skeletal allochems observed in the packstone, wackestone, and mudstone lithofacies, listed in decreasing order of relative abundance, are shown in Table 5. The major non-skeletal allochems consist of pisolites, peloids, ooids, intraclasts, and pellets. The main skeletal fossils found in the Wayne beds include calcispheres, gastropods, ostracods, forams, pelecypods, brachiopods, stromatolites, corals, and crinoids. The lithofacies can be further described by using the terms dolomitic and/or anhydritic.

Almost every conceivable combination of carbonate fabric, non-skeletal allochems, and skeletal allochems has been observed in the Wayne beds in the study area. The non-skeletal allochems and skeletal allochems have been used to divide the main lithofacies into a number of sublithofacies.

Packstone Sublithofacies

The sublithofacies of the packstone lithofacies are presented in Table 6. The packstone sublithofacies of the Wayne beds can occur as unaltered, dolomitized and/or anhydritized carbonate. The major non-skeletal allochems in the packstone sublithofacies are pisoliths (Figure 18), peloids (Figure 19), ooids, intraclasts, and pellets.

TABLE 5: WAYNE BEDS LITHOFACIES, ALLOCHEMS, AND MODIFIERS

| <u>Lithofacies</u> | <u>Non-Skeletal</u> | <u>Skeletal</u> | <u>Modifiers</u> |
|--------------------|---------------------|-----------------|------------------|
| Packstone | Pisoliths | Calcispheres | Dolomitic |
| | Peloids | Gastropods | Anhydritic |
| | Ooids | Ostracods | |
| | Intraclasts | Forams | |
| | Pellets | Pelecypods | |
| Wackestone | Peloids | Ostracods | Dolomitic |
| | Pisoliths | Gastropods | Anhydritic |
| | Ooids | Calcispheres | |
| | Intraclasts | Pelecypods | |
| | | Stromatolites | |
| Mudstone | (Massive) | Stromatolites | Dolomitic |
| | Peloids | Gastropods | Anhydritic |
| | Intraclasts | Pelecypods | |
| | | Ostracods | |
| | | Brachiopods | |
| | | Corals | |
| | | Crinoids | |
| | | Calcispheres | |

TABLE 6: WAYNE BEDS PACKSTONE SUBLITHOFACIES
IN DECREASING ORDER OF ABUNDANCE

1. Pisolitic packstone
 2. Peloidal packstone
 3. Oolitic packstone
 4. Skeletal packstone
 5. Pisolitic-peloidal packstone
 6. Pisolitic-oolitic packstone
 7. Pisolitic-skeletal packstone
 8. Peloidal-oolitic packstone
 9. Peloidal-skeletal packstone
 10. Oolitic-skeletal packstone
-

Figure 18.- (A) Photomicrograph of a pisolitic packstone.

White is equant calcite cement (NDIC-2176; 3,135 feet; plane light; field of view (FOV) 6.3 mm). (B) Core photograph of a pisolitic packstone (NDIC-1159; 3,237 feet; 10 cm wide).

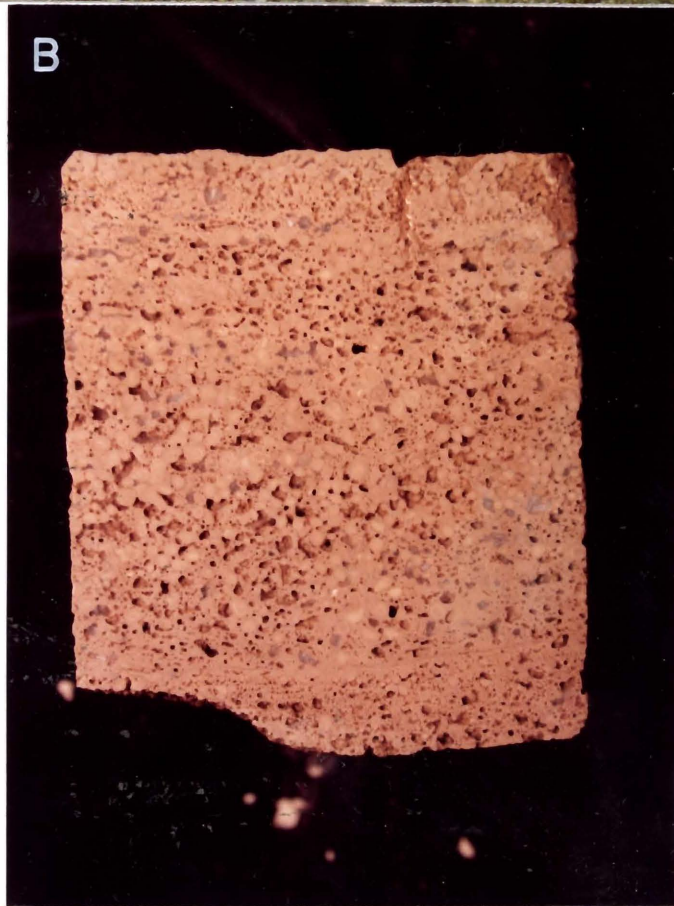
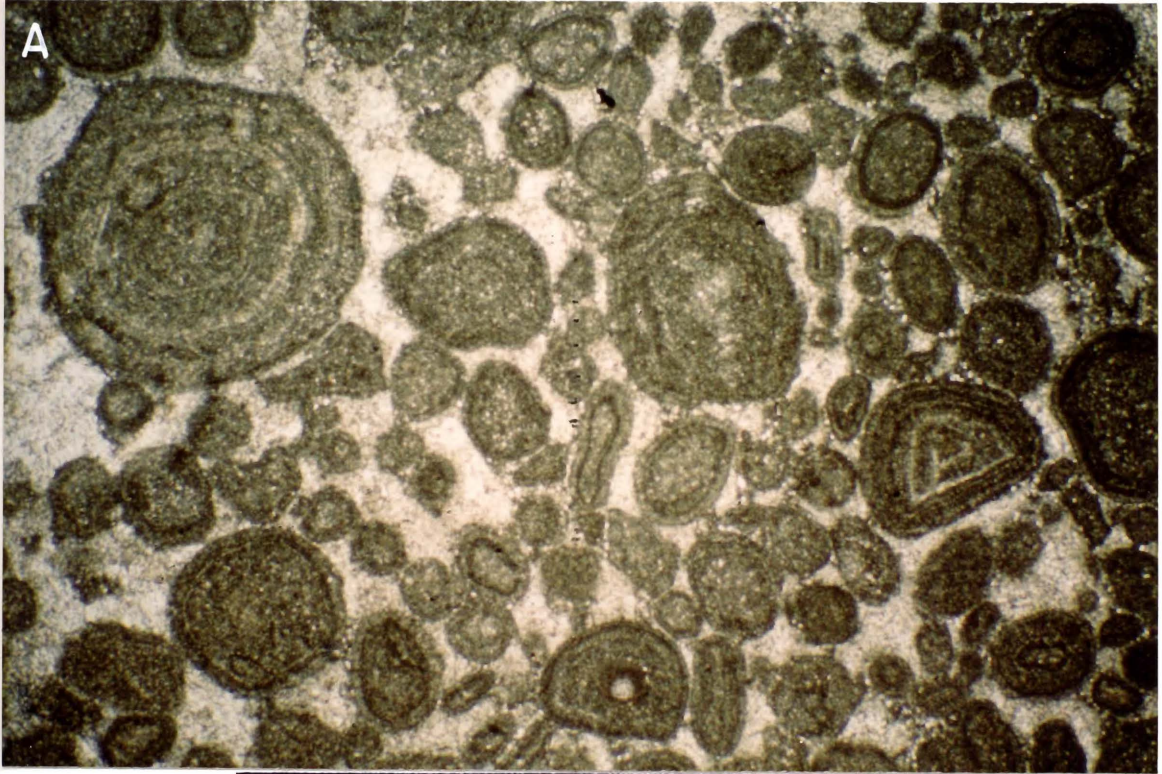
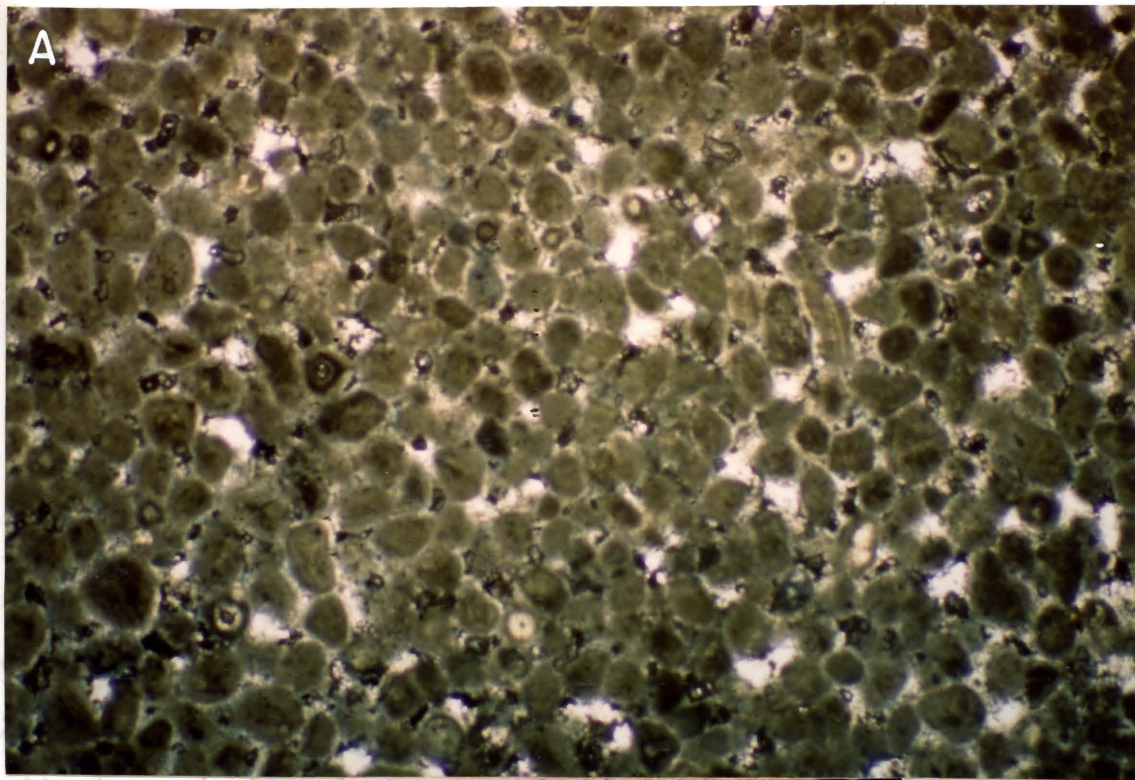


Figure 19.- (A) Photomicrograph of a peloidal packstone.

White is equant calcite cement (NDIC-3577; 3,107 feet; plane light; FOV 3.3 mm). (B) Core photograph of a peloidal packstone (NDIC-1159; 3,234 feet; 10 cm wide).



allochems in
skeletal and
gastropods, d

Mudstone Subl

The muds
presented in
anhydritized
beds. These
(Figure 12)
allochems. The
peloids and in



initial
s,
assisted.

eds are
and for
in the wagg
assive
keleta)
exist in
allochems.

Calcispheres, gastropods, ostracods, foraminifera, and pelecypods are the main skeletal allochems in the packstone sublithofacies. Skeletal packstones are shown in Figure 20.

Wackestone Sublithofacies

The sublithofacies of the Wayne beds wackestone lithofacies are shown in Table 7. The wackestone sublithofacies of the Wayne beds can be unaltered, dolomitized and/or anhydritized. Peloids, pisoliths (Figure 21), ooids, and intraclasts are the main non-skeletal allochems in the wackestone sublithofacies. Principal skeletal allochems (Figure 22) include ostracods, gastropods, calcispheres, pelecypods, and stromatolites.

Mudstone Sublithofacies

The mudstone sublithofacies of the Wayne beds are presented in Table 8. Unaltered, dolomitized, and/or anhydritized mudstone lithofacies are observed in the Wayne beds. These mudstone lithofacies are usually massive (Figure 23), but may contain non-skeletal and skeletal allochems. The major non-skeletal allochems consist of peloids and intraclasts. The primary skeletal allochems are

Figure 20.- (A) Photomicrograph of a skeletal packstone.

Shown are gastropods, pelecypods, and calcispheres.

Blue is interparticle porosity (NDIC-1977; 3,169 feet; plane light; FOV 6.3 mm). (B) Core photograph of a skeletal packstone (NDIC-2176; 3,123 feet; 10 cm wide).

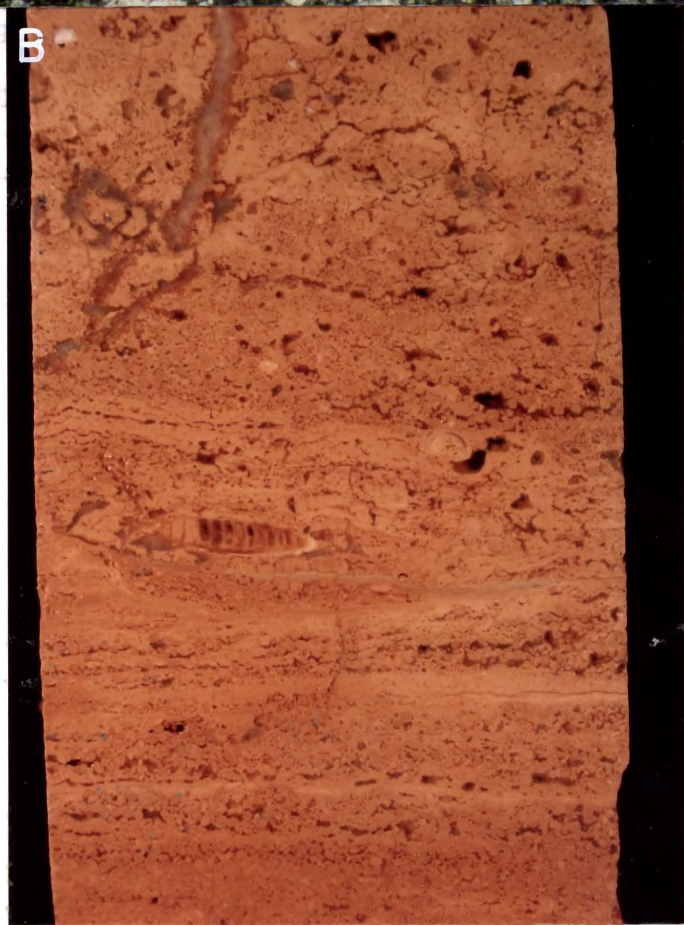
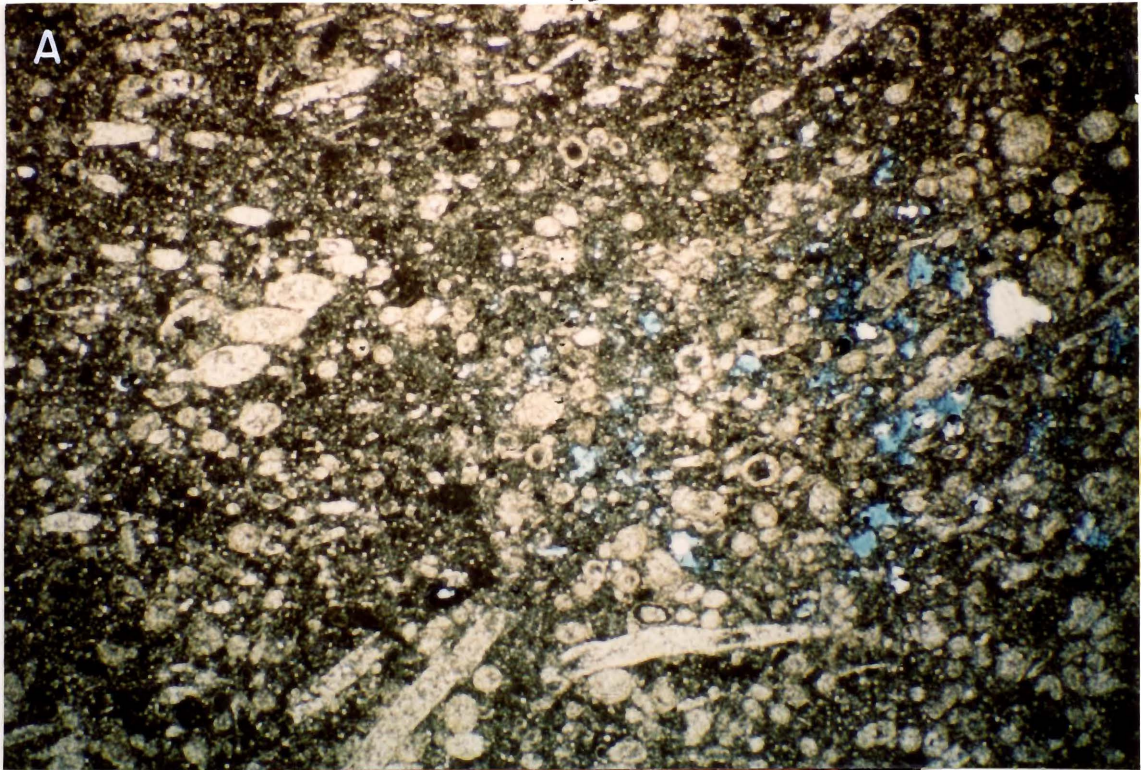


TABLE 7: WAYNE BEDS WACKESTONE SUBLITHOFACIES
IN DECREASING ORDER OF ABUNDANCE

1. Peloidal wackestone
 2. Stromatolitic wackestone
 3. Pisolitic wackestone
 4. Skeletal wackestone
 5. Peloidal-stromatolitic wackestone
 6. Peloidal-pisolitic wackestone
 7. Peloidal-skeletal wackestone
 8. Stromatolitic-pisolitic wackestone
 9. Stromatolitic-skeletal wackestone
 10. Pisolitic-skeletal wackestone
-

Figure 21.- (A) Photomicrograph of a pisolitic wackestone. Black is vugular porosity. Large, light blue crystal is pore-bridging anhydrite cement (NDIC-1159; 3,230 feet; crossed nicols; FOV 6.3 mm). (B) Core photograph of a pisolitic wackestone (NDIC-1159; 3,214 feet; 10 cm wide).

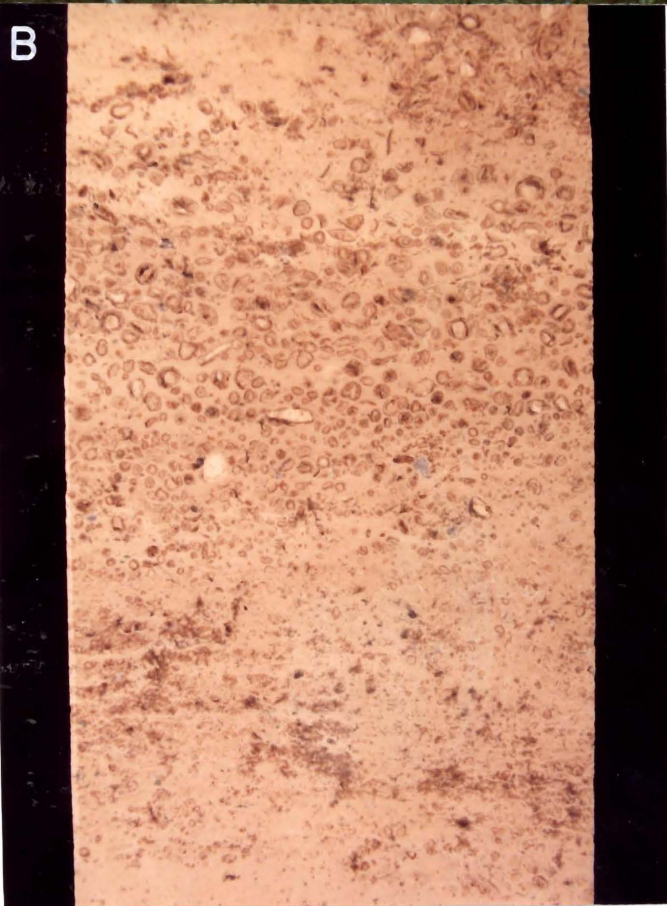
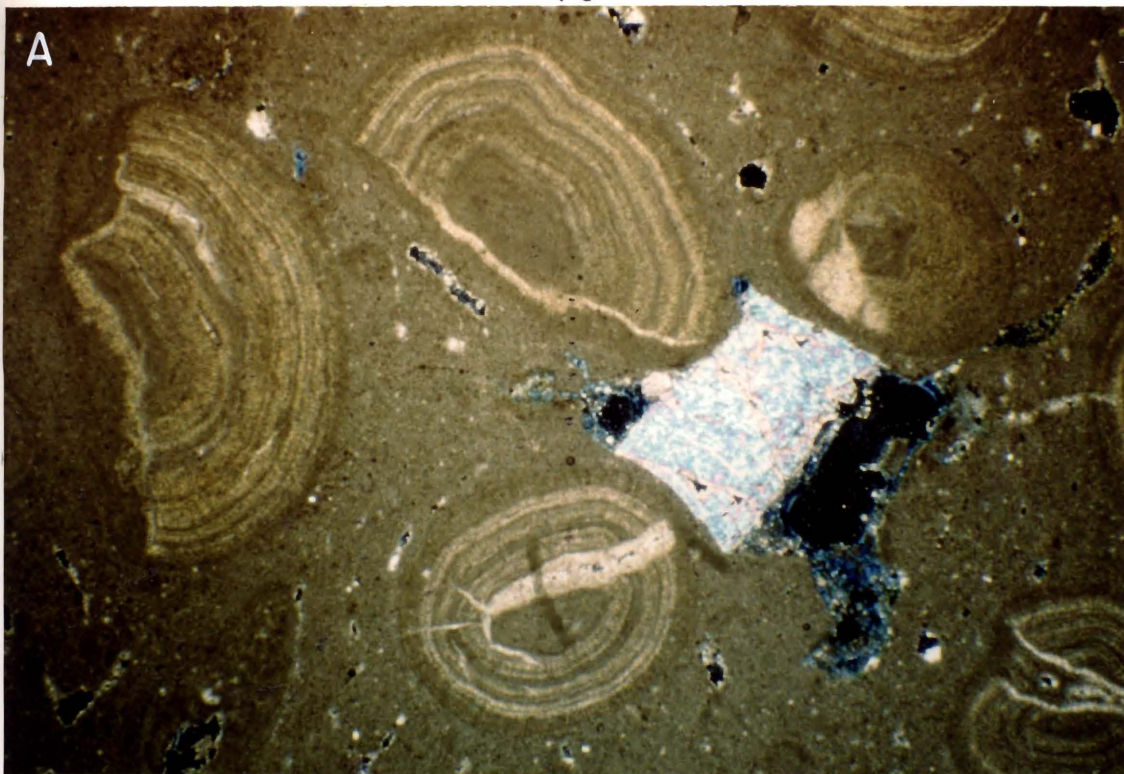


Figure 22.- Photomicrograph of a skeletal wackestone.
Shown are pelecypods, ostracods, and calcispheres
(NDIC-1159; 3,236 feet; plane light; FOV 6.3 mm).

TABLE 8: WAYNE COUNTY DETRITUS SAMPLES
..... IN DECKLEMAN SERIES OF SPERMATOPHYTES

- 1. *Abies balsamea*
- 2. *Pinus strobus*
- 3. *Taxus canadensis*

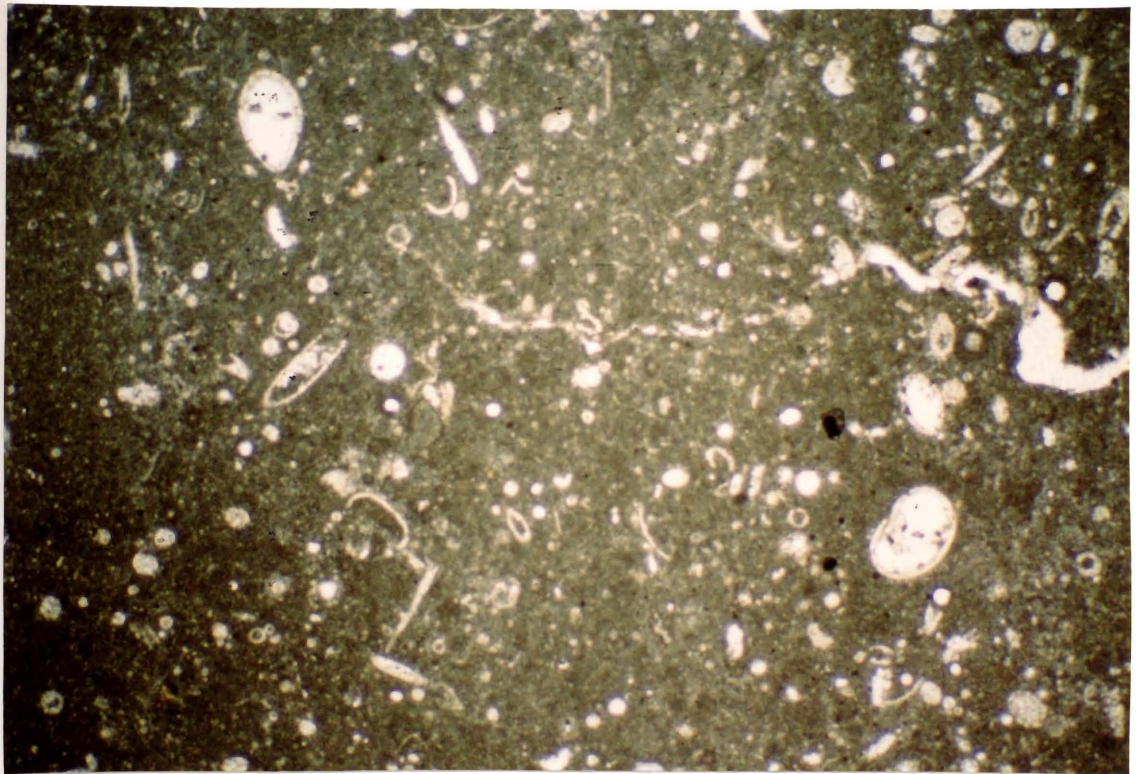
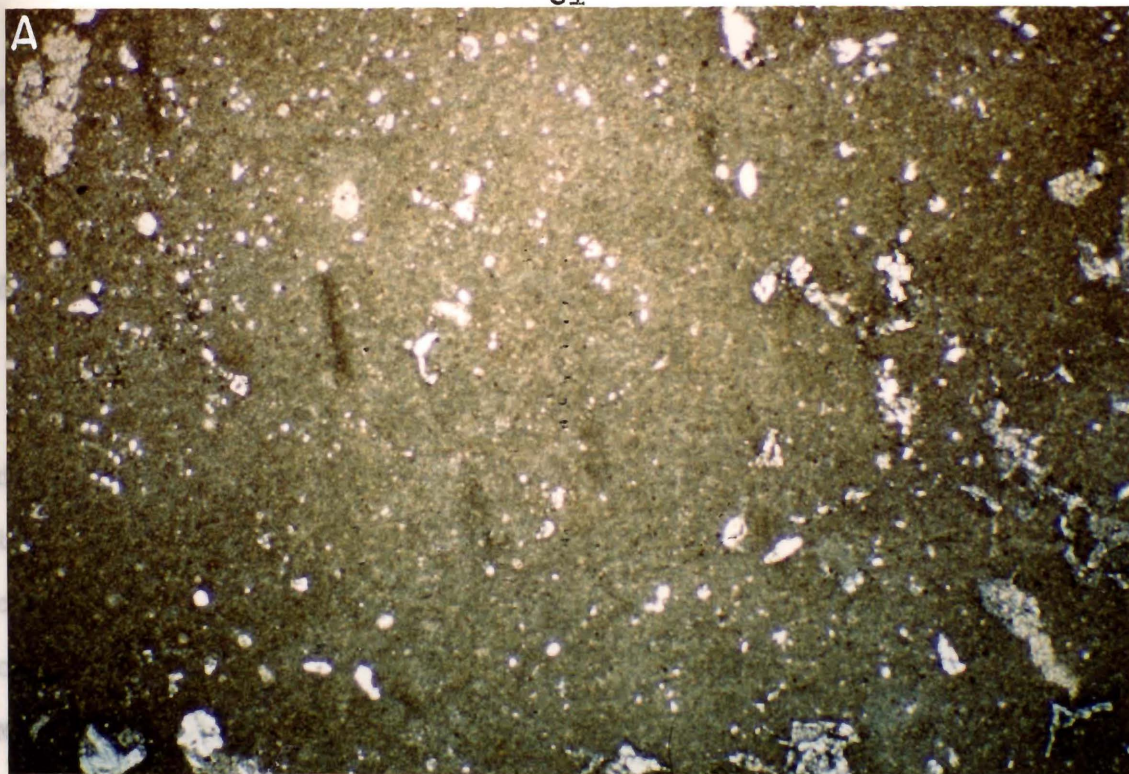


TABLE 8: WAYNE BEDS MUDSTONE SUBLITHOFACIES
IN DECREASING ORDER OF ABUNDANCE

1. Massive mudstone
 2. Stromatolitic mudstone
 3. Peloidal mudstone
 4. Skeletal mudstone
 5. Stromatolitic-peloidal mudstone
 6. Stromatolitic-skeletal mudstone
 7. Peloidal-skeletal mudstone
 8. Intraclastic mudstone
-

Figure 23.- (A) Photomicrograph of a massive mudstone.

White is vugular porosity (NDIC-1977; 3,189 feet; plane light; FOV 6.3 mm). (B) Core photograph of a massive mudstone (NDIC-1159; 3,218 feet; 10 cm wide).



photomicrogra
are shown in



anhydrous

stromatolites (Figure 24), gastropods, pelecypods, ostracods, brachiopods, corals, crinoids, and calcispheres.

Anhydrite Sublithofacies

The anhydrite lithofacies of the Wayne beds has been divided into sublithofacies based mainly on sedimentary textures as shown in Table 9. No allochems have been observed in the anhydrite sublithofacies. The anhydrite classification scheme and textural descriptions suggested by Maiklem et al. (1969) are used in this thesis. A photomicrograph and core photograph of a bedded anhydrite are shown in Figure 25.

Figure 24.- (A) Photomicrograph of a stromatolitic mudstone (NDIC-2176; 3,160 feet; plane light; FOV 6.3 mm). (B) Core photograph of a stromatolitic mudstone (NDIC-1159; 3,239 feet; 10 cm wide).

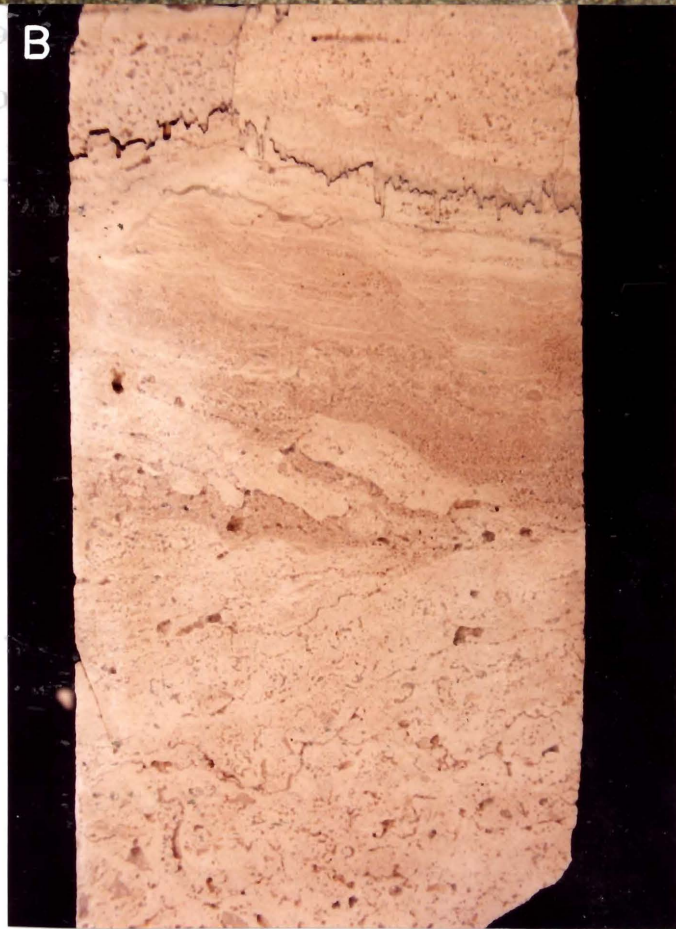
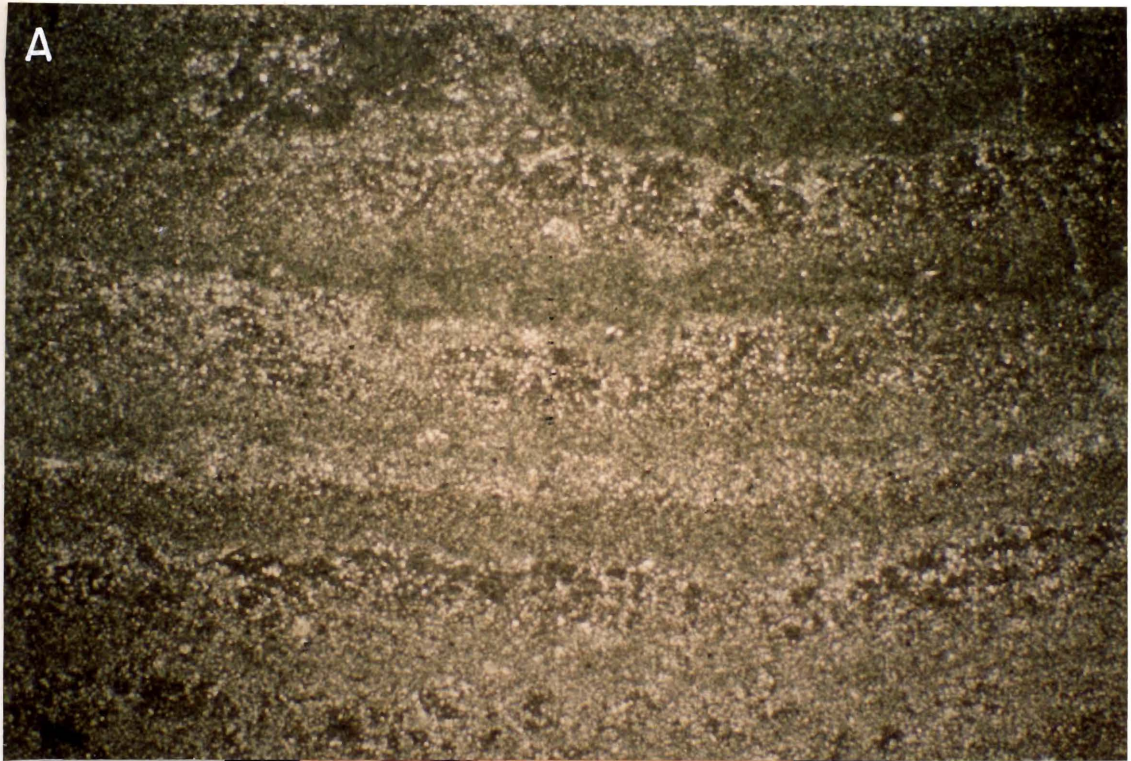


TABLE 9: WAYNE BEDS ANHYDRITE SUBLITHOFACIES
IN DECREASING ORDER OF ABUNDANCE

1. Massive anhydrite
 2. Distorted massive anhydrite
 3. Bedded massive anhydrite
 4. Mosaic anhydrite
 5. Distorted mosaic anhydrite
 6. Bedded mosaic anhydrite
 7. Nodular anhydrite
 8. Distorted nodular anhydrite
 9. Nodular mosaic anhydrite
 10. Bedded nodular anhydrite
-

Figure 25.- (A) Photomicrograph of bedded anhydrite with enterolithic micrite (NDIC-3451; 3,111 feet; plane light; FOV 6.3 mm). (B) Core photograph of bedded anhydrite (NDIC-1159; 3,180 feet; 10 cm wide).

DEPOSITIONAL ENVIRONMENTS

Previous Work

Most Mission Canyon Formation researchers agree that the Frobisher-Alida beds were deposited on a carbonate platform or carbonate shelf. Shanley (1983) described the Frobisher-Alida interval as having been deposited in a peritidal environment next to a low-lying coastal plain and lagoon complex. The Frobisher-Alida was considered to be the result of a digitate shoreline, shallowing upward, lime-mud to sabkha sequence by Obelenus (1985).

Luther (1988) contended that the lithofacies distribution in the Frobisher-Alida beds was due to the presence of a horizontal salinity gradient in a shallow marine environment. The Frobisher-Alida beds were interpreted to have been deposited on a carbonate tidal-flat/shoreline complex by Ahmed and Last (1991). A summary of the Frobisher-Alida depositional environments suggested by these studies, together with the investigations of Wilson (1975, p. 283-285), Quinn (1986), Stephens (1986), and Schwartz (1987), are given in Table 10.

TABLE 10: FROBISHER-ALIDA DEPOSITIONAL ENVIRONMENTS

| <u>Author (Year)</u> | <u>Depositional Environments</u> |
|----------------------|--|
| Wilson (1975) | Open Marine, Oolitic to Peloidal Shoals, Lagoons, Tidal Flats, Sabka |
| Shanley (1983) | Subtidal, Peritidal, Evaporitic Lagoon, Coastal Plain |
| Obelenus (1985) | Open Marine, Major Shoals, Protected Marine, Restricted Lagoon, Tidal Flat, Marginal Sabkha, Inner Sabkha |
| Stephens (1986) | Sublittoral, Littoral, Supralittoral |
| Quinn (1986) | Open Marine, Ooid Shoal, Ponged Lime Mud Flat, Evaporitic Lagoon, Sabkha |
| Schwartz (1987) | Shallow Marine, Shallow Sublittoral, Restricted Sublittoral, Supralittoral |

Luther (1988)

Open Marine Sublittoral,
Hypersaline Moderate Energy
Sublittoral, Hypersaline Low Energy
Sublittoral, Supratidal, Sabkha

Ahmed & Last (1991)

Shallow Open Marine, Shoals, Tidal
Channels, Intertidal Flats, Cut-off
Lagoons, Restricted Coastal Ponds

As can be seen in Table 10, these researchers are in general agreement as to the depositional environments of the Frobisher-Alida even in widely separated studies. In general, these models suggest that the Mississippian in the Williston Basin consisted of shallow, open-marine, shoal, subtidal-lagoon, tidal-flat, and evaporitic environments of deposition.

Wayne Beds Depositional Model

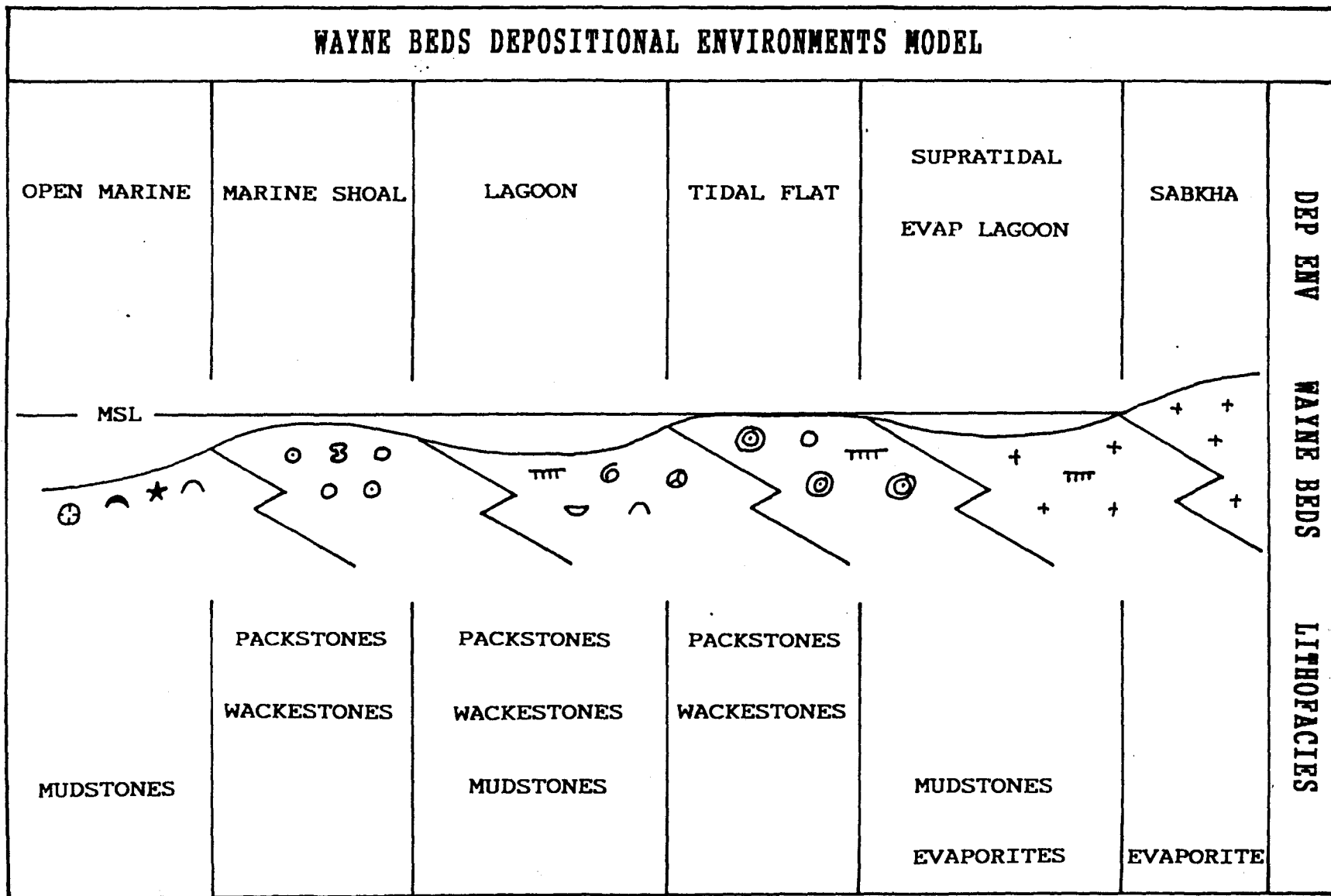
The Wayne beds in the study area were probably deposited on a shallow, open-marine to shallow semi-restricted marine shelf. A generalized depositional-environment model for the Wayne beds in the study area is shown in Figure 26. This model is based on megascopic and petrographic core observations in the study area together with comparisons to previous studies and the work of Wilson (1975). From basinward to landward, the depositional environments are open marine, marine shoal, lagoon, tidal flat, supratidal flat to evaporitic lagoon, and sabkha.

The depositional-environments model proposed in this thesis generally agrees with the models suggested by the above authors (Table. 10), and most closely agrees with the models of Wilson (1975) and Obelenus (1985). However, neither the digitate shoreline proposed by Obelenus (1985),

Figure 26.- Wayne beds depositional environments model.

Also shown are the allochems and lithofacies observed in the various depositional environments. Not to scale. A legend describing the various symbols used in this figure is shown in Appendix A.

WAYNE BEDS DEPOSITIONAL ENVIRONMENTS MODEL



nor the horizontal salinity gradient evaporite sedimentation controls suggested by Luther (1988), have been recognized in the study area.

Based on petrographic examination, the productive intervals of wells in the Cimbel, Leonard, and Roth fields are all completed within the packstone-wackestone lithofacies of the tidal flat environment (Figure 26). No significant lithofacies or depositional environment variations were observed either between wells within a field or between fields.

DISCUSSION: OIL PRODUCTION ANOMALIES

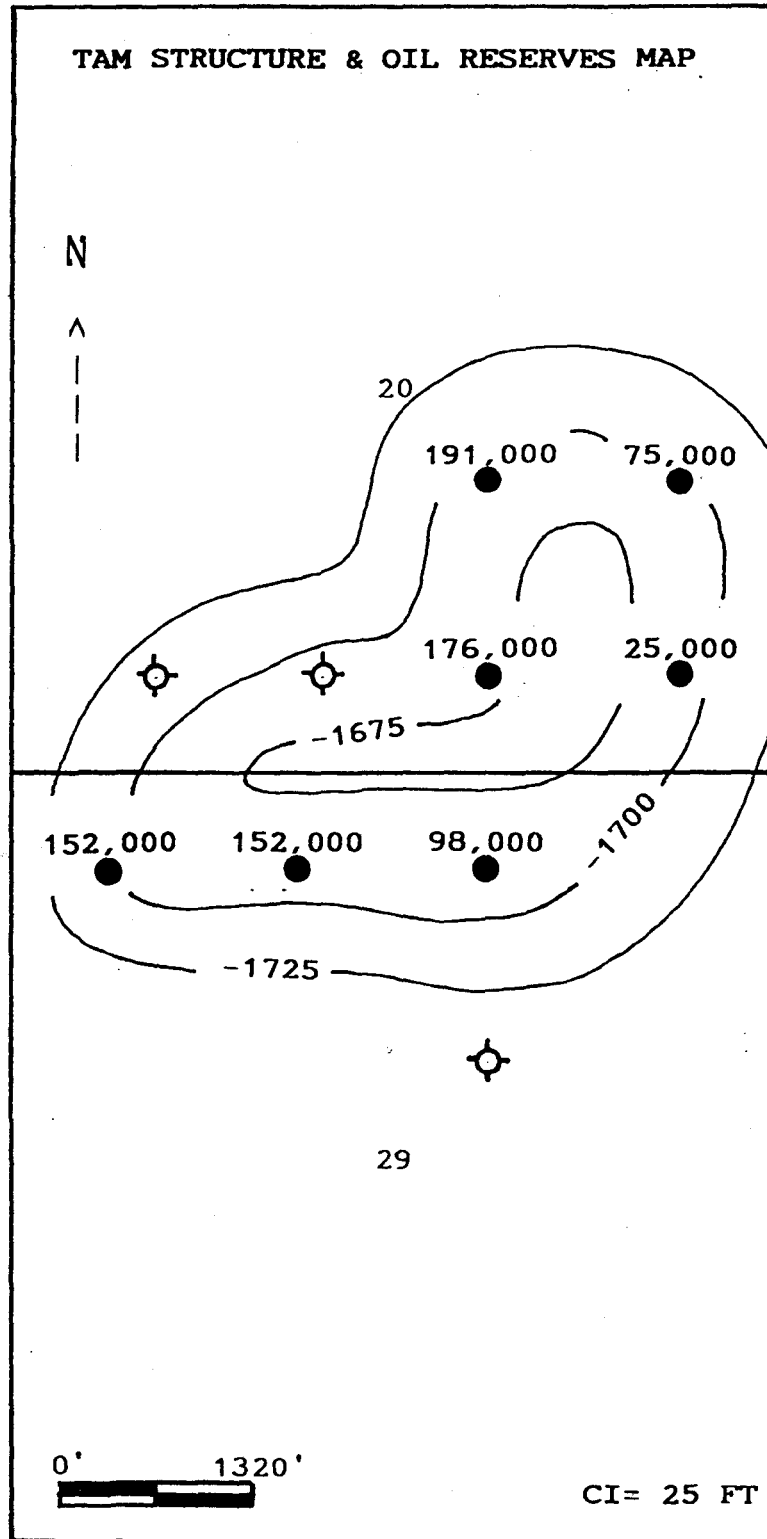
Structure

Detailed Tilston argillaceous marker (TAM) structure maps, together with ultimate recoverable oil reserves for the Cimbel, Leonard, and Roth fields are presented in Figures 27, 28, and 29, respectively. Comparing the structure to oil production reveals that wells drilled below the oil-water transition zone do not produce oil and that wells drilled above the oil-water transition zone may or may not produce oil.

The base of the oil-water transition zone in the Cimbel field appears to occur at approximately 1,725 feet below sea level (Figure 27). Wells drilled below this elevation are dry holes. However, the Cimbel field also has two dry holes above this elevation. Apparently, the amount of oil production per well is not controlled by structure. The best producer (191,000 bbls) is one of the structurally lowest wells in the field, and the poorest producer (25,000 bbls) is one of the structurally highest wells in the field.

Figure 27.- Cimbel field Tilston argillaceous marker (TAM) structure contour map with ultimate recoverable oil reserves per well. Datum is sea level. Contour interval is 25 feet. Symbols are as defined in Figure 3.

TAM STRUCTURE & OIL RESERVES MAP



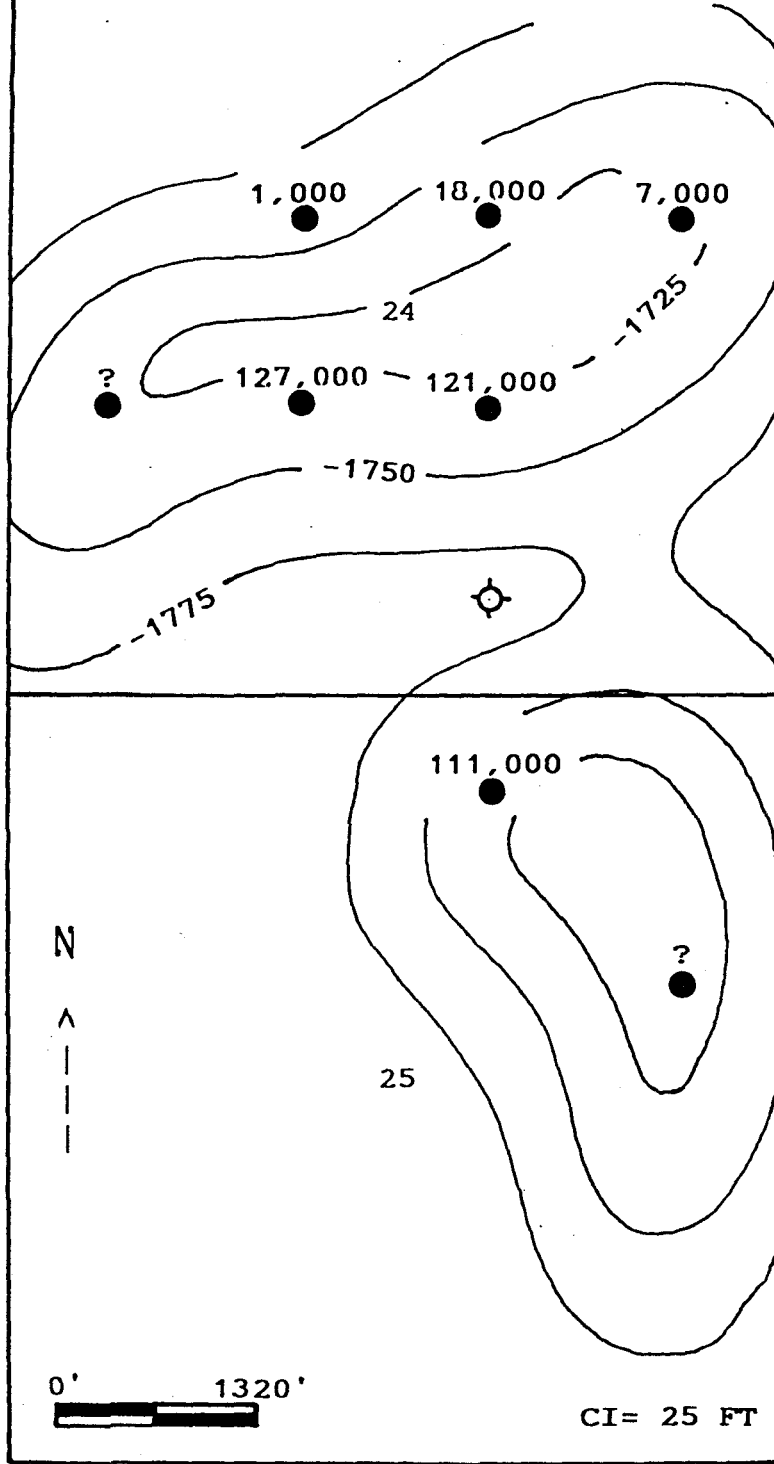
T 163 N

R 78 W

CIMBEL FIELD

Figure 28.- Leonard field Tilston argillaceous marker (TAM) structure contour map with ultimate recoverable oil reserves per well. Question marks denote wells whose production data were unavailable. Datum is sea level. Contour interval is 25 feet. Symbols are as defined in Figure 3.

TAM STRUCTURE & OIL RESERVES MAP



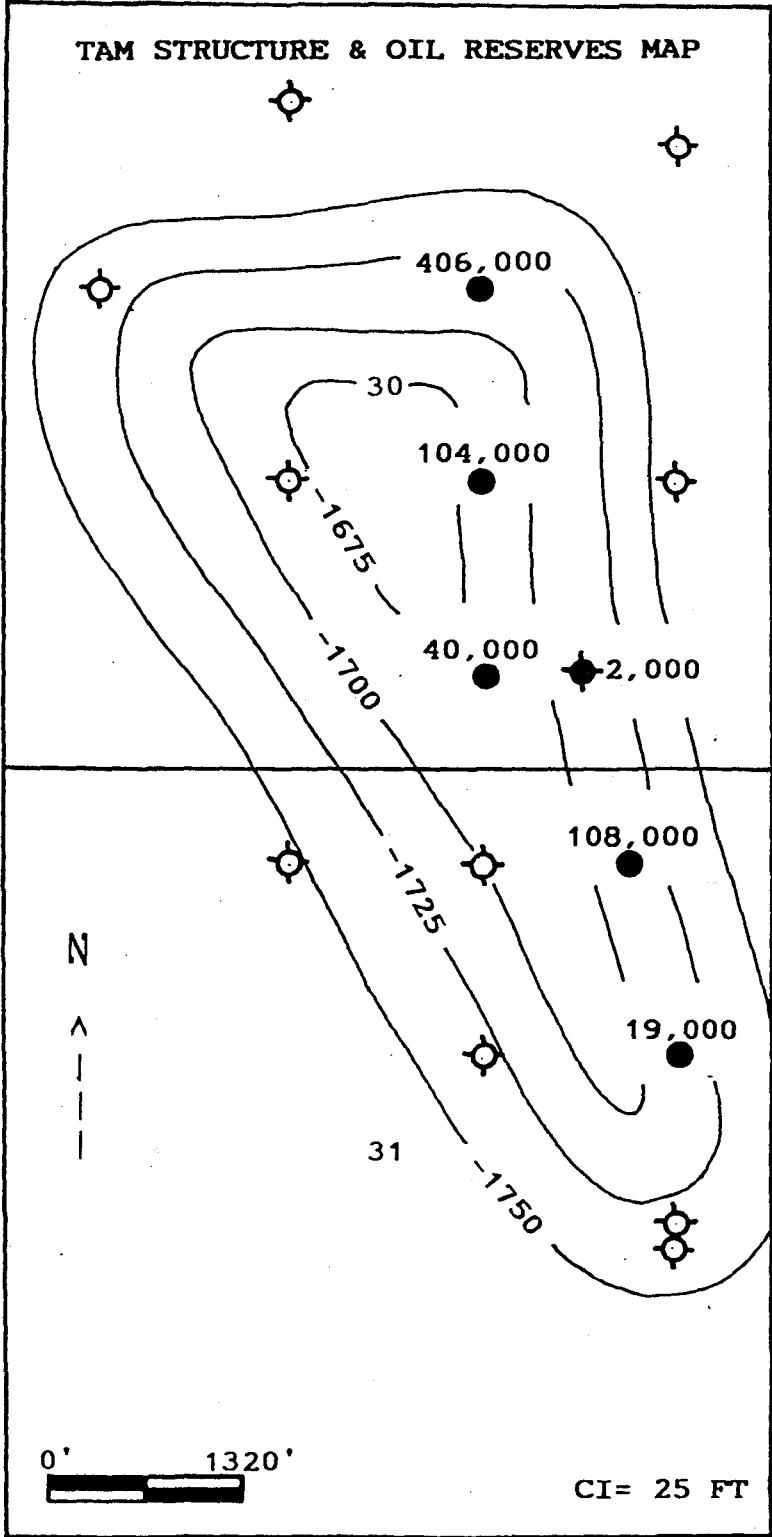
T 163 N

R 79 W

LEONARD FIELD

Figure 29.- Roth field Tilston argillaceous marker (TAM) structure contour map with ultimate recoverable oil reserves per well. Datum is sea level. Contour interval is 25 feet. Symbols are as defined in Figure 3.

101



R 78 W

ROTH FIELD

The Leonard field has an oil-water transition zone whose base is at about 1,750 feet below sea level (Figure 28). The structurally highest well in the field is one of the poorest producers at only 7,000 bbls. The best well in the field (127,000 bbls) is also one of the structurally lowest wells in the field.

The oil-water transition zone in the Roth field occurs at approximately 1,725 feet below sea level (Figure 29). Two dry holes in this field are located above that elevation. The best producer (406,000 bbls) occurs at about the same structural elevation as wells which will produce 2,000, 108,000, and 19,000 bbls.

A comparison of the production figures together with the structures for the Cimbel, Leonard, and Roth fields tends to rule out hydrodynamics and the accompanying tilted oil-water contacts as possible solutions to the production anomalies. The dry holes and poor producers are on the west and east sides of Cimbel field, the northeast side of Leonard field, and the west side of Roth field. Regional hydrodynamics is an unlikely mechanism to cause tilted oil-water contacts with three different orientations in these three closely spaced oil fields.

Two factors must be considered regarding the exploration and development of Wayne oil fields in the study area. First, the well must encounter the Wayne beds above

the oil-water transition zone. Second, above the oil-water transition zone, structure is not a guide to the amount of oil an individual well will produce over its lifetime.

Depositional Environments and Lithofacies

As discussed above, across the Cimbel, Leonard, and Roth fields the Wayne beds consist of the packstone-wackestone lithofacies, which was probably deposited in a tidal flat depositional environment (Figure 26).

Petrographic analysis of the core from these three fields does not reveal differences in Wayne lithofacies between the fields and between individual wells within those fields that could account for the observed production anomalies. For example, the Wayne beds in NDIC-2902 (104,000 bbls producer) and NDIC-2176 (dry hole) in the Roth field (Figure 29), and the NDIC-12357 (152,000 bbls producer) and NDIC-12401 (25,000 bbls producer) in the Cimbel field (Figure 27), were all deposited in a tidal flat environment. However, total recoverable oil reserve estimates for these wells vary greatly.

DIAGENESIS

Previous Work

The Frobisher-Alida beds are interpreted to have undergone marine phreatic diagenetic processes such as cementation, micritization, dolomitization, and anhydritization (Shanley, 1983; Obelenus, 1985; Luther, 1988; Ahmed and Last, 1991). These beds have also experienced diagenesis in the freshwater vadose and freshwater phreatic diagenetic environments, resulting in mineralogical stabilization, dissolution, and cementation (Obelenus, 1985; Ahmed and Last, 1991). Burial diagenetic features such as compaction, pressure solution, fracturing, and dolomitization have also been described in the Frobisher-Alida interval (Shanley, 1983; Obelenus, 1985).

Dolomitization of the Frobisher-Alida interval is extensive in some areas of the Williston Basin and lacking in others. Lindsay and Roth (1982) reported that the Mission Canyon Formation in the Little Knife field, Billings County, is heavily dolomitized. The Frobisher-Alida in north-central North Dakota has been described as

undolomitized (Shanley, 1983). Other studies have reported amounts of dolomitization which vary between these two extremes (Obelenus, 1985; Luther, 1988; Ahmed and Last, 1991).

Marine Phreatic Diagenesis

Cementation

One of the first diagenetic processes to affect carbonate sediments is the cementation of the allochems in the marine phreatic diagenetic environment (Figure 30). Later generations of calcite cement often overgrow marine cements. Marine cements can be controlled by either inorganic or organic mechanisms (Alexandersson, 1971) and form isopachous, bladed or fibrous rims around allochems (Longman, 1980).

Figure 31A is a photomicrograph showing marine phreatic cement consisting of isopachous rims around pisoliths. The Wayne beds in the study area have experienced cementation in the marine phreatic diagenetic environment.

Figure 30.- Paragenetic sequence for the Wayne beds (CMT=
cement; DOL= dolomite; ANHY= anhydrite; FW=
freshwater; DISS= dissolution; MIN STAB=
mineralogical stabilization; SOL= solution).

PARAGENETIC SEQUENCE FOR THE WAYNE BEDS

| DIAGENETIC EVENT | SHALLOW | EXPOSURE | BURIAL |
|----------------------|---------|----------|--------|
| MARINE CMT | | | |
| MICRITIZATION | | --- | |
| SUBTIDAL DOL | | --- | |
| HYPERSALINE DOL | | | --- |
| HYPERSALINE ANHY | | | --- |
| FW VADOSE DISS | --- | --- | |
| FW MIN STAB | --- | --- | --- |
| FW CMT | --- | --- | --- |
| COMPACTION | | | |
| PRESSURE SOL | | | |
| BURIAL DOL & CALCITE | | | |
| BURIAL ANHY | | | |

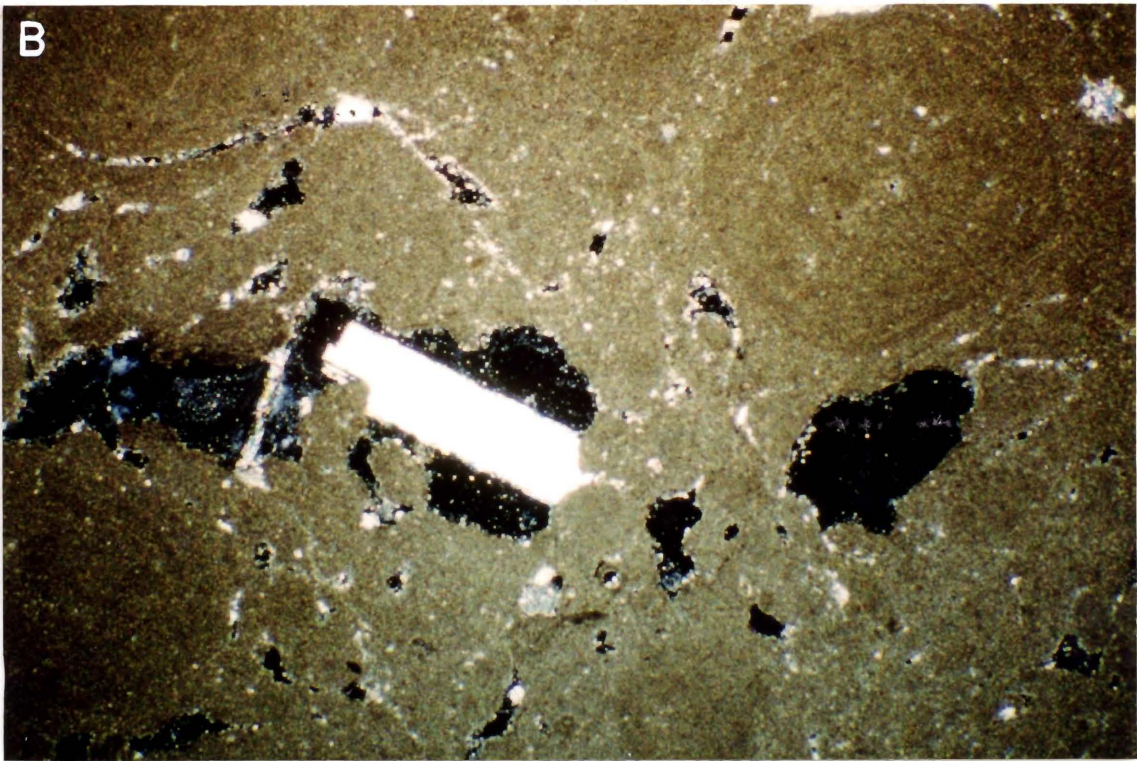
Figure 31.- Photomicrographs of marine phreatic cements.

(A) Isopachous rims of calcite around allochems in a pisolitic packstone. Black is interparticle porosity.

(NDIC-12357; 3,129 feet; crossed nicols; FOV 6.3 mm).

(B) Micrite rims around allochems in a pisolitic-peloidal packstone. Black is vugular porosity. Bright

white crystal is pore-bridging anhydrite cement (NDIC-2902; 3,136 feet; crossed nicols; FOV 6.3 mm).



Micritization

Micritization of carbonates results from infilling of the microborings of endolithic organisms, such as algae and fungi, by lime mud (Margolis and Rex, 1971; Rooney and Perkins, 1972). Endolithic algae can also add a micritic layer to the outside of a carbonate grain, thus reducing primary porosity (Kobluk and Risk, 1977).

Soon after deposition, at or near the sediment-water interface, some of the grains and marine cements in the Wayne beds were micritized (Figure 30). Many of the peloids in the Wayne beds are believed to have originally been ooid grains which have undergone micritization. Figure 31B is a photomicrograph showing micrite cement binding pisoliths and peloids.

Dolomitization

Dolomites can form in a wide variety of environments including the marine phreatic environment. Subtidal dolomite has been found in recent (Behrens and Land, 1972) as well as ancient (Qing and Mountjoy, 1989; Amthor and Friedman, 1992) shallow marine sediments. Also, dolomitization by normal seawater can occur at shallow depths below the seafloor (Saller, 1984).

UNIVERSITY OF MICHIGAN LIBRARY

Some Wayne dolomite may have been penecontemporaneous (Figure 30). Some of this primary dolomite could have been the result of direct precipitation in a lagoon depositional environment. The quantity of subtidal dolomite precipitated in the Wayne beds, if any, is unknown.

Hypersaline Phreatic Diagenesis

Dolomitization

In modern supratidal flats, primary dolomites have been found that precipitated directly from pore fluids (Shinn et al., 1965; Butler, 1969; Kinsman, 1969; McKenzie, 1981; Pierre et al., 1984). Modern dolomites may also form in evaporitic lagoons and hypersaline lakes (Clayton et al., 1968). Dolomitization of carbonates in similar depositional environments can also occur due to brine reflux or flow of dolomite-saturated brines through the subsurface (Adams and Rhodes, 1960; Kinsman, 1969; Supko, 1977; Patterson and Kinsman, 1982).

Figure 32A is a photomicrograph showing possible hypersaline phreatic matrix dolomite concentrated in a fracture. Hypersaline phreatic replacement dolomite, with remnant pisolith ghosts, is shown in Figure 32B. During Wayne beds time, contemporaneous with carbonate

Figure 32.- Photomicrographs of possible hypersaline.

phreatic dolomite. (A) Dolomite rhombs concentrated in a fracture in a peloidal wackestone. White is equant calcite cement (NDIC-12357; 3,119 feet; crossed nicols; FOV 6.3 mm). (B) Pisolith ghosts in a finely crystalline replacement dolomite. Black is interparticle (?) porosity (NDIC-12357; 3,123 feet; crossed nicols; FOV 6.3 mm).

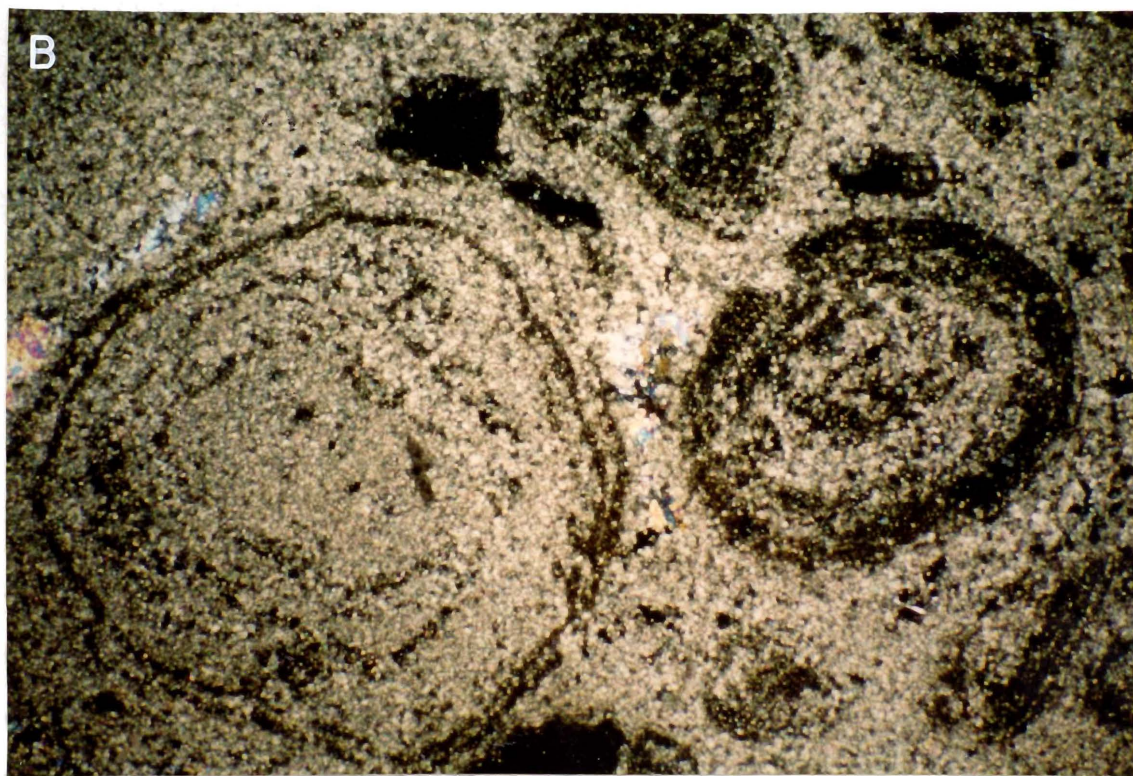
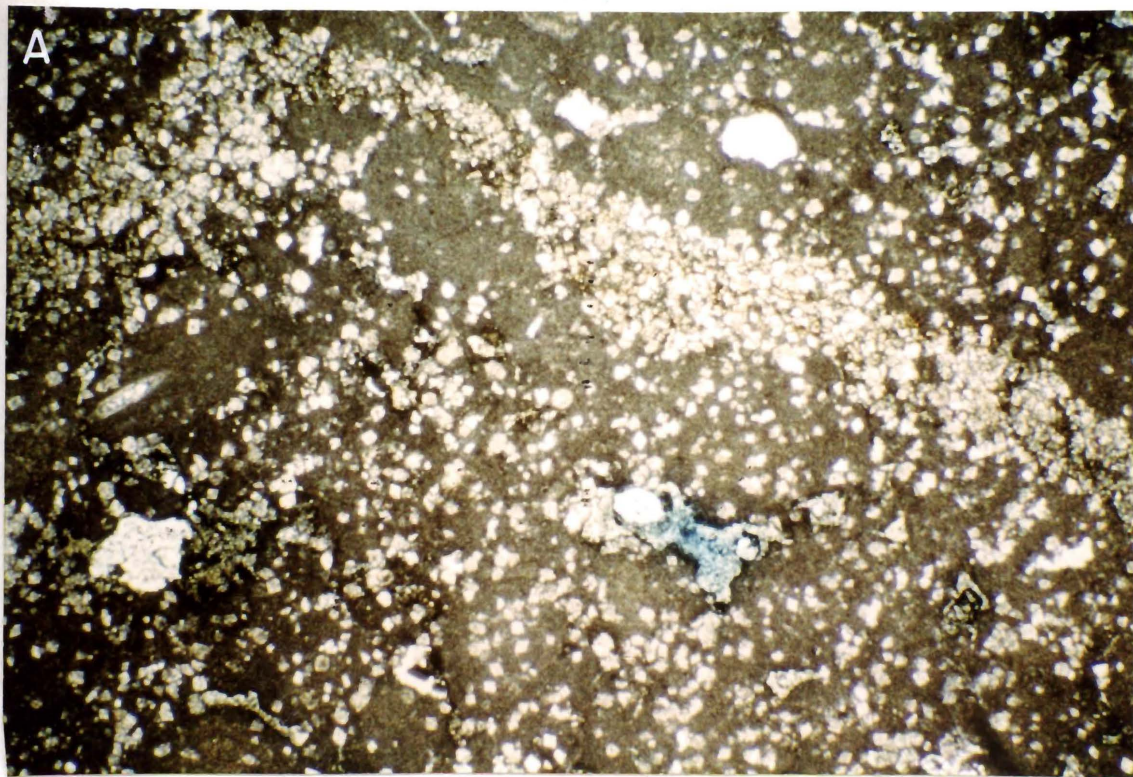


FIGURE 1. (A) The surface of the pollen grain.

sedimentation in the tidal flat depositional environment, dolomite could have formed in the supratidal-evaporitic lagoon and sabkha depositional environments (Figure 30). Waters saturated with dolomite below these environments could have been pumped or refluxed basinward through the subsurface resulting in dolomitization of the packstone-wackestone lithofacies of the tidal-flat depositional environment.

As the Triassic seas transgressed the study area over the pre-Mesozoic unconformity, the Wayne beds could have once again been subjected to dolomitization in the hypersaline environment (Figure 30). The amount of dolomitization due to re-submergence in the hypersaline phreatic environment, if any, has not been quantified.

Dissolution and Replacement by Anhydrite

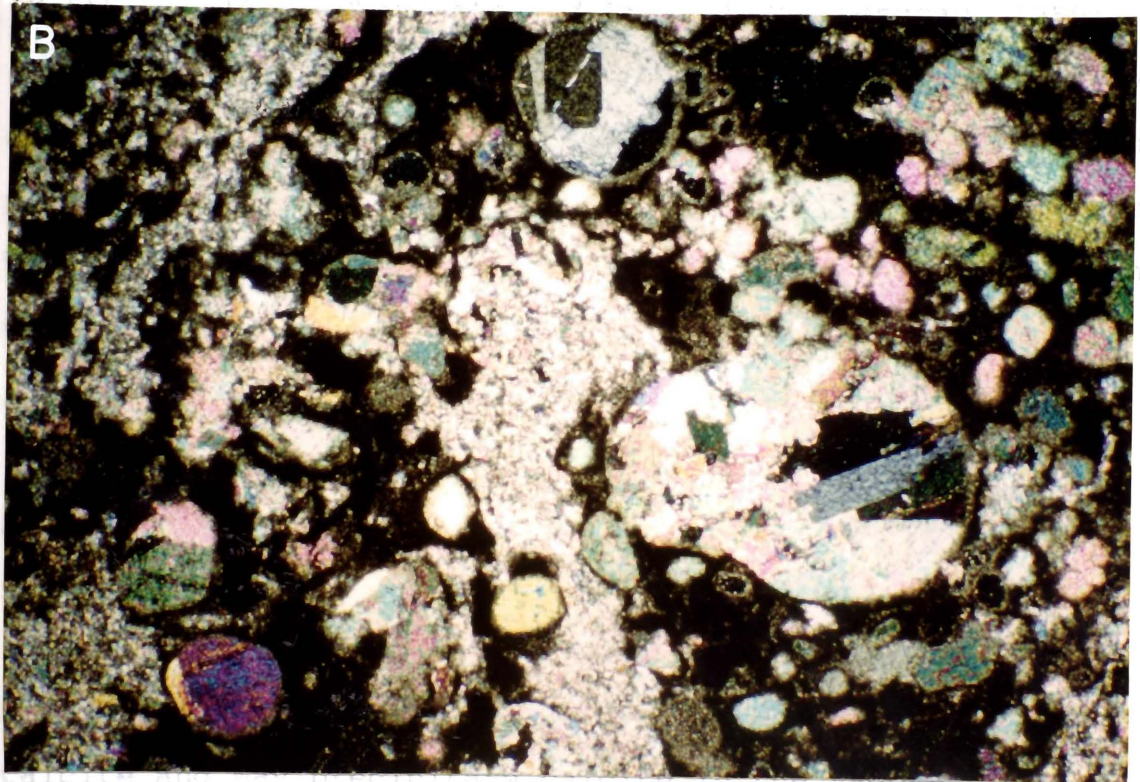
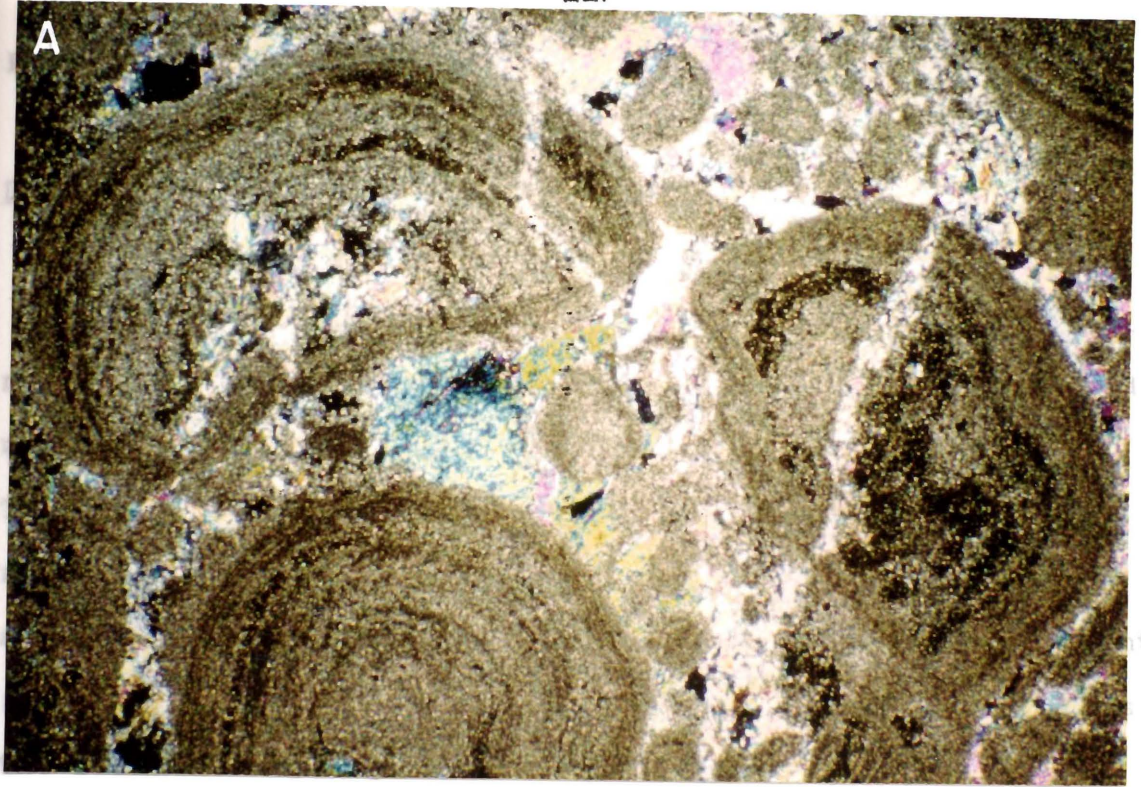
Anhydrite cements form by either direct precipitation in pore spaces or by a dissolution and replacement process (Sloss, 1969; Vai and Lucchi, 1977; Patterson and Kinsman, 1981). Formation waters which are undersaturated with respect to calcite and saturated with respect to calcium sulfate can result in the dissolution and replacement of calcite by anhydrite (Vai and Lucchi, 1977). These processes can occur in the subsurface as the result of

regional groundwater flow, evaporitic pumping, and/or brine reflux (Patterson and Kinsman, 1981; Bein and Land, 1982).

The carbonates in the Wayne beds are interpreted to contain small amounts of replacement anhydrite. In general, the yellow to brown anhydrites found in the Frobisher-Alida are due to replacement in a hypersaline environment, and the clear to white, pore-occluding anhydrites are a burial-diagenesis product (Murray, 1964). Contemporaneous with Wayne beds deposition, waters saturated with respect to gypsum and undersaturated with respect to calcite may have been pumped or refluxed basinward from the supratidal flats and evaporitic lagoon depositional environments through the subsurface resulting in carbonate replacement by anhydrite (Figure 30). Replacement of pisoliths and cement by hypersaline phreatic anhydrite may be partial (Figure 33A) or complete (Figure 33B).

A hypersaline diagenetic environment may have re-occurred in the study area after formation of the pre-Mesozoic unconformity due to the transgression of the Triassic seas (Figure 30). A second episode of Wayne beds hypersaline anhydritization may have resulted from the processes described above. Evidence for this is provided by sulfur isotope data discussed below.

Figure 33.- Photomicrographs of interpreted hypersaline phreatic anhydrite. (A) Anhydrite that partially replaced allochems and cement in a pisolitic packstone (NDIC-12357; 3,127 feet; crossed nicols; FOV 6.3 mm). (B) Anhydrite that completely replaced allochems and cement in a peloidal packstone (NDIC-3933; 3,057 feet; crossed nicols; FOV 6.3 mm).



Freshwater Vadose Diagenesis

Dissolution of Grains and Cement

Shallow marine cements and allochems have an original mineralogy consisting primarily of metastable aragonite and magnesium calcite together with a small amount of calcite. The movement of freshwater, which is undersaturated with respect to magnesium calcite and aragonite, through these sediments can result in the dissolution of grains and cement (Longman, 1980). The result of this dissolution process is the formation of vugular and solution-enlarged porosity (Matthews, 1967; Choquette and Pray, 1970; Longman, 1980).

Sometime after deposition of the Wayne beds, the study area was subjected to subaerial exposure as evidenced by the pre-Mesozoic unconformity (Figure 30). This event subjected the Wayne beds to a freshwater vadose diagenetic environment where dissolution resulted in the formation of vugular- (Figure 34A) and solution-enlarged secondary porosity.

Cementation

Freshwater trickling downward through carbonate sediment eventually becomes saturated with respect to calcite and may precipitate calcite in the vadose

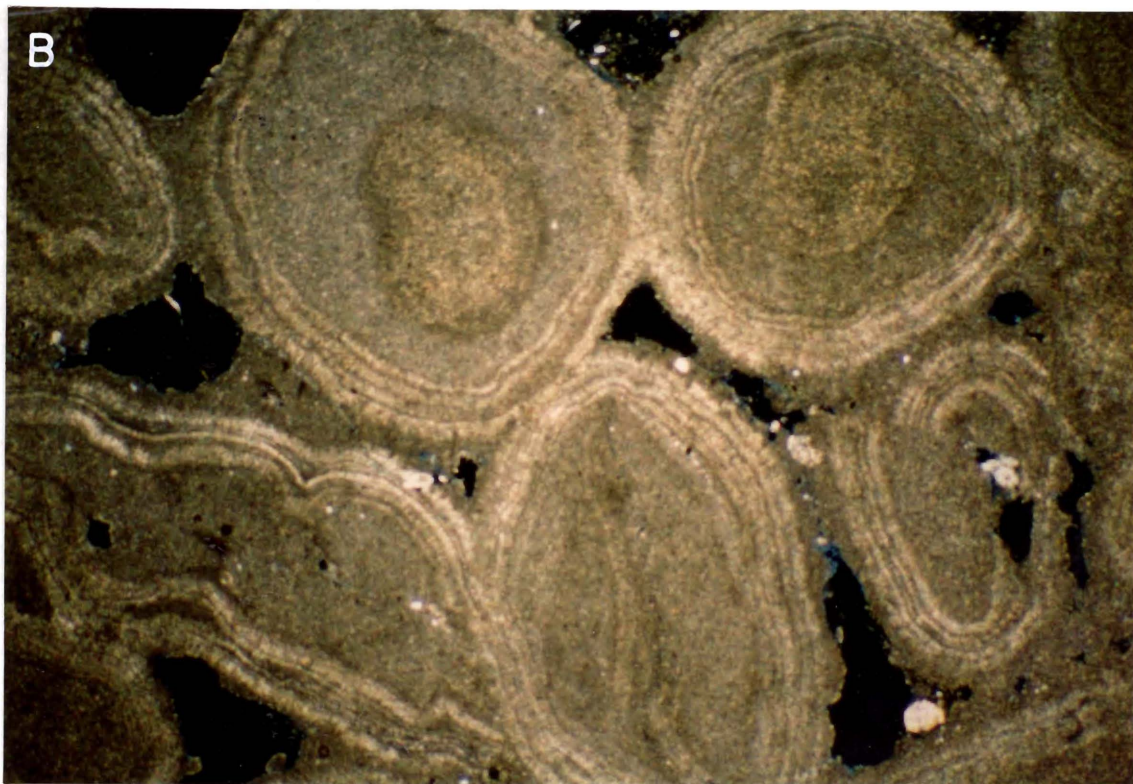
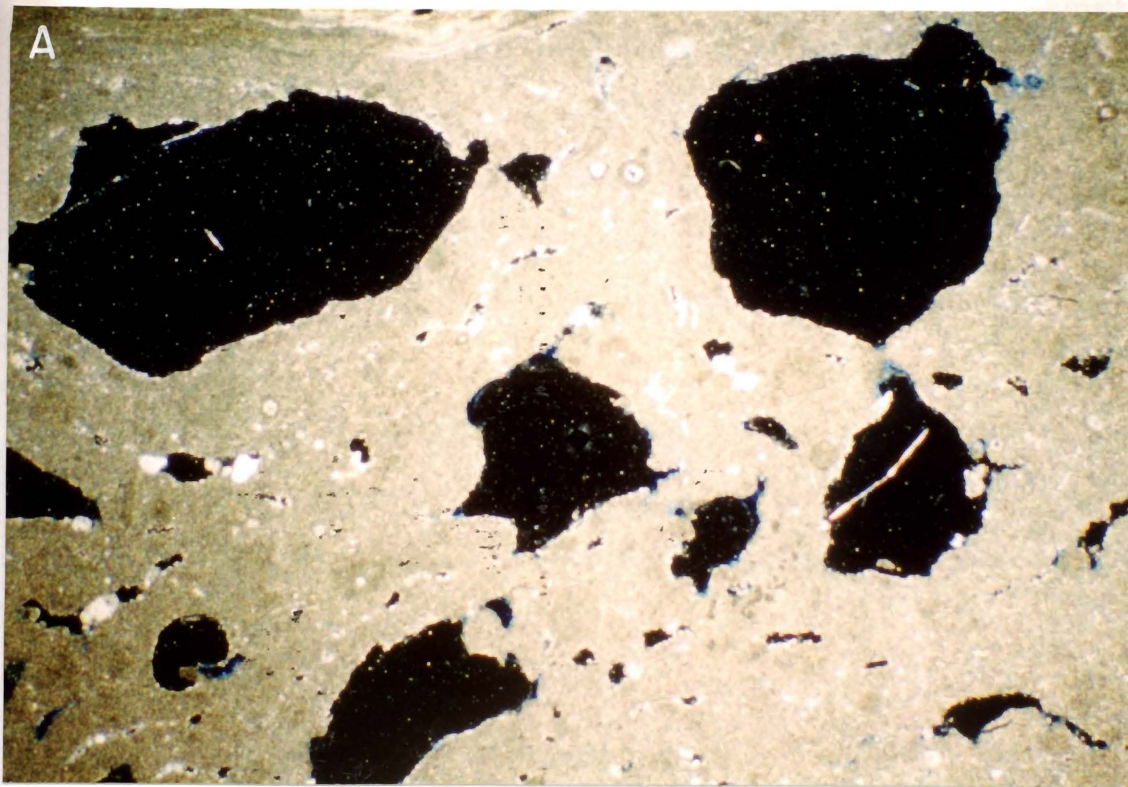
Figure 34.- Photomicrographs of freshwater vadose features.

(A) Vugular porosity (black) in a peloidal wackestone.

(NDIC-1159; 3,232 feet; crossed nicols; FOV 6.3 mm).

(B) Meniscus cements in a pisolitic packstone. Black is interparticle porosity (NDIC-2776; 3,251 feet;

crossed nicols; FOV 6.3 mm).



environment (Matthews, 1964; Longman, 1980). The resultant cements can sometimes be recognized by their pendant or meniscus forms. However, vadose cements may also be equant or micritic, forms not diagnostic of the vadose environment (Thorstenson et al., 1972; Halley and Harris, 1979; Longman, 1980).

Subaerial exposure of the Wayne beds in the study area resulted in the formation of vadose cements (Figure 30). Freshwater-vadose micritic, meniscus cements in a pisolitic packstone are shown in Figure 34B.

Freshwater Phreatic Diagenesis

Mineralogical Stabilization

One of the more important processes that occurs in the freshwater phreatic zone is the mineralogical stabilization of carbonate allochems and cements (Friedman, 1964; Matthews, 1968; Steinen and Matthews, 1973). This mineralogical stabilization involves the transformation of metastable aragonite and magnesium calcite to stable calcite (Land and Epstein, 1970). Stabilization of mineralogy early in the diagenetic history of a carbonate can result in preservation of reservoir-quality rock because porosity may not be totally occluded by burial processes such as

compaction and cementation (Wagner and Matthews, 1982). Carbonates not stabilized during early diagenesis will be stabilized in the burial environment. Burial stabilization can release calcium and magnesium carbonate into the pore fluids leading to precipitation of pore-occluding burial dolomite and calcite cements.

Thin areas on the Spearfish Formation isopach map (Figure 17) suggest that highs existed at the time of Spearfish deposition. These paleohighs could have become islands as the Triassic seas transgressed the study area. Freshwater lenses may have developed beneath these islands and resulted in the mineralogical stabilization of the Wayne limestones (Figure 30). The Wayne beds beneath these paleohighs exhibit much less burial dolomite and calcite cementation than beneath the paleolows (Appendix A). Thus, carbonates outside of the paleoislands may have experienced less freshwater diagenesis and more burial dolomite and calcite cementation.

Cementation

The freshwater phreatic diagenetic environment can be a zone of abundant calcite-cement precipitation (Friedman, 1964; and Land, 1970). Equant calcite cements are commonly interpreted as having precipitated in a freshwater phreatic

environment (Longman, 1980). In the short term, these cements tend to occlude both primary and secondary porosity. However, in the long term, they may make the rock less susceptible to porosity occlusion due to burial processes (Wagner and Matthews, 1982). Thus, some freshwater-phreatic diagenesis may be beneficial for porosity preservation as long as cementation is not too extensive.

The Wayne beds contain only rare examples of cements which can be conclusively identified as having a freshwater-phreatic origin. Figure 35 is a photomicrograph displaying a rim of bladed to equant freshwater phreatic cement on the inside of a gastropod shell. Other equant cements are common, but they could have precipitated in the freshwater-vadose, freshwater-phreatic, or burial environments.

Burial Diagenesis

Compaction

Sediment loading compacts carbonate grains and matrix (Coogan, 1970; Shinn and Robbin, 1983). Laboratory experiments have shown that significant compaction occurs at overburden pressures simulating 1,000 feet of overlying sediment (Shinn and Robbin, 1983). Compaction can obliterate primary porosity (Shinn and Robbin, 1983).

Figure 35.- Photomicrograph of freshwater phreatic cement.

A rim of bladed to equant cements on the inside of a gastropod shell in a skeletal wackestone. Black is intraparticle porosity (NDIC-2176; 3,123 feet; crossed nicols; FOV 6.3 mm).

After the pre-Montana was saturated approximately to 3,200 feet of thickness, the sandstone and shale were deposited over the Na, brines. The pre-Montana sequence for the sandstone is a partially saturated sandstone. Compaction problems have been reported for sandstone.



Pressure

commercial
 loading resulted not only in
 selection of
 the medium
 environment (Figure 108,)

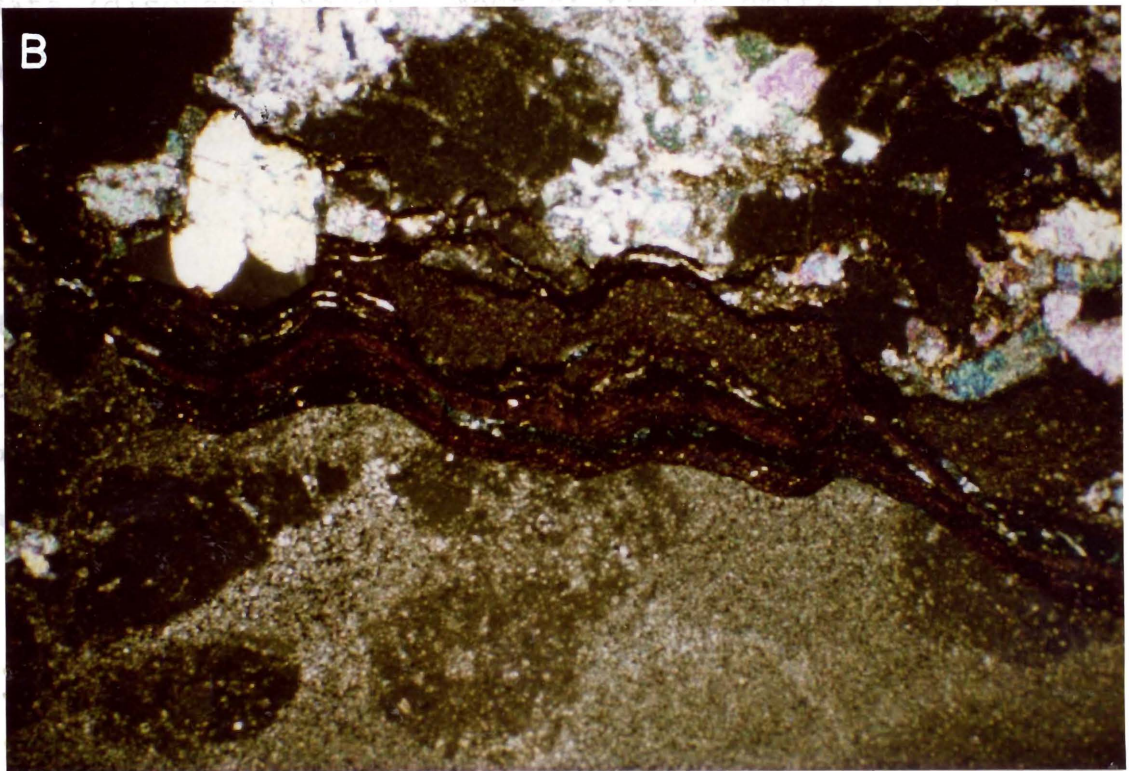
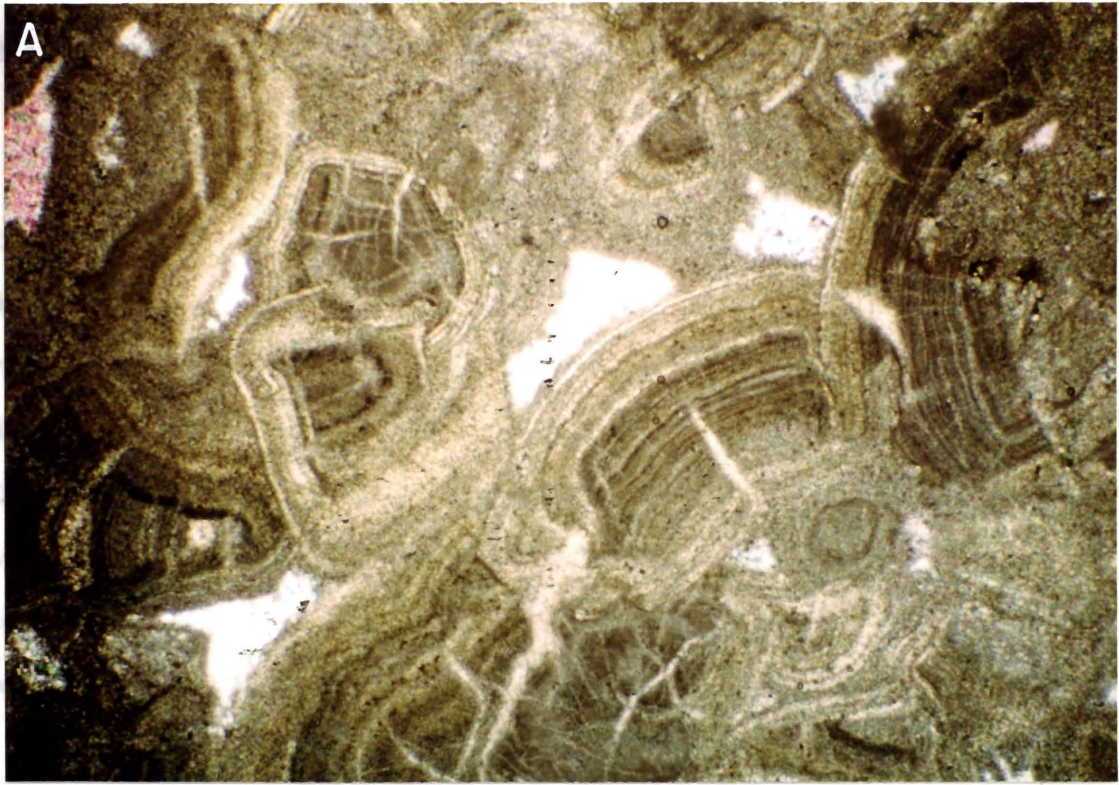
After the pre-Mesozoic unconformity approximately 3,100 to 3,200 feet of Triassic through Quaternary age sediments were deposited over the Wayne beds. The paragenetic sequence for the Wayne beds is presented in Figure 30. Compaction probably began soon after deposition and continued to the end of the Cretaceous. Those sediments that experienced the greatest amount of freshwater diagenesis probably underwent the least amount of compaction.

Pressure Solution

The onset of stylolitization is believed to be initiated by overburden-loading and pressure-solution processes (Shinn and Robbin, 1983). Sediment loading can also cause the melding of grains due to pressure solution at grain-to-grain contacts.

Pressure solution processes in the Wayne beds probably commenced soon after burial began (Figure 30). Sediment loading resulted not only in compaction but also in pressure solution of grains (Figure 36A). Stylolites are common in the mudstone lithofacies of the open-marine depositional environment (Figure 36B).

Figure 36.- (A) Photomicrograph showing pressure solution between allochems in a pisolitic packstone. White is anhydrite cement (NDIC-12358; 3,123 feet; crossed nicols; FOV 6.3 mm). (B) Photomicrograph showing stylolite formed in a peloidal mudstone. White is anhydrite cement (NDIC-2176; 3,158 feet; crossed nicols; FOV 6.3 mm).

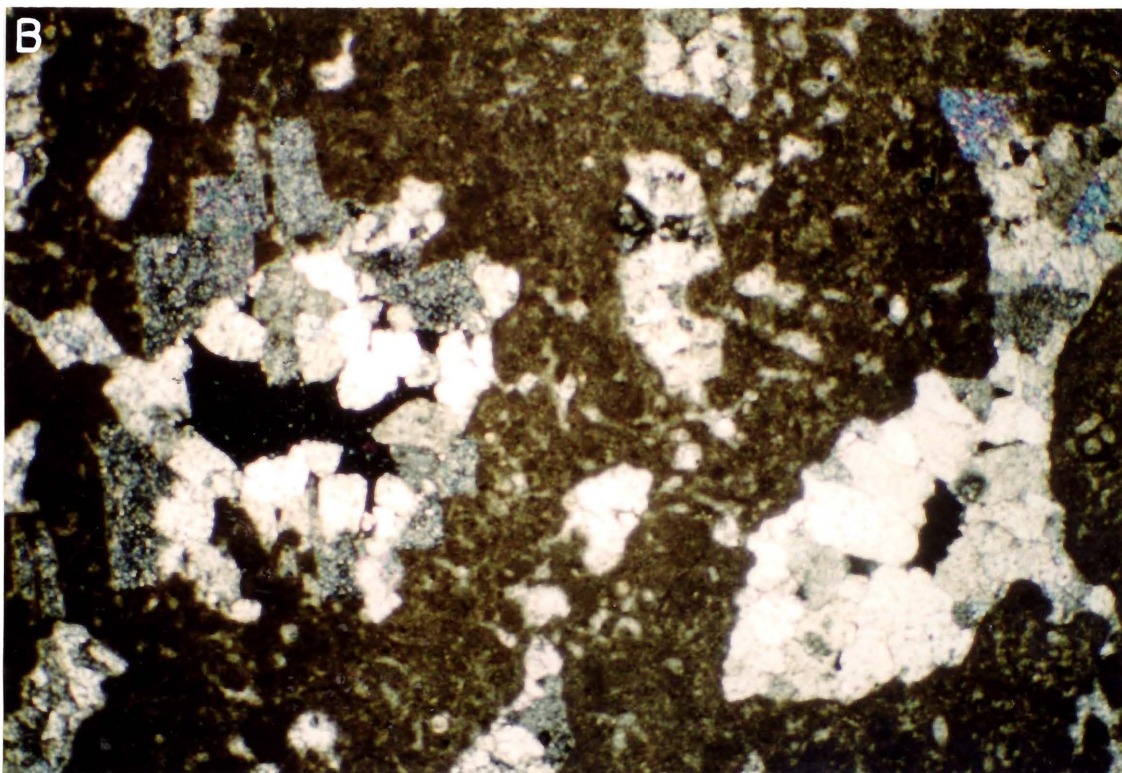
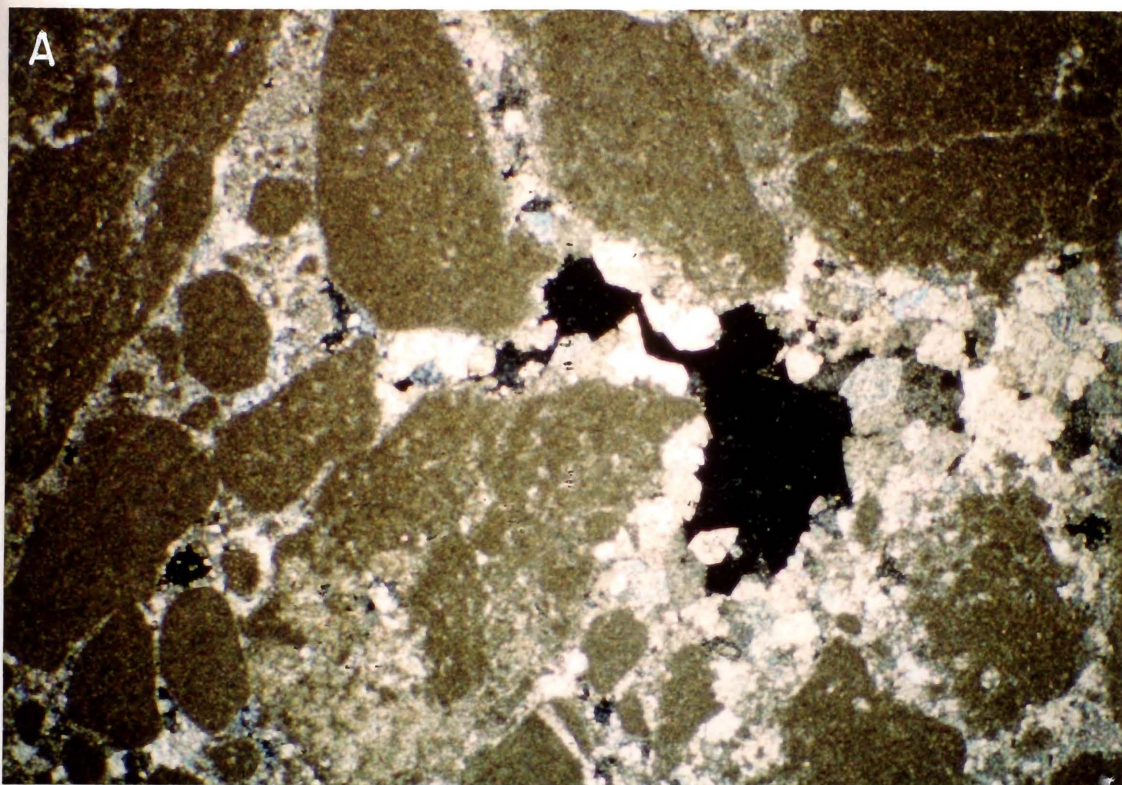


Dolomite and Calcite Cementation

As temperature and pressure increase with burial, the introduction of internal and external sources of calcium and magnesium carbonate results in pore fluids saturated with respect to dolomite and calcite and in the precipitation of dolomite and calcite cement (Qing and Mountjoy, 1989; Kaufman et al., 1990). Magnesium calcite which has not been stabilized to calcite during early diagenesis can be a source of calcium and magnesium carbonate for this type of burial dolomite and calcite cementation.

Based on petrographic observations and oxygen isotope data (discussed below), most of the dolomite in the study area probably formed due to burial processes (Figure 30). The burial dolomite post-dates isopachous, micrite, and equant cements and vugular porosity development. Figure 37 is a pair of photomicrographs showing pore-occluding burial dolomite and calcite cement in peloidal packstones. This type of dolomite and calcite cement, which lines pores and occludes porosity, is abundant in the Wayne beds in areas not associated with paleohighs.

Figure 37.- Photomicrographs of burial dolomite and calcite cements. (A) Burial dolomite and calcite cement in a peloidal packstone. Black is interparticle porosity (NDIC-12358; 3,153 feet; crossed nicols; FOV 6.3 mm). (B) Burial dolomite and calcite cement in a peloidal packstone. Black is interparticle (?) porosity (NDIC-3238; 3,061 feet; crossed nicols; FOV 6.3 mm).

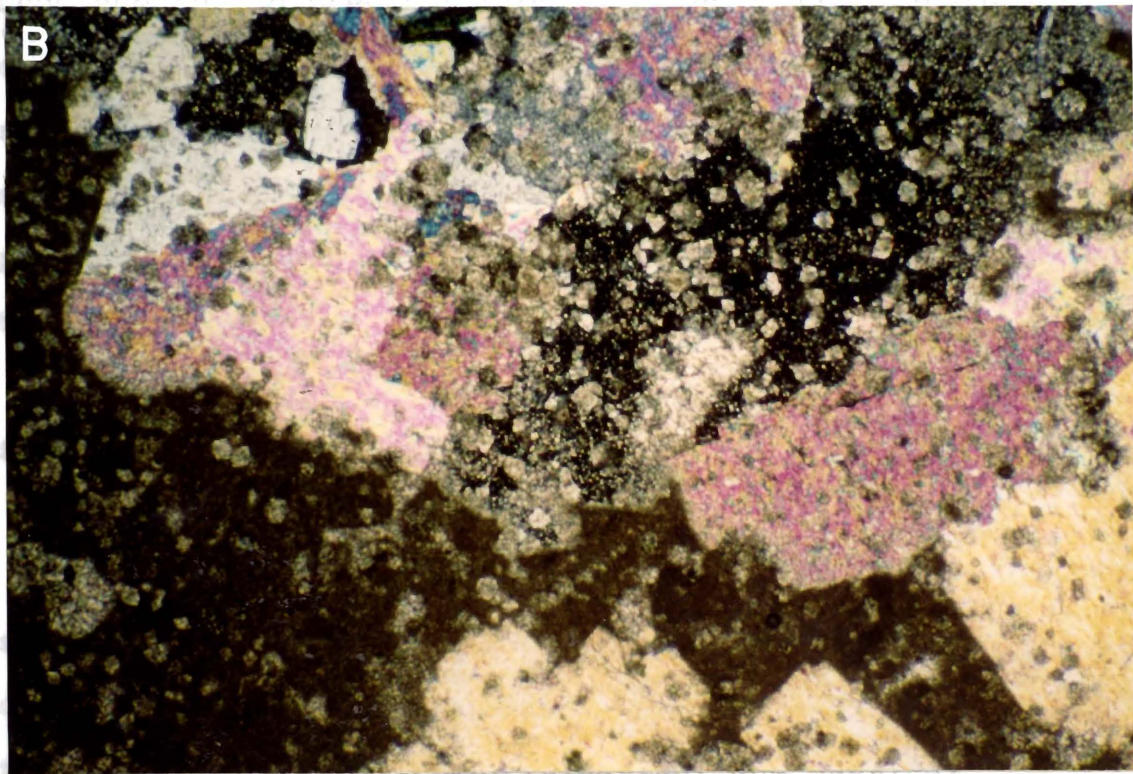
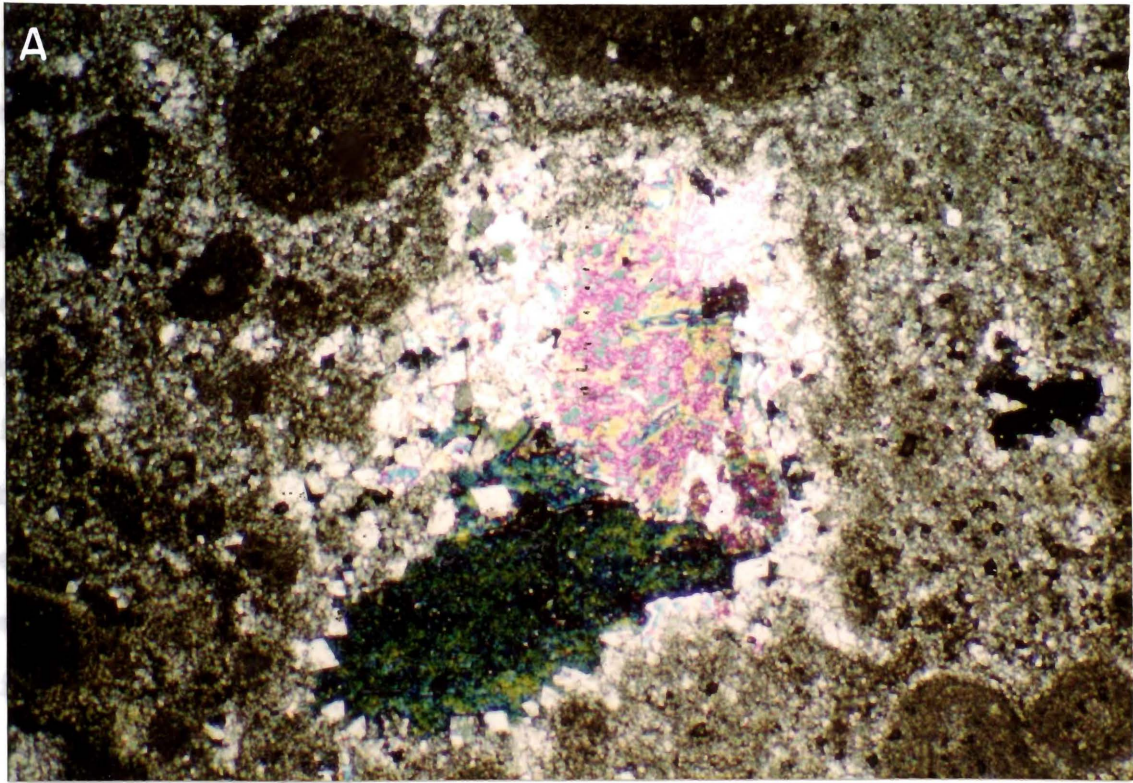


Anhydritization

The evaporites of the Glenburn beds were probably deposited originally as gypsum. Depending on the salinity of the formation water and the geothermal gradient, gypsum begins to transform into anhydrite at depths of about 1,800 feet below the surface due to elevated temperatures (Holser, 1979). Dewatering of gypsum to anhydrite results in the release of water, which is saturated with respect to calcium sulfate, into the pore fluids (Warren, 1989). The amount of water released is approximately 38% of the volume of the original gypsum (Warren, 1989). Anhydrite may then precipitate from this expelled water. Anhydrite cements can form both displacively and replacively in carbonates (Machel and Burton, 1991).

In the Wayne beds, anhydrite cements generally overlie burial dolomite and calcite cements (Figure 38A). In addition, these anhydrite cements sometimes have floating rhombs of dolomite as inclusions (Figure 38B). This petrographic evidence indicates that most of the anhydrite cements post-date the marine, freshwater, and burial-dolomite and calcite cements. This evidence also suggests that the anhydrite cements are a product of burial diagenesis (Figure 30).

Figure 38.- (A) Photomicrograph of burial anhydrite that overlies burial dolomite and calcite in a peloidal packstone. The dolomite and calcite cements line the vug while the anhydrite occludes the pore space. Timing of the cements is based on the principle of superposition (NDIC-3577; 3,103 feet; crossed nicols; FOV 6.3 mm). (B) Photomicrograph of floating euhedral dolomite rhombs in burial anhydrite in a peloidal wackestone. Burial dolomite pre-dates anhydrite based on the principle of inclusions (NDIC-2176; 3,119 feet; crossed nicols; FOV 6.3 mm).



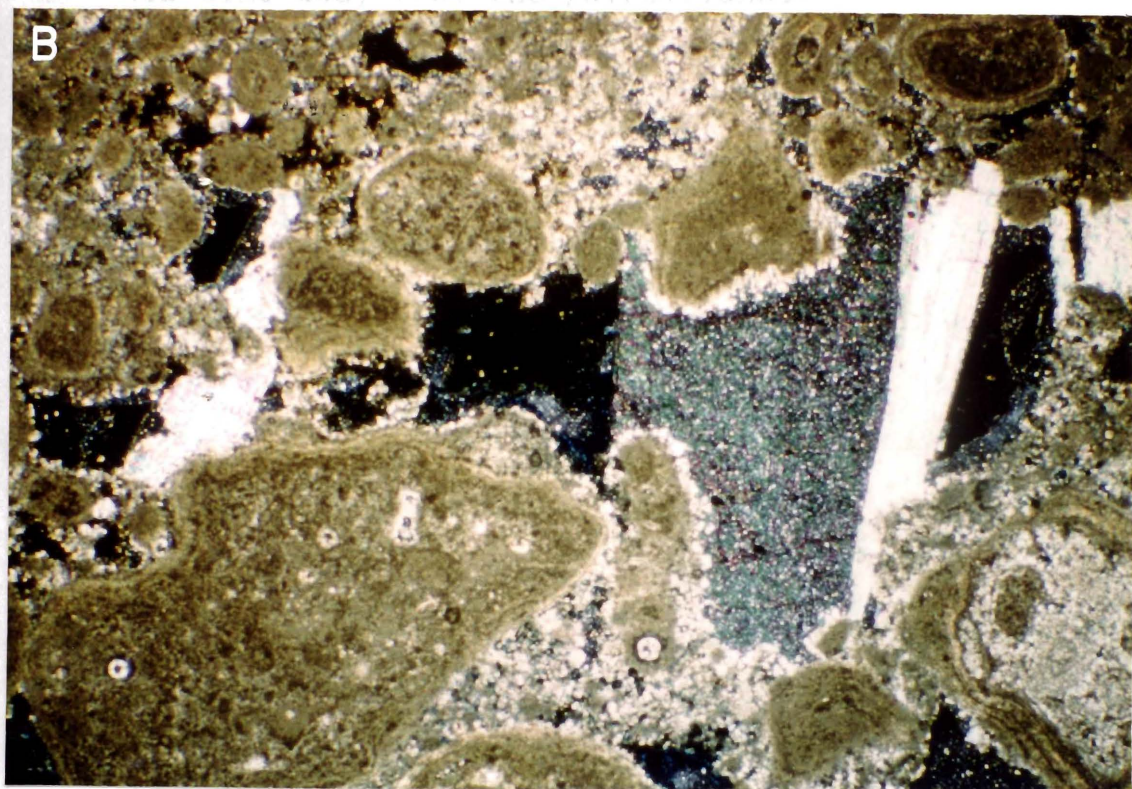
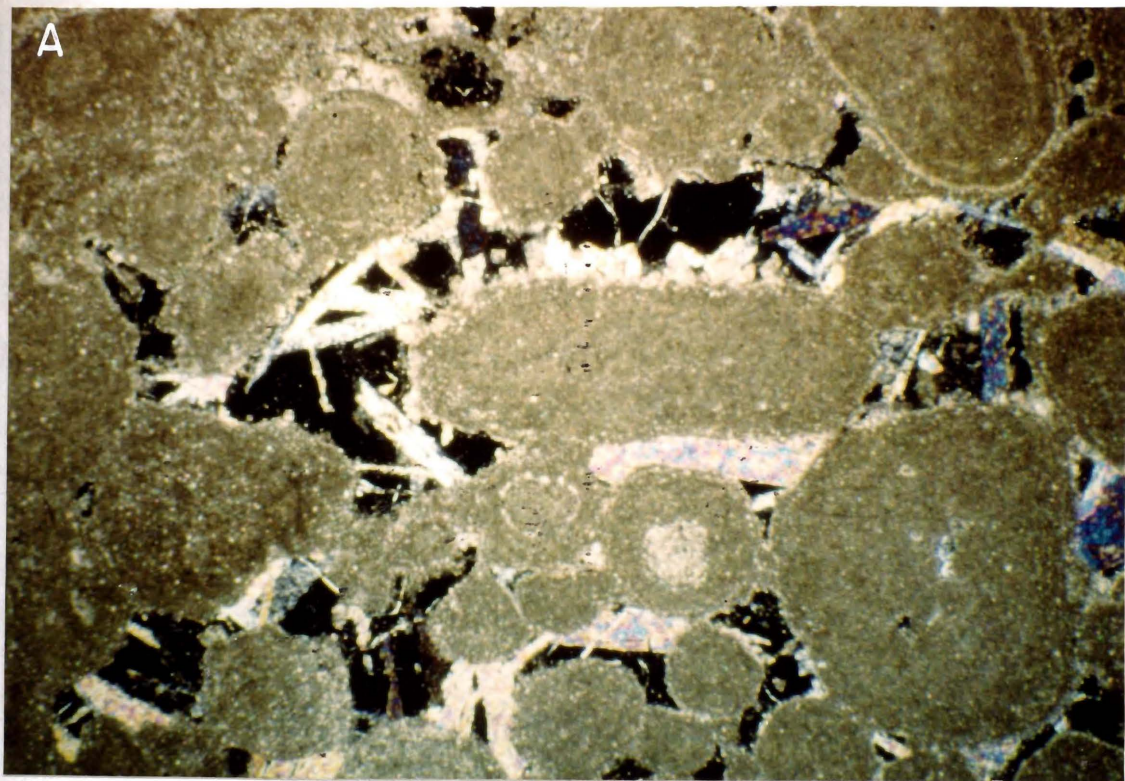
The sulfate in the anhydrite cements in the Wayne beds may have originated from the bedded anhydrites in the overlying Glenburn beds. Sulfur isotope data (discussed below) suggest that these anhydrite cements are in isotopic equilibrium with the anhydrites of the overlying Glenburn beds. Elevated temperatures and pressures at depth resulted in the gypsum-to-anhydrite transformation of the Glenburn beds. In a relatively static burial environment, the expelled water, saturated with respect to calcium sulfate, may not have traveled very far before anhydrite precipitated in the pore spaces of the underlying Wayne beds.

Permeability (discussed below) was reduced in the Wayne beds due to the precipitation of pore-bridging anhydrite cements (Figure 39). Before burial, the Glenburn beds were removed due to erosional processes over paleohighs in the study area. Because of this, the Wayne beds beneath paleohighs exhibit less burial anhydrite cement and, thus, have higher permeabilities.

Summary of Diagenetic History

The paragenetic sequence for the Wayne beds in the study area is shown in Figure 30. Contemporaneous with deposition or soon thereafter, the Wayne beds were subjected to marine cementation, micritization, and subtidal

Figure 39: Photomicrographs of pore-bridging anhydrite cements. (A) Whisker anhydrite cements in a pisolitic packstone. Black is interparticle porosity (NDIC-2176; 3,137 feet; crossed nicols; FOV 6.3 mm). (B) Anhydrite cements in a pisolitic packstone. Black is interparticle porosity (NDIC-3933; 3,064 feet; crossed nicols; FOV 6.3 mm).



dolomitization in the marine diagenetic environment. At the same time, some of the sediments may have been slightly dolomitized and anhydritized by hypersaline phreatic diagenesis.

After Mississippian deposition, the Wayne beds were subaerially exposed during the formation of the pre-Mesozoic unconformity. This was a time of freshwater vadose dissolution. As the Triassic seas transgressed the study area, mineralogical stabilization and cementation in the freshwater phreatic diagenetic environment continued beneath paleoislands. A small amount of hypersaline phreatic dolomitization and anhydritization may have also taken place at this time away from the paleoislands.

From the Triassic through the Quaternary, the Wayne beds were buried beneath 3,100 to 3,200 feet of overburden. This loading resulted in compaction and pressure solution, which obliterated some of the porosity in the limestones, especially in those that were not at least partially cemented and mineralogically stabilized as a result of freshwater diagenesis. Burial-dolomite and calcite cementation followed, which also occluded porosity. As the gypsum of the Glenburn beds was buried, it transformed to anhydrite and expelled calcium-sulfate-saturated waters into the underlying Wayne beds. The anhydrite precipitated as pore-bridging and pore-occluding cements.

STABLE-ISOTOPE DATA

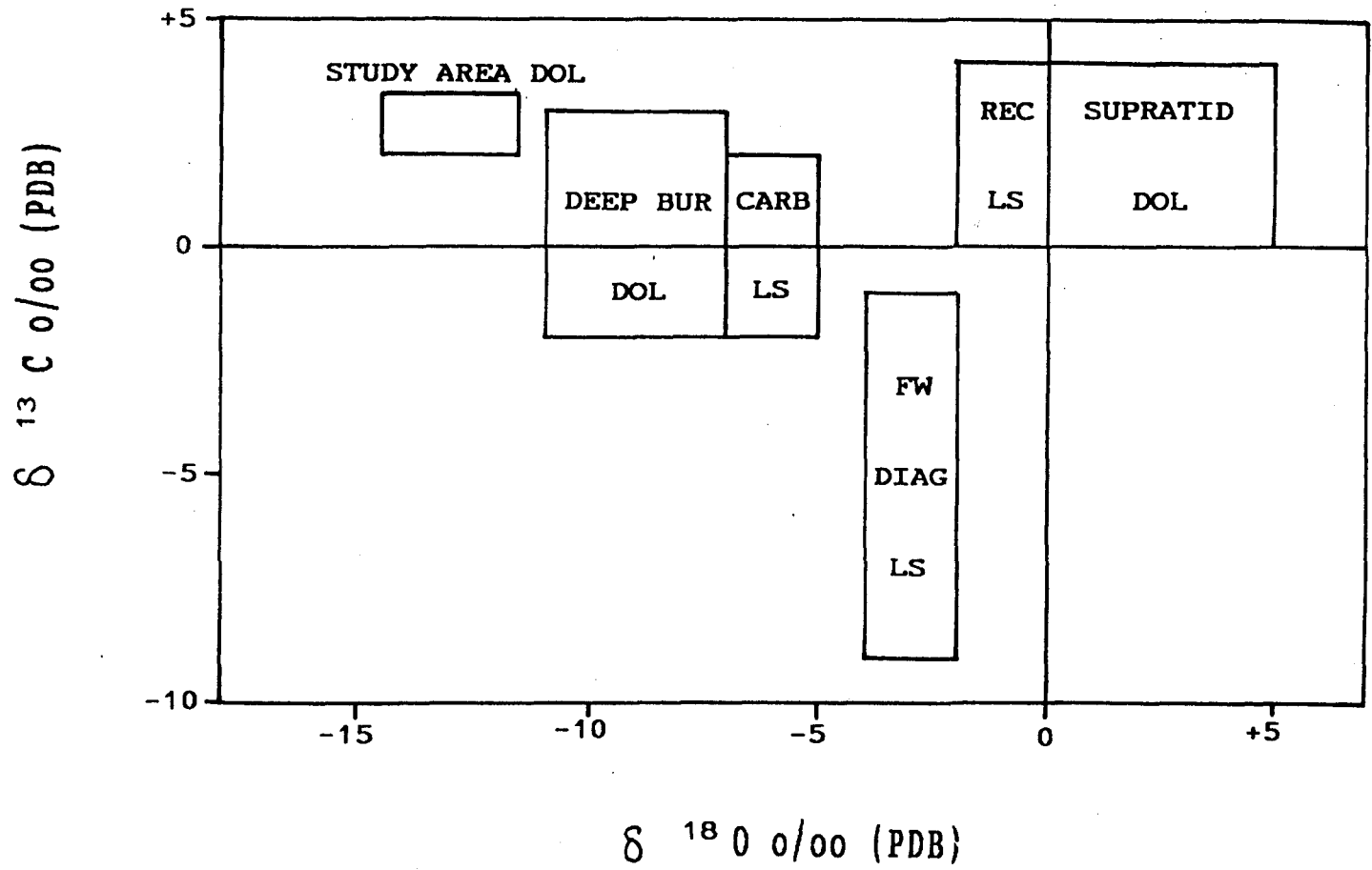
Carbon- and Oxygen-Isotope Geochemistry

In recent carbonate sediments, $\delta^{13}\text{C}$ varies from approximately 0 to +4‰ PDB and $\delta^{18}\text{O}$ varies from approximately -2 to 0‰ (Gross, 1964). In Mississippian and Pennsylvanian (Carboniferous) marine carbonates, $\delta^{13}\text{C}$ varies from about -2 to +2‰ and $\delta^{18}\text{O}$ from about -7 to -5‰ (Keith and Weber, 1964). Much of this variation in the Carboniferous data is probably due to diagenesis (Veizer and Hoefs, 1976). The ranges of carbon and oxygen in the recent and the Carboniferous are shown in Figure 40.

The diagenetic environments which have affected a carbonate sediment can sometimes be determined by analysis of carbon and oxygen stable isotopes. Carbonates which have undergone diagenesis in freshwater vadose and freshwater phreatic diagenetic environments may be recognized by their ^{12}C enrichment (Gross and Tracey, 1966; Allan and Matthews, 1982; Given and Lohmann, 1986). This ^{12}C enrichment results from the presence of organically derived carbon dioxide in

Figure 40.- $\delta^{13}\text{C}$ versus $\delta^{18}\text{O}$. Recent limestone (REC LS) values from Gross (1964). Carboniferous (CARB) from Keith and Weber (1964). Isotope ratios in limestones altered by freshwater diagenesis (FW DIAG LS) from Allan and Matthews (1977). Ancient supratidal dolomites (SUPRATID DOL) isotopic compositions from Supko (1977). Deep burial dolomites (DEEP BUR DOL) values from Kaufman et al. (1990). Study area dolomites (STUDY AREA DOL) measured from whole rock core and drill cutting samples (discussed above).

$\delta^{13}C$ VS $\delta^{18}O$



the diagenetic fluid of the freshwater environment (Gross, 1964; Budd and Land, 1990).

This relationship between light carbon and freshwater diagenesis has been used to define both modern and ancient subaerial exposure surfaces (Allan and Matthews, 1977; Allan and Matthews, 1982; Rush and Chafetz, 1990). $\delta^{13}\text{C}$ and $\delta^{18}\text{O}$ resulting from freshwater diagenesis are shown in Figure 40 (Allan and Matthews, 1977). These values range from approximately -9 to -1‰ for $\delta^{13}\text{C}$ and -4 to -2‰ for $\delta^{18}\text{O}$.

$\delta^{18}\text{O}$ of dolomites can be either heavy or light depending on the environment in which the dolomite precipitated. Dolomites precipitated under evaporitic conditions, such as supratidal or brine reflux dolomite, tend to be enriched in ^{18}O due to evaporation (Degens and Epstein, 1964; Gross and Tracy, 1966; Clayton et al., 1968; Rothe et al., 1974; Supko, 1977; McKenzie, 1981; Pierre et al., 1984). $\delta^{13}\text{C}$ and $\delta^{18}\text{O}$ for ancient supratidal dolomites, ranging from about 0 to +4‰ for $\delta^{13}\text{C}$ and 0 to +4‰ for $\delta^{18}\text{O}$, are shown in Figure 40 (Supko, 1977).

Dolomite which has formed in the deep burial diagenetic environment is usually enriched in ^{16}O due to the temperature dependence of the carbonate-water fractionation factor (Gregg and Sibley, 1984; Taylor and Sibley, 1986; Lee and Friedman, 1987; Qing and Mountjoy, 1989; Gao, 1990;

Gregg and Shelton, 1990; Kaufman et al., 1990). $\delta^{13}\text{C}$ and $\delta^{18}\text{O}$ of burial dolomites, ranging from approximately -2 to +3‰ in $\delta^{13}\text{C}$ and from -11 to -7‰ in $\delta^{18}\text{O}$, are shown in Figure 40 (Kaufman et al., 1990).

$\delta^{13}\text{C}$ and $\delta^{18}\text{O}$ of whole-rock core and drill cutting samples (mixed calcite and dolomite mineralogies) of the Wayne beds are listed in Table 11. These samples can be identified by their North Dakota Industrial Commission (NDIC) well file number and by their depth below kelly bushing (KB). The location of the wells sampled for isotopic analysis are shown in Figure 41.

Sulfur-Isotope Geochemistry

The sulfur-isotope age curve (modified after Holser and Kaplan, 1966, and Claypool et al., 1980) presented in Figure 42 indicates that $\delta^{34}\text{S}$ of sulfates precipitated from seawater have varied throughout geologic time. $\delta^{34}\text{S}$ ranges from a low of approximately +10‰ CDT in the Late Permian to Early Triassic to a high of approximately +35‰ in the Early Cambrian. The sulfur age curve can be used as a stratigraphic-correlation and age-determination

TABLE 11: CARBON AND OXYGEN ISOTOPIC COMPOSITION ⁽¹⁾

| <u>NDIC No.</u> | <u>DEPTH (ft)</u> | <u>$\delta^{13}\text{C}$</u> <u>(‰ PDB)</u> | <u>$\delta^{18}\text{O}$</u> <u>(‰ PDB)</u> |
|---------------------------------|-------------------|---|---|
| CORE SAMPLES: | | | |
| 12357 | 3113 | +2.31 | -5.13 |
| 12357 | 3115 | +2.72 | -7.00 |
| 12357 | 3117 | +2.72 | -3.99 |
| 12357 | 3119 | +2.63 | -2.83 |
| 12357 | 3121 | +2.60 | -5.39 |
| 12357 | 3126 | +2.95 | -3.47 |
| 12357 | 3131 | +3.11 | -1.59 |
| 12357 | 3136 | +3.05 | -0.68 |
| 12357 | 3146 | +3.09 | -1.47 |
| 12357 | 3156 | +3.12 | -2.50 |
| BOREHOLE DRILL CUTTING SAMPLES: | | | |
| 843 | 3210 | +2.97 | -2.18 |
| 1476 | 3168 | +2.98 | -2.51 |
| 12280 | 3140 | +3.11 | -2.02 |
| 12409 | 3130 | +3.07 | -1.76 |

⁽¹⁾- All data from in and around the Cimbel field

Figure 41.- Stable-isotope sample-location map. Shown are the locations and well file numbers for each well from which core or drill cuttings were sampled for carbon, oxygen, and/or sulfur isotope analysis.

STABLE ISOTOPE SAMPLE LOCATION MAP

LEONARD-ROTH AREA
BOTTINEAU CO., N.D.
DRAWN BY: M.J. WETMORE, 1991



0 1000 2000 3000 4000
FEET

EXPLANATION:

- PRODUCER
- ◆ PRODUCER NOW ABANDONED
- ◇ DRY HOLE
- ◊ WATER INJECTION

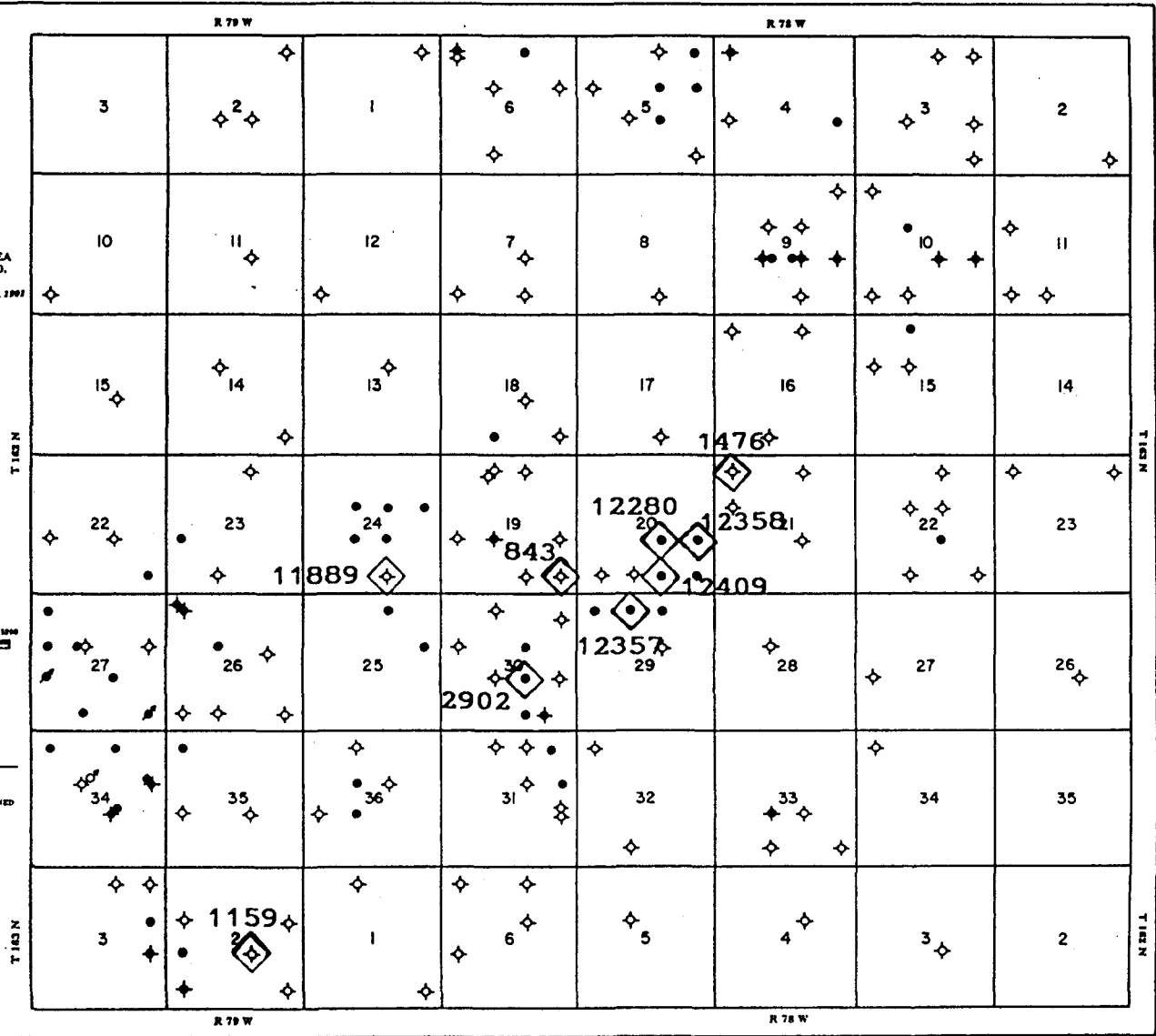
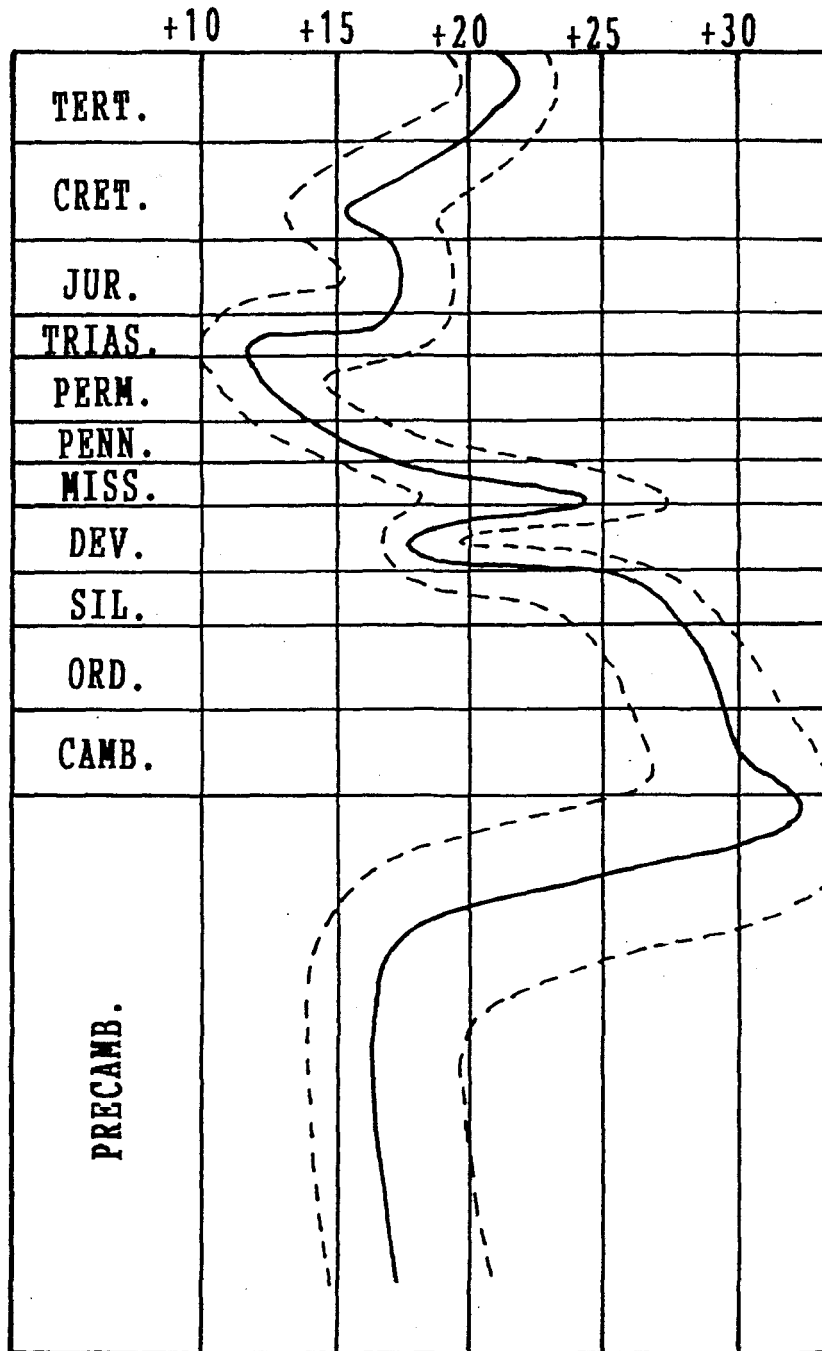


Figure 42.- Sulfur isotope age curve (modified after Holser and Kaplan, 1966, and Claypool et al., 1980). Dashed lines represent the estimated maximum and minimum $\delta^{34}\text{S}$ (Claypool et al., 1980).

$\delta^{34}\text{S} \text{ ‰}$ 

SULFUR ISOTOPE AGE CURVE

tool (Butler et al., 1973; Pierre and Rouchy, 1986; Kaufman et al., 1990).

The processes which control fluctuations of sulfur-isotope ratios in marine-associated sulfate deposits are not well understood (Faure, 1986, p. 531-534). The most important control of isotopic fractionation of sulfur is bacterial reduction of sulfate to sulfide (Ault and Kulp, 1959; Veizer et al., 1980). Sulfide mineralization in shales due to bacterial activity tends to result in depletion of seawater in ^{32}S , while the inflow of sulfate from the weathering of shales tends to enrich seawater in ^{32}S (Holser and Kaplan, 1966). Thus, the variability of sulfur isotope ratios throughout geologic time is primarily a function of movement of sulfur to and from sedimentary environments (Holser and Kaplan, 1966; Rees, 1970; Holland, 1973; Schidlowski et al., 1977; Claypool et al., 1980).

Bedded anhydrites from the Glenburn beds and replacement and pore-occluding anhydrites from the Wayne beds were sampled from core for sulfur-isotope analysis. These samples are identified by their NDIC well-file number and by their depth below KB. The locations of the wells sampled is shown in Figure 41, and the sulfur data is presented in Table 12.

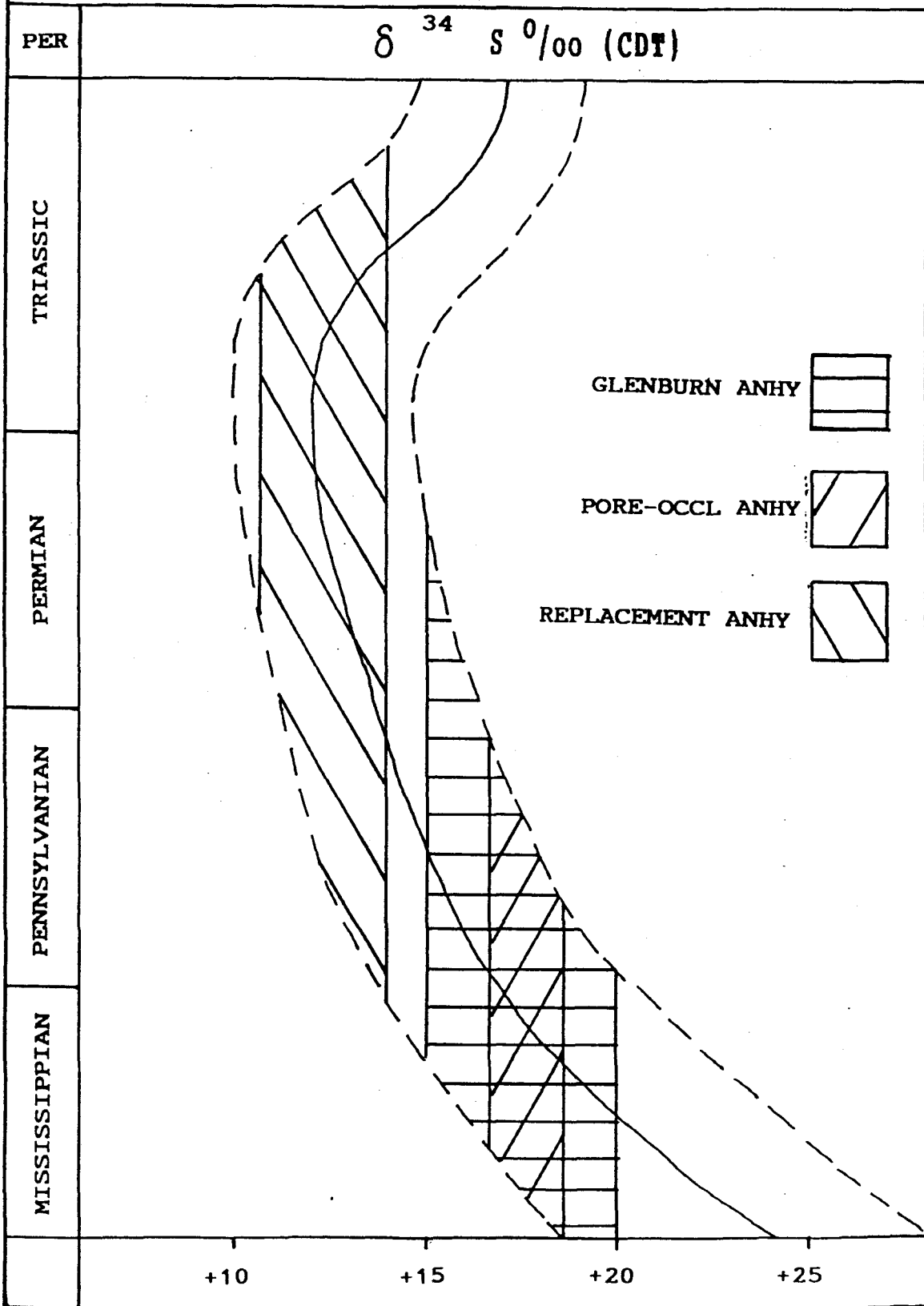
A plot of the sulfur data in an expanded version of the sulfur isotope age curve is shown in Figure 43. As

TABLE 12: SULFUR ISOTOPIC COMPOSITION

| <u>NDIC No.-DEPTH (ft)</u> | <u>ANHYDRITE TYPE</u> | $\delta^{34}\text{S}$ <u>(‰ CDT)</u> |
|----------------------------|-----------------------|---|
| 1159-3172 | Bedded | +20.0 |
| 1159-3177 | Bedded | +18.9 |
| 1159-3182 | Bedded | +15.3 |
| 1159-3187 | Bedded | +19.1 |
| 1159-3192 | Bedded | +19.2 |
| 1159-3197 | Bedded | +20.0 |
| 11889-3155 | Bedded | +19.9 |
| 1159-3212 | Replacement | +14.1 |
| 11889-3184 | Replacement | +10.5 |
| 1159-3225 | Pore Occluding | +16.5 |
| 2902-3125 | Pore Occluding | +18.5 |
| 2902-3133 | Pore Occluding | +17.4 |
| 2902-3142 | Pore Occluding | +17.8 |
| 11889-3192 | Pore Occluding | +18.4 |
| 11889-3205 | Pore Occluding | +16.8 |
| 12357-3115 | Pore Occluding | +18.3 |
| 12358-3121 | Pore Occluding | +18.3 |
| 12358-3147 | Pore Occluding | +17.9 |

Figure 43.- Expanded sulfur isotope age curve (modified after Holser and Kaplan, 1966, and Claypool et al., 1980). Dashed curves depict the approximate upper and lower ranges for sulfur isotopes from Mississippian through Triassic evaporites. As expected, bedded anhydrites from the Glenburn match Mississippian sulfur values. Pore-occluding anhydrites also match Mississippian sulfur isotopes within the error given (Holser and Kaplan, 1966; and Claypool et al., 1980). Replacement anhydrites match Permian or Triassic $\delta^{34}\text{S}$.

EXPANDED SULFUR ISOTOPE AGE CURVE



expected, the bedded Glenburn anhydrites match Mississippian-seawater sulfur values. The pore-occluding anhydrites are also consistent with a Mississippian-seawater origin and therefore the sulfur may have been derived from the gypsum-dehydration waters expelled from the Glenburn. The replacement anhydrites have $\delta^{34}\text{S}$ consistent with sulfur derived from Permian or Triassic seawater.

POROSITY AND PERMEABILITY

Porosity Formation and Preservation

After deposition of the Wayne beds, the study area was subaerially exposed during the formation of the pre-Mesozoic unconformity. During this time, the Wayne beds were diagenetically altered in the freshwater vadose environment. The creation of vugular and solution-enlarged porosity in the Wayne carbonates is a result of exposure to the freshwater vadose diagenetic zone.

In addition to petrographic observations, carbon isotope data also suggest that the Wayne beds were subjected to freshwater vadose diagenesis. Due to the presence of ^{12}C enriched carbon dioxide in the pore fluid at the time of diagenesis, the freshwater diagenetic environment commonly has a characteristically light carbon signature (Gross, 1964; Gross and Tracey, 1966; Allan and Matthews, 1982; Given and Lohman, 1986; Budd and Land, 1990). This light carbon flag is common beneath subaerial exposure surfaces (Allan and Matthews, 1977; Rush and Chafetz, 1990).

A plot of $\delta^{13}\text{C}$ versus depth beneath the pre-Mesozoic unconformity surface for NDIC-12357 is shown in Figure 44. $\delta^{13}\text{C}$ is lowest near the subaerial exposure surface and gets higher with depth. These carbon-isotope data provide evidence that the Wayne beds underwent diagenesis in the freshwater vadose environment and that the secondary porosity formed in these beds is probably the result of dissolution during the time of the pre-Mesozoic unconformity.

The vadose carbon flag documented in the study area is not as dramatic as those presented elsewhere in the literature (Gross, 1964; Gross and Tracey, 1966; Allan and Matthews, 1977; Allan and Matthews, 1982; Given and Lohmann, 1986; Budd and Land, 1990; Rush and Chafetz, 1990; among others). This modest vadose flag may be due to scant available organic matter so that the carbon dioxide dissolved in the diagenetic fluid was not extremely depleted in ^{13}C . Megascopic examination of the Wayne beds cores did not reveal evidence of a soil horizon or vegetation on the pre-Mesozoic unconformity surface indicating the relatively small vadose carbon flag could be due to the lack of substantial vegetative cover associated with the exposure surface. Or, the ^{13}C -depleted carbonate may have been removed during transgression.

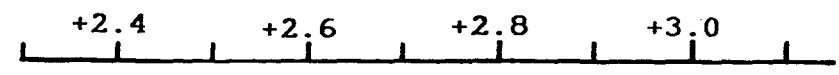
Figure 44.- Whole rock $\delta^{13}\text{C}$ versus depth below KB for NDIC-12357. Error bars are approximately ± 0.1 ‰. The general trend is for Wayne carbonates to become enriched in ^{12}C as they approach the pre-Mesozoic unconformity.

UNIVERSITY OF MICHIGAN LIBRARY

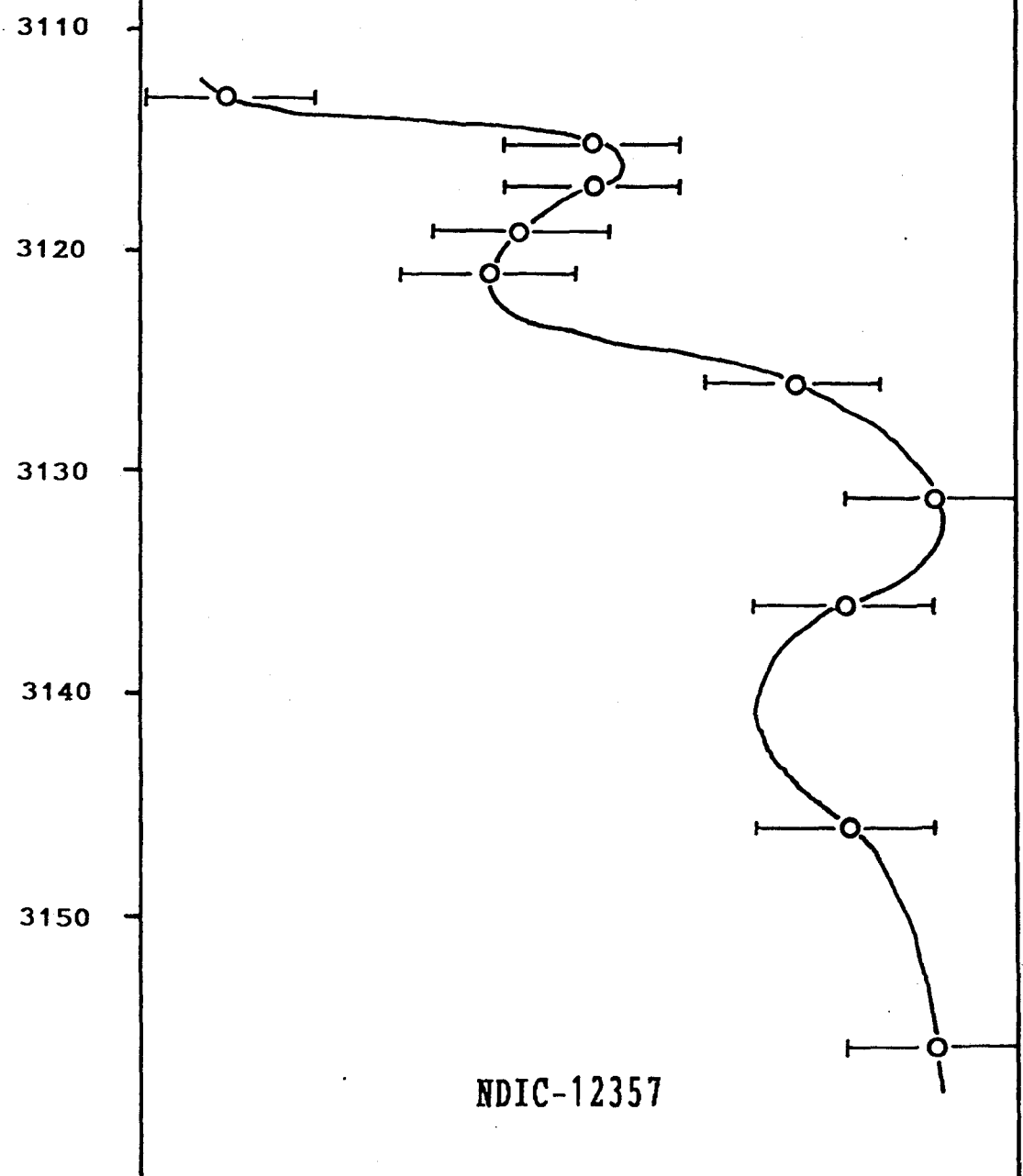
CARBON ISOTOPES VS DEPTH

$\delta^{13}C^0/100$ (PDB)

DEPTH (FT)



PRE-MESOZOIC UNCONFORMITY



NDIC-12357

Porosity formed during freshwater vadose diagenesis was subsequently preserved by freshwater phreatic diagenesis. The presence of freshwater cements (Figure 35) in portions of the Wayne beds suggests that these beds have undergone diagenesis in the freshwater phreatic environment.

The recrystallization of metastable aragonite and magnesium calcite to calcite is an important effect of freshwater diagenesis (Friedman, 1964; Matthews, 1968; Land and Epstein, 1970; Steinen and Matthews, 1973). Early stabilization of calcite reduces the likelihood of extensive compaction during burial (Wagner and Matthews, 1982).

Porosity Occlusion

The loss of even a small amount of porosity can have a dramatic effect on the potential reserves of an oil well. To illustrate this point, the oil reserves lost due to a 5% porosity reduction employing simple volumetric calculations are shown in Table 13. These example calculations, using typical Wayne beds reservoir parameters, show that the loss of even 5% porosity can result in the loss of 33% of the reserves or 26,000 barrels of oil in the example shown.

A plot of core porosity versus weight percent dolomite (well NDIC-12357) as determined by x-ray diffraction shows that as dolomite content in the Wayne beds increases,

TABLE 13: EXAMPLE OF RESERVES LOST DUE TO POROSITY REDUCTION

| <u>RESERVOIR PARAMETER</u> | <u>GOOD POROSITY</u> | <u>POOR POROSITY</u> |
|----------------------------|----------------------|----------------------|
| Porosity | 15% | 10% |
| Oil Saturation | 50% | 50% |
| Acres Drained | 40 | 40 |
| Feet of Pay | 20 | 20 |
| Recoverability Factor | 20% | 20% |
| Formation Volume Factor | <u>1.2</u> | <u>1.2</u> |
| Reserves (Barrels Oil) | 78,000 | 52,000 |

porosity decreases (Table 14 and Figure 45). The correlation coefficient (R) of this negative relationship is -0.67 with one standard deviation (SD) of +/- 4.21% porosity. Porosity in the Wayne beds was occluded by burial-dolomite and calcite cement with minor amounts of marine and freshwater calcite and burial anhydrite cements. Of the cement types, burial dolomite and calcite is believed to have had the most damaging effect on the porosity. Such a pore-filling dolomite cement has been noted in other studies (Qing and Mountjoy, 1989; Kaufman et al., 1990; Amthor and Friedman, 1992).

The data in Figure 45 can be interpreted in the following manner. First, the secondary-vugular and solution-enlarged porosity in the Wayne beds formed in the freshwater vadose diagenetic environment. Second, mineralogical stabilization and some cementation took place in the freshwater phreatic environment, which left the rocks resistant to compaction and cementation during burial. Porosity at this time was between 12 and 20% (porosity at 0% dolomite, Figure 45). Finally, dolomite and calcite cementation in the burial diagenetic environment took place which occluded porosity in some zones but not in others. Porosity in some of the more heavily dolomitized zones is as low as 4%.

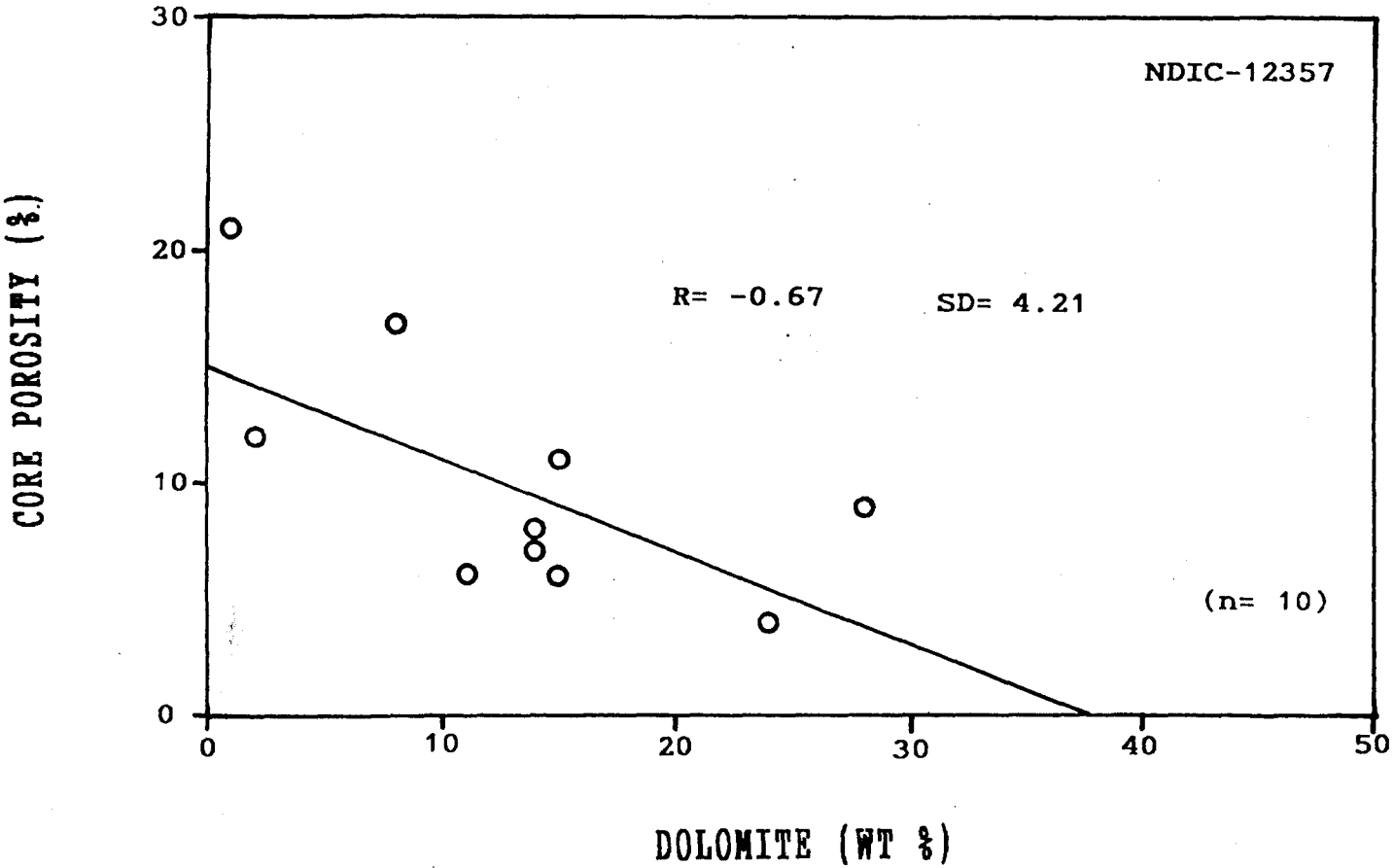
TABLE 14: CORE POROSITY AND DOLOMITE WEIGHT PERCENT

(WELL NDIC-12357)

| <u>Depth (feet)</u> | <u>Core Porosity (%)</u> | <u>Dolomite (Wt %)</u> |
|---------------------|--------------------------|------------------------|
| 3113 | 6 | 11 |
| 3115 | 4 | 24 |
| 3117 | 7 | 14 |
| 3119 | 17 | 8 |
| 3121 | 9 | 28 |
| 3126 | 8 | 14 |
| 3131 | 21 | 1 |
| 3136 | 12 | 2 |
| 3146 | 11 | 15 |
| 3156 | 6 | 15 |

Figure 45.- Core porosity versus dolomite weight percent
(based on XRD analysis) for well NDIC-12357. Wayne
beds exhibit a negative correlation between porosity
and dolomite content. Correlation coefficient = -0.67.
One standard deviation = +/-4.21% porosity.

CORE POROSITY VS DOLOMITE %



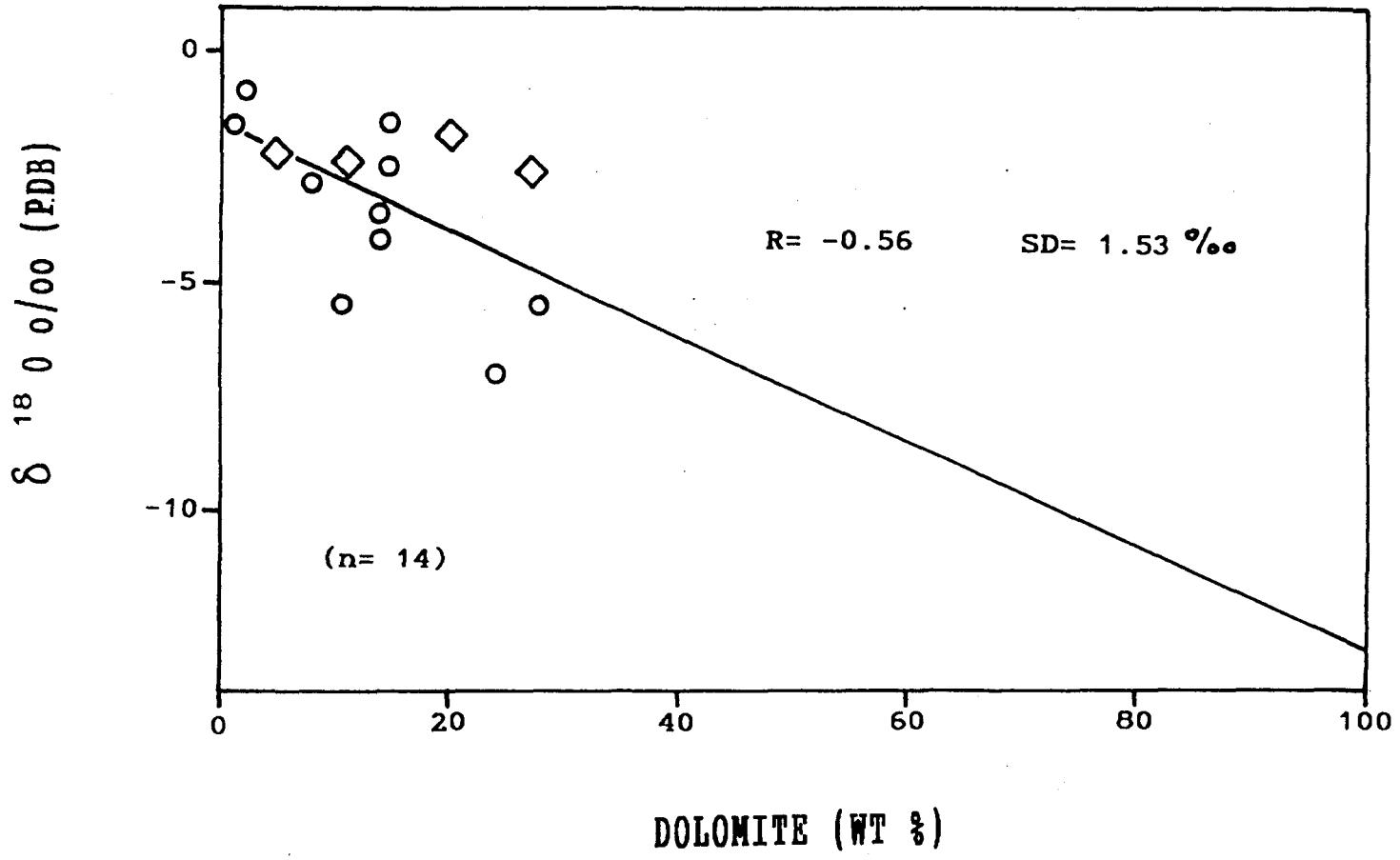
Pore-occluding dolomite in the Wayne beds probably formed during burial diagenesis. A plot of $\delta^{18}\text{O}$ from core and drill cutting samples versus dolomite weight percent (Figure 46) illustrates that increasing dolomite content results in decreased $\delta^{18}\text{O}$. The correlation coefficient (R) of this negative relationship is -0.56 and one standard deviation (SD) is $\pm 1.53\text{‰}$.

If the regression line in Figure 46 is extrapolated to 100% dolomite, $\delta^{18}\text{O}$ ranges between approximately -11.5 and -14.5‰, which may be the oxygen isotope value of the pore-occluding dolomite. Carbonates which are depleted in oxygen-18 are usually associated with either elevated temperatures or freshwater precipitation, especially at high latitudes (McCrea, 1950; Urey, 1951; Emiliani and Shackleton, 1974; Hays and Grossman, 1991). Extrapolated $\delta^{18}\text{O}$ values for dolomite in the Wayne beds (Figure 40) are more similar to the oxygen composition of dolomites formed during burial diagenesis noted in other studies than to those formed in any other diagenetic environment.

Although elevated temperatures result in carbonate with light oxygen, the extrapolated values for the Wayne beds are less than expected as these rocks were probably never buried deeper than 3,200 feet. These light oxygen values may be due, in part, to error introduced by using mixed

Figure 46.- $\delta^{18}\text{O}$ versus dolomite weight percent (XRD analysis) for well NDIC-12357. Open circles are core sample data, and open diamonds are drill cutting sample data. Oxygen isotope values display a negative correlation with dolomite content in the Wayne beds. Correlation coefficient = -0.56. One standard deviation = $\pm 1.53\text{‰}$ $\delta^{18}\text{O}$.

$\delta^{18}O$ ‰ (PDB) VS DOLOMITE ‰



mineralogies, error in the XRD or isotope analyses, and/or the method used to extrapolate the oxygen ratios.

Permeability Reduction

Table 15 shows the permeability and point count data from well NDIC-12357. Pores which have been occluded or partially occluded by burial dolomite and calcite cement are tabulated in the pore occluded by dolomite or calcite cement column. Pores which have been bridged or occluded by anhydrite are tabulated in the pores bridged or occluded by anhydrite cement column. Thus, effective porosity rather than total porosity was counted by these point counts. Permeability was reduced in the Wayne beds by anhydrite cementation. X-ray diffraction analysis indicates that the anhydrite content of the carbonates ranges from 0 to 3%. However, the point count data indicate that pores containing pore-bridging or pore-occluding anhydrite ranges from 0 to 39%. Figure 47 is a plot of whole-core permeability versus percentage of pores or former pores bridged or occluded by anhydrite based on point count data for NDIC-12357 (the same well used for oxygen and carbon isotope analysis). This plot shows how small amounts of effective porosity-reducing, pore-bridging anhydrite can have a very adverse effect on the permeability of the reservoir.

TABLE 15: PERMEABILITY AND POINT COUNT DATA

(WELL NDIC-12357) ⁽¹⁾

| Depth (ft) | Effective | | | | |
|---------------|--|-----------------|---------------------------|----------------|-----------------------|
| | Perm. (md) | Porosity (%) | Isopachous Cal Cmt (%) | Micrite (%) | Equant Cal Cmt (%) |
| 3111 | No permeability analysis | | | | |
| 3113 | 0.20 | 3 | 8 | 7 | 0 |
| 3115 | 0.03 | 1 | 0 | 11 | 0 |
| 3117 | 0.42 | 4 | 0 | 16 | 0 |
| 3119 | 27 | 14 | 0 | 14 | 0 |
| 3120 | 36 | 11 | 0 | 15 | 3 |
| 3123 | 12 | 3 | 0 | 0 | 0 |
| 3126 | 0.45 | 4 | 0 | 30 | 0 |
| 3127 | 0.45 | 3 | 0 | 9 | 0 |
| 3129 | 2.5 | 4 | 21 | 0 | 0 |
| 3135 | 36 | 18 | 0 | 5 | 1 |
| 3140 | 0.44 | 2 | 0 | 17 | 0 |
| 3143 | 18 | 15 | 0 | 10 | 0 |
| 3145 | 5.2 | 19 | 0 | 14 | 0 |
| 3146 | Permeability analysis affected by fracture | | | | |
| 3149 | 4.9 | 10 | 0 | 5 | 8 |
| 3155 | 2.1 | 7 | 0 | 15 | 0 |
| 3162 | 0.12 | 4 | 0 | 17 | 0 |

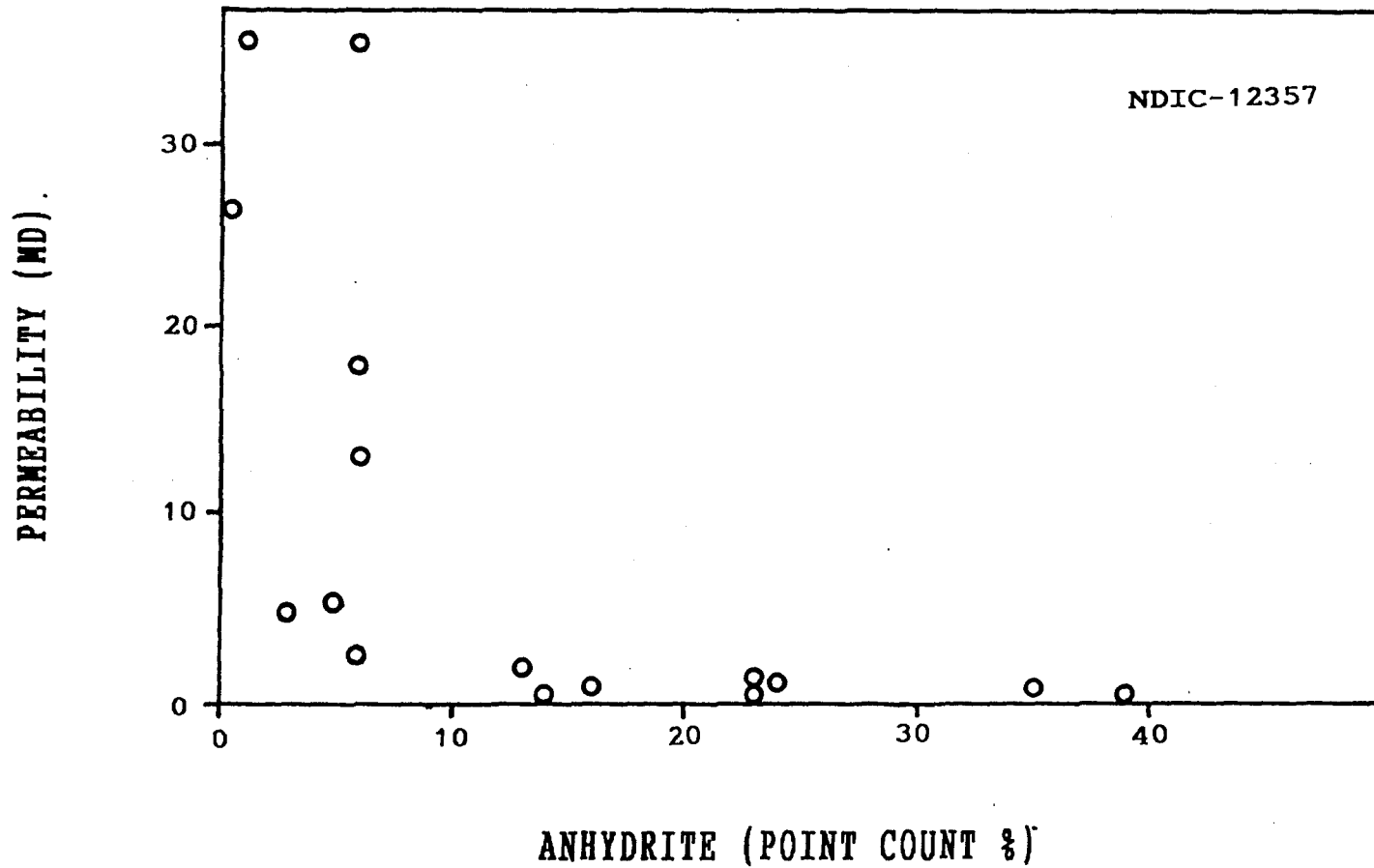
| Depth (ft) | Pore Occl | | Pore Bridged | |
|---------------|--|----------------|-------------------------|--------------------------|
| | by Dolomite (%) | by Cal Cmt (%) | or Occl by Anhy Cmt (%) | or Occl by Allochems (%) |
| 3111 | No permeability analysis | | | |
| 3113 | 4 | 11 | 23 | 44 |
| 3115 | 30 | 7 | 39 | 12 |
| 3117 | 16 | 14 | 23 | 27 |
| 3119 | 34 | 0 | 0 | 36 |
| 3120 | 10 | 0 | 6 | 55 |
| 3123 | 90 | 1 | 6 | 0 |
| 3126 | 4 | 15 | 16 | 31 |
| 3127 | 2 | 0 | 35 | 51 |
| 3129 | 6 | 0 | 6 | 63 |
| 3135 | 0 | 0 | 1 | 75 |
| 3140 | 19 | 0 | 24 | 38 |
| 3143 | 0 | 0 | 6 | 69 |
| 3145 | 1 | 0 | 5 | 61 |
| 3146 | Permeability analysis affected by fracture | | | |
| 3149 | 4 | 0 | 3 | 70 |
| 3155 | 0 | 24 | 13 | 41 |
| 3162 | 8 | 20 | 14 | 37 |

(1)- Permeability values from commercial core analysis.

Cement and effective porosity percentages from point count data.

Figure 47.- Core permeability versus pore-bridging
anhydrite percent (based on point count data) for well
NDIC-12357.

PERMEABILITY VS PORE-BRIDGING ANHYDRITE %



As can be seen in Figure 47, in unfractured samples with an anhydrite content below 6%, the permeability ranges from 2.5 to 36 millidarcies with an average of 17.7 millidarcies. The permeability in samples with an anhydrite content above 6% anhydrite content averages only 0.53 millidarcies. Thus, as the pore-bridging anhydrite cement content of the rock increases, the permeability decreases. The other cement types point counted in the Wayne beds, which include isopachous, micrite, and equant calcite cements, and burial dolomite and calcite cements, do not exhibit statistically significant correlations with permeability. The occurrence of burial calcite cement with burial dolomite cement was used to differentiate burial calcite cement from equant calcite cement.

As discussed earlier, the permeability-reducing anhydrite cements in the study area probably precipitated during burial diagenesis. Other authors have shown that anhydrite can form in a burial diagenetic environment (Machel and Burton, 1991). The anhydrite cements in the Wayne beds are probably the result of the gypsum-to-anhydrite transformation in the overlying Glenburn beds. Calcium-sulfate-saturated waters expelled from the gypsum during dewatering were probably the source of the anhydrite cements. As discussed earlier, burial-anhydrite cementation

occurred at depth relatively late in the diagenetic history of the study area (Figure 30).

Sulfur isotope data (Figure 43) suggest that the pore-occluding anhydrites are in isotopic equilibrium with the evaporites in the Glenburn beds. Petrographic observations indicate the anhydrite cements precipitated after the burial dolomite and calcite cements. Taken together, the petrographic and isotopic data indicate that the permeability-reducing anhydrite cements originated from the Glenburn beds and precipitated in a burial-diagenetic environment.

Based on petrographic observations (Appendix A), pore-bridging and pore-occluding anhydrite cements appear to be less common in those portions of the study area where the Glenburn beds were eroded during the time of the pre-Mesozoic unconformity. The abundance of anhydrite cement in the Wayne beds appears to be proportional to the thickness of overlying Glenburn evaporites (discussed below; and Appendix A). In general, permeability is highest where the Glenburn is absent.

PETROLEUM EXPLORATION MODELS

Previous Work

In the Wayne beds, porosity is diminished by pore-occluding, burial-dolomite and calcite cements and the permeability is reduced by pore-bridging anhydrite cement which postdates the dolomite. But, why did these burial processes affect only selected portions of the Cimbel, Leonard, and Roth fields? A search of the Williston Basin literature did not reveal previous investigations which specifically address the relationship between burial processes and paleotopography.

Easy solutions (e.g., structure and depositional environments) to the anomalous petroleum production patterns observed in the Wayne beds reservoirs cannot be found. Two exploration and development models, the paleoisland model and the eroded paleohigh model, are proposed herein to account for the production anomalies. Examples are found in the literature suggesting that freshwater lenses beneath carbonate paleoislands can account for reservoir development in carbonates (Wagner and Matthews, 1982; Budd and Vacher,

1991). Nothing similar to the eroded paleohigh model has been encountered in the literature. The processes involved in these two models occur at different times in the diagenetic history of the Wayne beds. Both of these models may have affected the reservoirs in the study area, one after the other; therefore, the two models are not mutually exclusive.

Paleoisland Model

As discussed earlier, the diagenetic history of the Wayne beds involves porosity formation due to dissolution in the freshwater vadose, porosity preservation due to mineralogical stabilization in the freshwater phreatic, porosity occlusion by burial-dolomite and calcite cements, and permeability reduction by burial anhydrite cements. Reservoirs in the study area have been damaged as a result of either porosity occlusion and/or permeability reduction. The paleoisland model addresses the problem of porosity occlusion due to compaction and burial dolomite and calcite cementation. The paleoisland model is dependent upon four factors: (1) the timing of the diagenetic event which resulted in pore-occluding dolomite and calcite cementation, (2) the presence of paleoislands, (3) the existence of freshwater lenses beneath these paleoislands, and (4) the

location of the pore-occluding dolomite and calcite cements within the Wayne beds.

Based on petrographic observations and oxygen-isotope data, the dolomite cements formed in the burial diagenetic environment. The pore-occluding dolomites post-date all isopachous, micrite, and equant cements.

Evidence for the existence of paleoislands in the study area is provided by isopach maps and sulfur-isotope data. Thin areas on the Spearfish Formation isopach map (Figure 17) indicate that before and during Spearfish deposition paleohighs existed on the pre-Mesozoic unconformity surface. Sulfur isotope data for replacement anhydrites in the Wayne beds indicate precipitation from waters in isotopic equilibrium with Triassic seawater (Figure 43). Thus, as the Triassic seas transgressed the study area, the highs may have become islands.

Freshwater lenses may have formed beneath these islands. As discussed earlier, the transformation of magnesium calcite and aragonite to calcite is one of the more important processes resulting from freshwater diagenesis. This mineralogical stabilization was more extensive beneath the islands than in the surrounding lows. Thus, the stabilized carbonates beneath the islands would have undergone much less compaction and burial dolomitization than the less mineralogically stabilized

carbonates in the lows. The lack of extensive burial dolomite and calcite cements beneath the paleohighs suggests freshwater lenses existed beneath the paleoislands. Static conditions in the burial diagenetic environment kept most, but not all, of the late cements out of the paleohighs.

The paleoisland and eroded-paleohigh (discussed below) models for the Cimbel, Leonard, and Roth fields are shown in Figures 48, 49, and 50, respectively. The datum for these cross-sections is the red shale unit at the top of the Spearfish Formation that is thought to have been deposited as a nearly horizontal surface. The best and poorest producers in each field are shown for comparison. According to these models, the best producers in each field are associated with a freshwater lens beneath a paleoisland that ultimately resulted in porosity preservation.

Eroded Paleohigh Model

As stated earlier, study area reservoirs have been damaged by either porosity occlusion or permeability reduction. The eroded paleohigh model addresses the problem of permeability reduction. Permeability in the Wayne beds was reduced by precipitation of burial anhydrite cements. The occurrence of these pore-bridging cements within the reservoirs is related to four factors: (1) the timing of

Figure 48.- Paleoisland and eroded-paleohigh model for Cimbrel field. Good oil producers are associated with the freshwater lenses beneath paleoislands and/or paleohighs where the Glenburn was eroded. Poor producers are located on the flanks of the paleoislands and in paleolows where the Glenburn is preserved. The location of cross-section A-A' is shown in Figure 3.

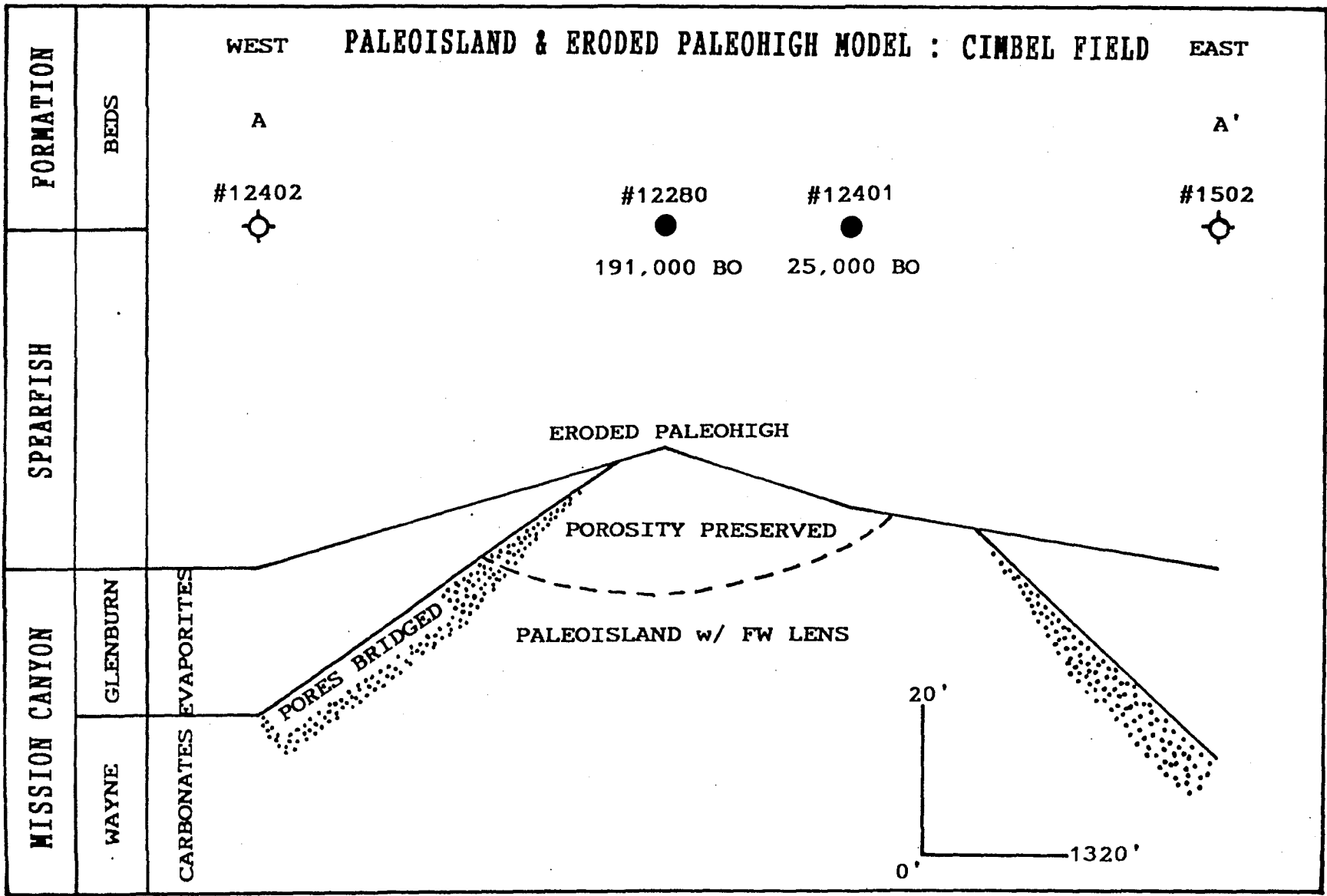


Figure 49.- Paleoisland and eroded-paleohigh model for Leonard field. Poor oil producers are located on flanks of paleoislands and in paleolows where the Glenburn is preserved. Good producers are associated with freshwater lens development beneath paleoislands and/or paleohighs where the Glenburn was eroded. The location of cross-section B-B' is shown in Figure 3.

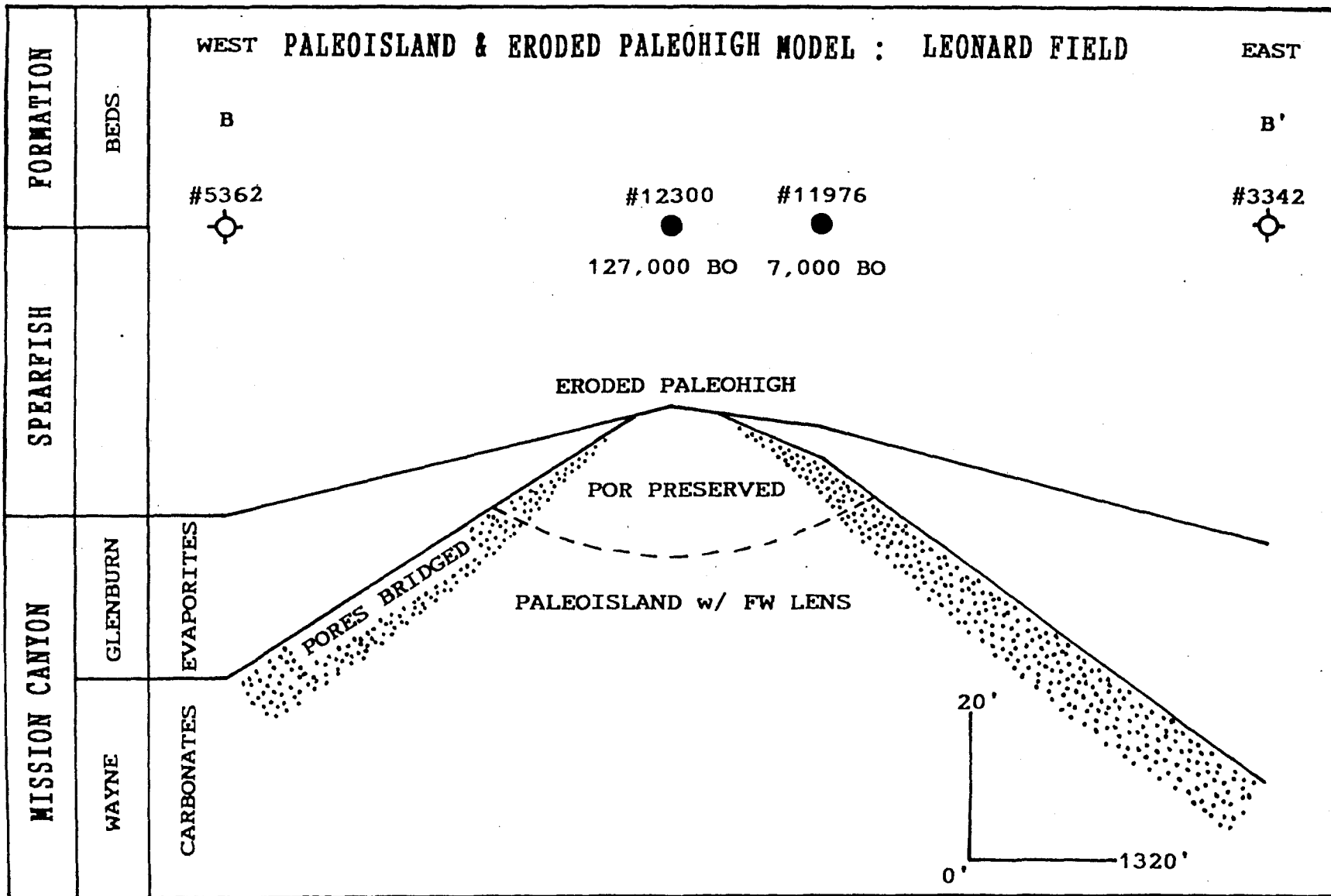
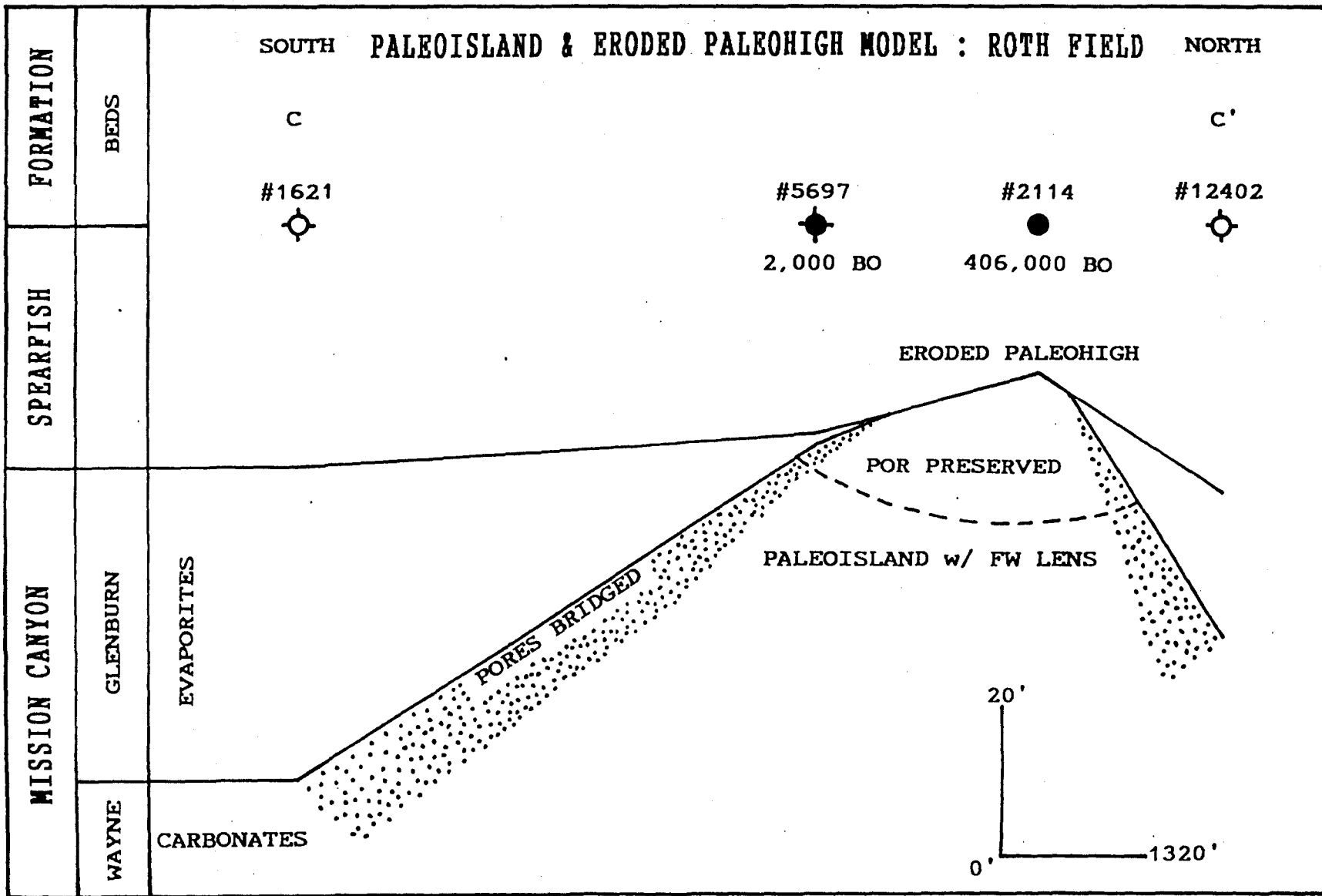


Figure 50.- Paleoisland and eroded-paleohigh model for Roth field. The good oil producers are associated with freshwater lens development beneath paleoislands and/or paleohighs where the Glenburn was eroded. Poor producers are located on flanks of paleoislands and paleolows where the Glenburn is preserved. The location of cross-section C-C' is shown in Figure 3.



the diagenetic event which resulted in anhydrite cementation, (2) the source of calcium sulfate for anhydrite precipitation, (3) the amount of calcium sulfate introduced into the Wayne beds, and (4) the location of the pore-bridging anhydrites within the reservoirs.

The pore-bridging anhydrite cements are interpreted to be burial cements based on the principles of inclusions and superposition. The pore-occluding dolomite and calcite cements formed as a result of burial diagenesis. Anhydrite cements postdate the dolomite and calcite cements and inclusions of the dolomite can be found in the anhydrite (Figure 38). Therefore, the pore-bridging anhydrite cements must also be due to burial diagenesis.

The sulfur isotope data suggest that the evaporites of the overlying Glenburn beds could be the source of the sulfate required for anhydrite precipitation. The Glenburn beds were originally deposited as gypsum. Burial resulted in gypsum-to-anhydrite transformation of the Glenburn evaporites. The sulfur isotope data indicate that the pore-bridging anhydrites in the Wayne beds are in isotopic equilibrium with the bedded anhydrites of the Glenburn (Figure 43). Thus, the calcium sulfate in water expelled during the Glenburn gypsum-to-anhydrite transformation precipitated as pore-bridging anhydrite in the underlying Wayne beds.

Based on megascopic and petrographic core examination, the amount of pore-bridging anhydrite in the Wayne beds appears to be directly related to the thickness of the overlying Glenburn beds. In those areas where the Wayne beds are overlain by the Glenburn beds, such as on the flanks of paleohighs or in paleolows, extensive pore-bridging anhydrite cementation has occurred. Those areas beneath paleohighs which have been completely eroded of Glenburn evaporite contain much less pore-bridging anhydrite in the Wayne beds.

The eroded paleohigh model, in conjunction with the paleoisland model for the Cimbel, Leonard, and Roth fields, is also shown in Figures 48, 49, and 50, respectively. These cross-sections illustrate that the amount of oil production from wells within these fields is related to the thickness of the overlying Glenburn beds, and the occurrence of pore-bridging anhydrite cement. Wells which are located on eroded paleohighs are good oil producers. Wells which are located on the flanks of the paleohighs, where some of the Glenburn survived erosion, are generally poor producers.

The best producers in the Cimbel, Leonard, and Roth fields are not affected by either compaction, pore-occluding dolomite and calcite, or pore-bridging anhydrite cements. Reservoir quality in some study area wells is diminished only by compaction and pore-occluding burial dolomite and

calcite cements (paleoisland model). Other oil wells are only affected by pore-bridging burial anhydrite cements (eroded paleohigh model). The poorest producers contain abundant pore-occluding dolomite and calcite and pore-bridging anhydrite cements.

SUMMARY AND CONCLUSIONS

Continued discoveries of new oil fields with good production at shallow depths have created a renewed interest in the Mission Canyon Formation in the Williston Basin. During the past few years, production in the Bluell and Sherwood beds has extended southward from north-central North Dakota into central North Dakota. In Bottineau County, individual wells are capable of producing over 400,000 barrels of oil from the Wayne beds at depths of only 3,100 feet. Extending the search for production in the Wayne beds southward into central North Dakota might, therefore, make economic sense. Determining what processes control the amount of production in current oil fields will facilitate the exploration for new oil fields in the Wayne beds.

The Wayne beds in the study area produce oil from structural traps formed by the multistage, differential dissolution of the underlying Devonian Prairie Formation. Structural mapping on either the Tilston argillaceous marker (TAM) or the Wayne argillaceous marker (WAM) can readily identify these structures. Comparing the oil production

from individual wells to the present-day structure reveals that, above the oil-water transition zone, the quality of oil production is not controlled by structure.

The Wayne beds were deposited on an upward-shoaling, shallow water carbonate shelf. The tidal-flat depositional environment consists of pisolitic-peloidal-skeletal packstones and wackestones. The Wayne beds in the Cimbel, Leonard, and Roth oil fields are all situated within this broad lithofacies belt. Lithofacies variations in the study area do not control the amount of oil that either an individual well or a field will produce.

The Wayne beds underwent diagenesis in a variety of diagenetic environments. Cementation, micritization, and perhaps minor amounts of subtidal dolomitization occurred in the marine phreatic diagenetic environment. Hypersaline diagenesis during the Mississippian resulted in minor amounts of dolomitization and anhydritization. Sulfur isotope data indicate that hypersaline diagenesis also occurred as the early Triassic seas transgressed the study area.

Following marine deposition, the study area was subaerially exposed during the time of the pre-Mesozoic unconformity. The presence of a light $\delta^{13}\text{C}$ flag beneath the unconformity surface indicates that the Wayne beds were diagenetically altered in the freshwater vadose

environment. Concomitant subaerial exposure resulted in the dissolution of carbonates and minor cementation.

During the Triassic transgression, the Wayne beds underwent freshwater phreatic diagenesis. Thin areas on the Spearfish Formation isopach map along with petrographic data suggest that freshwater diagenesis may have been localized in freshwater lenses beneath paleoislands. The freshwater phreatic diagenetic environment resulted in mineralogical stabilization of calcite along with minor amounts of cementation. Carbonates which contained metastable mineralogies were prone to dolomite and calcite cementation during burial. Paleolows in the study area experienced burial-dolomite and calcite cementation while paleohighs did not.

Burial diagenesis resulted in compaction, pressure solution, dolomite and calcite cementation, and anhydritization. Oxygen-isotope data suggest that the pore-occluding dolomites formed in a burial environment. Since the Wayne beds anhydrite cements post-date the burial dolomite and calcite cements, they too are believed to have precipitated in the burial environment. Sulfur isotope data suggests that pore-bridging burial anhydrites originated from the overlying Glenburn beds as a result of gypsum-to-anhydrite transformation.

Porosity formed in the Wayne beds due to dissolution during freshwater-vadose diagenesis. Porosity preservation occurred as a result of freshwater-phreatic diagenesis which was localized in freshwater lenses beneath paleoislands. Those areas not located under paleoislands experienced less mineralogical stabilization, which resulted in more porosity occlusion due to compaction and burial-dolomite and calcite precipitation. Permeability was reduced by pore-bridging, burial-anhydrite cements which precipitated from calcium-sulfate-saturated waters expelled during the gypsum to anhydrite transformation of the overlying Glenburn beds.

Oil production in the study area is controlled by burial processes involving compaction and precipitation of pore-occluding dolomite and calcite and pore-bridging anhydrite cements. However, the location and intensity of these burial diagenetic processes are controlled by earlier events involving freshwater diagenesis, paleotopography, and erosion. Relating early and late diagenetic events to paleotopography is the key to success in Wayne reservoir exploration and development.

APPENDIX A: PETROGRAPHIC DESCRIPTIONS

EXPLANATION OF SYMBOLS

| <u>SYMBOL</u> | <u>DESCRIPTION</u> |
|---------------|--------------------|
|---------------|--------------------|

Note: Each entry represents one thin section

| | |
|------|--------------------------------|
| P | Packstone |
| W | Wackestone |
| M | Mudstone |
| A | Anhydrite |
| D | Dolomite Cement-large crystals |
| d | Dolomite Rhombs-small crystals |
| C | Calcite Cement |
| arg | Argillaceous |
| ss | Sandstone |
| qtz | Quartz |
| mas | Massive |
| nod | Nodule |
| ? | Unidentified |
| lrg | Large |
| xls | Crystals |
| grns | Grains |

Non-skeletal Particle Types:

Pisoliths

Oolites

Intraclasts

Pellets

Peloids

Skeletal Particle Types:

Skeletals

Algal Stromatolites

Calcispheres

Filamentous Algae

Corals

Pelecypods

Gastropods

Brachiopods

Crinoids

Foraminifera

Ostracods

Sedimentary Structures:

| | |
|------|-------------------------|
| | Laminated |
| intl | Interlaminated |
| | Sealed Fractures |
| | Open Fractures |
| | Pore-occluded Vugs |
| | Pore-bridged Vugs |
| | Open Vugs |
| | Geopetal Structure |
| | Stylolites |
| | Wavy or Nodular Bedding |
| | Compacted Grains |

Reservoir Descriptors:

| | |
|----|-----------------------------------|
| | Porosity |
| | Visual Estimate of Porosity (15%) |
| | Interparticle Porosity |
| | Vugular Porosity |
| xl | Intercrystalline Porosity |
| | None or Very low (tight) Porosity |

PETROGRAPHIC DESCRIPTION

WELL NAME: Halvorson #1 (#1159)

LOCATION: NWSE 2-162 -79

| DEPTH | TEXTURE | PARTICLES | STRUCTURES | RESERVIOR |
|-------|--------------------|-------------------|------------------|-------------|
| 3212 | A & W _d | ⊙ ππ? O | ~ + _A | π |
| 3214 | | | | |
| 3216 | P _{D+A} | O? | + _A | π |
| 3218 | | | | |
| 3220 | | | | |
| 3222 | P _A | O? O? ⊙? | + _A | π |
| 3224 | W _D | ∩ O? ⊙ ⊙ | + _A | ⊕ 1-5 φ |
| 3226 | | | | |
| 3228 | | | | |
| 3230 | W | ⊙? O | + _A | ⊕ 1-5 φ |
| 3232 | W | ⊙ ˆ ˆ ˆ? ⊙ ⊙ ˆ | + _A | ⊕ Δ 15-20 φ |
| 3234 | | | | |

PETROGRAPHIC DESCRIPTION

WELL NAME: Halvorson #1 (#1159)

LOCATION: NWSE 2-162-79

| DEPTH | TEXTURE | PARTICLES | STRUCTURES | RESERVIOR |
|-------|---------|-------------|-------------------------------|-----------|
| 3236 | W | ⊙ ⊙ ⊙ λ? | ⊕ _{AIC} ≡ | ⊕ 5-10 φ |
| | W | ⊙ λ? ~? ⊙ ⊙ | ⊕ _A ⚡ _A | ⊕ 1-5 φ |
| 3238 | | | | |
| | W | ⌒ ^ ⊙ ⊙ ⊙ | ⊕ _A | ⊕ 10-15 φ |
| 3240 | | λ? | | |
| 3242 | | | | |
| 3244 | | | | |
| 3246 | | | | |

PETROGRAPHIC DESCRIPTION

WELL NAME: Nordmark #1 (#1977)

LOCATION: NENW 30-163-78

| DEPTH | TEXTURE | PARTICLES | STRUCTURES | RESERVIOR |
|-------|----------------|-----------------|---------------------|-------------|
| 3164 | P _d | ⊙ | ✦ _{A+D} | ✧ XL 5-10 φ |
| 3166 | M | ∩ ⊙ ⊙ | Anod ✦ _A | π |
| 3168 | P | ⊙ ∩ ✦? ∩ Σ | | Δ 1-5 φ |
| 3170 | | | | |
| 3172 | | | | |
| 3174 | W | ∩ ⊙ ∩ λ? ∩ | ✦ _{A+C} ≡ | ✧ 1-5 φ |
| 3176 | P | ∩ ⊙ ∩ ∩ λ? ⊙ | ✦ _A | ✧ 5-10 φ |
| 3178 | | | | |
| 3180 | M | ∩ ⊙ λ? | ✦ _A | ✧ 5-10 φ |
| 3182 | | | | |
| 3184 | M _d | ∩ ∩ | ✦ _A | ✧ 5-10 φ |
| 3186 | P | ⊙ ∩ ∩ λ? | | ✧ L 1-5 φ |

PETROGRAPHIC DESCRIPTION

WELL NAME: Skarpohl # 1 (# 2038)
















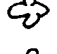


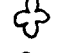






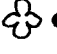





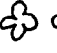

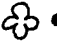

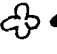







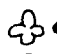

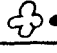

LOCATION: NENE 23-163-78

| DEPTH | TEXTURE | PARTICLES | STRUCTURES | RESERVIOR |
|-------|----------------|---------------------|----------------|--------------|
| 3078 | W | ○ ∩ ⊗ | ✱ _A | ✱ 10-15 φ |
| 3080 | | | | |
| 3082 | | | | |
| 3084 | M _D | | | ✱ XL 10-15 φ |
| 3086 | M _D | ∩ S m | = ∩ | ✱ XL 5-10 φ |
| 3088 | M _D | m ∩ | | ✱ XL 10-15 φ |
| 3090 | | | | |
| 3092 | | | | |
| 3094 | | | | |
| 3096 | | | | |
| 3098 | P | ● ⊗ S ∩ or ○? | | ✱ △ 15-20 φ |
| 3100 | | | | |

PETROGRAPHIC DESCRIPTION

WELL NAME: Akerlind #1 (2176)

LOCATION: NESW 30-163-78

| DEPTH | TEXTURE | PARTICLES | STRUCTURES | RESERVIOR |
|-------|----------------|-----------|--|-------------------------|
| 3114 | M _d | ??? |  | π |
| | P _d | ○ or ⊙ |  | π |
| 3116 | P _d | ∩ ○ or ⊙ |   | π |
| | P _d | ⊙ ⊙? |   | π |
| 3118 | P _d | ○ ∩ ⊙? |   | π |
| | P _d | ○ |  | π |
| 3120 | P _d | ○ |   | π |
| | P | ⊙ |   | |
| 3122 | P | ⊙ |   | 5-10 φ |
| | P | ∩ ⊙ ⊙ |    | 1-5 φ |
| 3124 | M _d | ∩ ⊙ ^ |   | 1 φ |
| | M _d | ⊙ ^ |    | 1-5 φ |
| 3126 | M _d | ⊙ |   | π |
| | P _d | ○ ⊙ ⊙ |   | 1-5 φ |
| 3128 | P _d | ○ ⊙ |   | 5-10 φ |
| | M _d | ⊙ ^ |   | 5-10 φ |
| 3130 | M _d | ○ ⊙ ∩ |   | 10-15 φ |
| | M _D | |   | XL 5-10 φ |
| 3132 | P | ○ |    | 1-5 φ |
| | M _D | ○ |    | XL 5-10 φ |
| 3134 | P _D | ○ ⊙ |   | (some Δ φ) XL 5-10 φ |
| 3136 | P | ○ ○ ^ |   | Δ 10-15 φ |
| | P | ○ ○ |   | Δ 10-15 φ |

PETROGRAPHIC DESCRIPTION

WELL NAME: Akerlind #1 (2176)

LOCATION: NESW 30-163-78

| DEPTH | TEXTURE | PARTICLES | STRUCTURES | RESERVIOR |
|-------|----------------|---------------|---------------------------------|------------------------|
| 3138 | P | ○ ∩ ⊙? | ✚ _A ⚡ _A | ✚ _A 10-15 φ |
| | M _d | ∩ ⊙ ∩ | ✚ _A | ✚ 5-10 φ |
| 3140 | P | ⊙ ○ | ✚ _A | ✚ _A 5-10 φ |
| 3142 | M | ○ | ✚ _A | ✚ 5-10 φ |
| 3144 | P | ○ ∩ ⊙ ∩? ⊙ | ✚ _A | ✚ 5-10 φ |
| | W _d | ∩? ∩ ⊙ ∩ ∩ | ✚ _A | ✚ XL 5-10 φ |
| 3146 | P _d | ○ ○? ⊙ | ✚ _{C+A} | ✚ _A 5-10 φ |
| | P | ∩ ○ ∩ ⊙ | ✚ _{C+A} ⚡ _A | ✚ _A 10-15 φ |
| 3148 | P _d | ∩ ⊙ ∩ | ✚ _{C+A} | ✚ 10-15 φ |
| | P | ∩ ∩ ○ ○ | ✚ _C | ✚ 1-5 φ |
| 3150 | P | ○ ⊙ ⊙ ∩ | ✚ _{C+A} | ✚ 5-10 φ |
| | P | ⊙ ○? ○ ∩ | ✚ _A | ✚ 5-10 φ |
| 3152 | M _d | ∩ ⊙ | ✚ _A | ✚ 5-10 φ |
| | M _d | ⊙ ⊙ ∩ | ✚ _A | ✚ 5-10 φ |
| 3154 | M _d | ⊙ ∩ | ✚ _A | ✚ 5-10 φ |
| | M _d | ⊙ ∩ ∩ | ✚ _A | ✚ 5-10 φ |
| 3156 | W _d | ○ ∩ ∩ | ✚ _A ∞ | ✚ XL 5-10 φ |
| | W _d | ○ | ✚ _A | ✚ 1-5 φ |
| 3158 | M _D | ○ ⊙ ∩ | ✚ _A ∩ | ✚ XL 1-5 φ |
| | M _D | ∩ ∩ ∩ | ✚ _A | ✚ XL 1-5 φ |
| 3160 | M _D | ∩ ∩ ∩ | ✚ _A ≡ | ✚ XL 1-5 φ |

PETROGRAPHIC DESCRIPTION

WELL NAME: Larson #1-A (#2776)

LOCATION: NWSE 15-163-79

| DEPTH | TEXTURE | PARTICLES | STRUCTURES | RESERVIOR |
|-------|----------------|-----------------------|------------|-------------|
| 3240 | P & A | O? | ✚ A | ✚ 1-5 φ |
| 3242 | M _d | ∩ ⊙ ⊗ ∪ λ? | ✚ A | ✚ 5-10 φ |
| 3244 | M _d | ∩ ∪ λ? ⊙ ⊗ III? | ✚ A | ✚ 5-10 φ |
| 3246 | | | | |
| 3248 | P | O? ⊙? | ✚ A or C? | ✚ 15-20 φ |
| 3250 | P | ○ or ⊙? λ? | ✚ A ~~~~~ | ✚ 5-10 φ |
| 3252 | M | ⊙ ∩ λ? ∪ | ✚ clay | ✚ 10-15 φ |
| 3254 | P _d | ○ or ⊙? | ✚ C? A | ✚ 10-15 φ |
| 3256 | W _D | ∩ ⊗ ○ ⊙ ∪ | | ✚ XL 5-10 φ |
| 3258 | P | ○ or ⊙? ⊗ ∩ λ? ⊙ ∪ | | ✚ 15-20 φ |
| 3260 | W | ∩ ⊙ ∪ λ? | ✚ A & Clay | ✚ 10-15 φ |
| | M | ∪ λ? ⊙ ∩ ∩ | ✚ A & clay | ✚ 5-10 φ |
| 3262 | P | ⊙ ⊙? ∪ ⊗ ∩ ∪ ∩ | | ✚ 15-20 φ |

PETROGRAPHIC DESCRIPTION

WELL NAME: Nordmark #3 (#2902)

LOCATION: NWSE 30-163-78

| DEPTH | TEXTURE | PARTICLES | STRUCTURES | RESERVIOR |
|-------|----------------|---|------------|--------------|
| 3122 | M | | | 10-15 ϕ |
| 3124 | P | | | 15-20 ϕ |
| 3126 | P | | | 10-15 ϕ |
| 3128 | P | | | 15-20 ϕ |
| | | Large vug completely filled with secondary anhy | | |
| 3130 | P | | | 5-10 ϕ |
| 3132 | P | | | 5-10 ϕ |
| 3134 | P | | | 10-15 ϕ |
| 3136 | P | | | 5-10 ϕ |
| 3138 | M _d | | | 1-5 ϕ |
| 3140 | M _d | | | 1-5 ϕ |
| 3142 | M | | | 5-10 |
| 3144 | P | | | 5-10 |

PETROGRAPHIC DESCRIPTION

WELL NAME: Norderhus #1 (#3238)

LOCATION: SESE 2-163-78

| DEPTH | TEXTURE | PARTICLES | STRUCTURES | RESERVIOR |
|-------|---------------------------------|-----------|------------------------|-------------|
| 3052 | | | | |
| 3054 | M _D | | ✚ _A | XL 10-15 ∅ |
| 3056 | M _D & W _D | ○ ^ ▯ | ≡ ≡ ≡ -w- | ✚ XL 5-10 ∅ |
| 3058 | P | ▯ ⊗ ○ | ✚ _A | ✚ 1-5 ∅ |
| | P | ▯ ○ ⊗ | ✚ _A ≡ | ✚ 1-5 ∅ |
| 3060 | P | ▯ ● ○ | ✚ _A † Qz ≡ | ✚ 1-5 ∅ |
| 3062 | P | ⊙ ○ ● | ✚ _C | ✚ 1-5 ∅ |
| | P | ○ ▯ ⊗ ● ^ | ✚ _C † A ≡ ≡ | ✚ 1-5 ∅ |
| 3064 | P | ▯ ○ ⊗ ∪ | ✚ _C † A | ✚ 10-15 ∅ |
| 3066 | W _D | ⊕ ^ ▯ | ≡ ≡ ≡ -w- | XL 10-15 ∅ |
| 3068 | W | ▯ ^ ∪ ⊗ | ✚ _A | ✚ 5-10 ∅ |
| 3070 | W | ∪ ^ | | ✚ 5-10 ∅ |
| 3072 | W | ∪ ^ | ✚ _C | ✚ 5-10 ∅ |
| 3074 | W _d | ⊕ | ✚ _C † A | ✚ 5-10 ∅ |
| | W | ^ ○ | ✚ _C † A | ✚ 5-10 ∅ |

PETROGRAPHIC DESCRIPTION

WELL NAME: Bernstein # 1 (# 3375)





LOCATION: NWNW 23-163-78

| DEPTH | TEXTURE | PARTICLES | STRUCTURES | RESERVIOR |
|-------|----------------|-----------|---------------------------------|-----------|
| 3054 | | | | |
| 3056 | A | | ≡ ∞ M | π |
| | M | | ≡ ↘ _{A+Qtz} | π |
| 3058 | | | ✦ _A π | |
| | M | | ≡ π ✦ _A A | π |
| 3060 | M & A | ? | ≡ | π |
| 3062 | M _D | πππ | A _{nod} ✦ _A | π |
| 3064 | | | | |
| 3066 | | | | |
| | A | | | π |
| 3068 | | | | |
| 3070 | A & M | πππ | | π |
| 3072 | | | | |
| | M _D | | ✦ _A | π |
| 3074 | | | | |
| 3076 | A | | | π |

PETROGRAPHIC DESCRIPTION

WELL NAME: Bernstein # 1 (# 3375)

LOCATION: NWNW 23-163-78

| DEPTH | TEXTURE | PARTICLES | STRUCTURES | RESERVIOR |
|-------|----------------|-----------|--|-----------|
| 3078 | P & A | O |  A nod | π |
| 3080 | P _D | O ● ⊕ |  A  A | π |
| 3082 | | | | |
| 3084 | A | | | π |
| 3086 | | | | |
| 3088 | A | | | π |
| 3090 | | | | |
| 3092 | A | |  Qz | π |
| | A & M | | | π |
| 3094 | | | | |
| | A | | | π |
| 3096 | | | | |
| 3098 | | | | |
| 3100 | A | | # | π |

PETROGRAPHIC DESCRIPTION

WELL NAME: Bernstein #1 (# 3375)

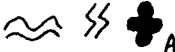
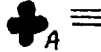



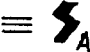
LOCATION: NWNW 23-163-78

| DEPTH | TEXTURE | PARTICLES | STRUCTURES | RESERVIOR |
|-------|--------------------|-----------|---------------------|-------------|
| 3102 | A & M _D | TTTT | ≡ + Qtz | TT |
| 3104 | W _D | ∩ ⊙ TTTT | + _A | TT |
| 3106 | P _D | ○ TTT Σ ^ | SS _{Qtz} ≡ | TT |
| 3108 | M _D | TTT | + _{clay} | + 1-5 φ |
| | W _d | ○ ∩ ⊙ | | + 5-10 φ |
| 3110 | P _D | ○ ⊙ ⊙ | + _{Calc} | △ + 1-5 φ |
| 3112 | W _d | TTT ○ ⊙ | + _A ≡ | + 1-5 φ |
| 3114 | P | ○ ⊙ ⊙ | + _{A+Calc} | + 1-5 φ |
| 3116 | W _D | ∧ ∩ ⊙ | + _A | + 1-5 φ |
| 3118 | W _D | ∩ ⊙ ∧ ^ | + _{A+Clay} | + 5-10 φ |
| 3120 | W _D | ∧ ∧ Σ | | XL 5-10 φ |
| | P | ∩ + ⊙ ○ | + _A | + 5-10 φ |
| 3122 | P | ● + ○ ^ | + _{Calc} | + 5-10 φ |
| 3124 | P _D | ○ ⊙ | | XL + 5-10 φ |

PETROGRAPHIC DESCRIPTION

WELL NAME: Kjelshus # 1 (# 3451)

LOCATION: NWSE 22-163-78

| DEPTH | TEXTURE | PARTICLES | STRUCTURES | RESERVIOR |
|-------|---------|-----------|---|---|
| 3086 | A | |  | π |
| 3088 | | | | |
| 3090 | | | | |
| 3092 | A | | | |
| 3094 | | | | |
| 3096 | | | | |
| 3098 | D | |  | XL  5-10 ∅ |
| 3100 | | | | |
| 3102 | | | | |
| 3104 | W | qtz |  |  5-10 ∅ |
| 3106 | M & A | |  | π |
| 3108 | | | | |

PETROGRAPHIC DESCRIPTION

WELL NAME: Kjelshus #1 (#3451)

LOCATION: NWSE 22-163-78

| DEPTH | TEXTURE | PARTICLES | STRUCTURES | RESERVIOR |
|-------|--------------------|-----------|--------------------|--------------|
| 3110 | M & A | | ≡ ~~~ | π |
| 3112 | | | | |
| 3114 | P | Σ ○ | ✚ _A | π |
| | P | ⊙ ⊗ ● Σ | ✚ _C ≡ | ✚ 1-5 φ |
| 3116 | P | ⊙ Σ ⊗ | | ✚ 15-20 φ |
| | P | | ✚ _A | ✚ 1-5 φ |
| 3118 | | | | |
| | P _d | ⊙ Σ | ✚ _A | ✚ XL 10-15 φ |
| 3120 | P | ⊙ Σ | ✚ _A | ✚ 1-5 φ |
| 3122 | | | | |
| 3124 | | | | |
| 3126 | A | | ✚ _A | ✚ 1-5 φ |
| | M _d & A | | ✚ _A | π |
| 3128 | M _d & A | | ✚ _A ~~~ | π |
| 3130 | | | | |
| | A & M | | ~~~~ | π |
| 3132 | | | | |

PETROGRAPHIC DESCRIPTION

WELL NAME: Kjelshus - State #1 (# 3472)

LOCATION: SE SW 22-163-78

| DEPTH | TEXTURE | PARTICLES | STRUCTURES | RESERVIOR |
|-------|----------------|----------------|---------------------|-----------|
| 3114 | | | | |
| 3116 | | | | |
| 3118 | A | qtz grns | ≡ arg | π |
| 3120 | M | ≡ ⊕ | ≡ | ⊕ 1-5 φ |
| 3122 | | | | |
| 3124 | A | Σ _m | | π |
| 3126 | | | | |
| 3128 | P _A | Σ | ⊕ _A | π |
| 3130 | P _d | ⊙ | ⊕ _A | ⊕ 5-10 φ |
| 3132 | | | | |
| 3134 | P | ⊙ ● | | ⊕ 15-20 φ |
| | W | ⊙ ≡ ∩ | ⊕ _A clay | ⊕ 5-10 φ |
| 3136 | | | | |

PETROGRAPHIC DESCRIPTION

WELL NAME: Kjelshus - State # 2 (# 3527)

LOCATION: SE NW 22-163-78

| DEPTH | TEXTURE | PARTICLES | STRUCTURES | RESERVIOR |
|-------|----------------|-----------|------------------------------|-----------|
| 3110 | D & A | | | π |
| 3112 | D & A | | ≡ | π |
| 3114 | A | | ✚ _A | π |
| 3116 | | | | |
| 3118 | M | | ✚ _A lrg anhyd nod | π |
| 3120 | P | | ✚ _A ● clay | ✚ 5-10 φ |
| 3122 | M | ⊙ ⊙ ⊙ | ✚ _A | ✚ 1-5 φ |
| 3124 | P _d | ⊙ ⊙ ππ | | ✚ 10-15 φ |
| 3126 | P | ⊙ ⊙ | ✚ _A | ✚ 15-20 φ |
| 3128 | | | | |

PETROGRAPHIC DESCRIPTION

WELL NAME: Foster - Kjelshus #1 (# 3577)

LOCATION: NWE 22-163-78

| DEPTH | TEXTURE | PARTICLES | STRUCTURES | RESERVIOR |
|-------|----------------|-----------|---------------------|--------------|
| 3094 | A | | ≡ w/ππ M | π |
| 3096 | | | | |
| 3098 | A | Σ of M | | π |
| 3100 | | | | |
| 3102 | A & M | πππ | ≡ | π |
| | P _d | ⊙ Σ ⊕ | ⊕ _A | ⊕ XL 5-10 φ |
| 3104 | | ○ | ⊕ _A | ⊕ XL 10-15 φ |
| | M _d | | | |
| 3106 | P _d | ⊙ ππ ⊕ | ⊕ _A clay | ⊕ XL 15-20 φ |
| | P _d | ⊙ ● ⊕ ^ ^ | ⊕ _A | ⊕ XL 10-15 φ |
| 3108 | | | | |
| 3110 | P _d | ⊙ ⊕ | ⊕ _A clay | ⊕ 5-10 φ |
| 3112 | | | | |
| 3114 | P | ○ | ⊕ _A c | π |
| | P | ○ ⊕ ⊙ | ⊕ _A | π |
| 3116 | | | | |

PETROGRAPHIC DESCRIPTION

WELL NAME: Brenden #1 (#3933)

LOCATION: NESE 10-163-78

| DEPTH | TEXTURE | PARTICLES | STRUCTURES | RESERVIOR |
|-------|---------|--|-------------------------|-----------------------|
| 3052 | A | Σ | \approx | Π |
| 3054 | | | | |
| 3056 | P_A | O | \oplus_A | Π |
| 3058 | | | | |
| 3060 | M_A | | \oplus_A | Π |
| 3062 | P | $\odot \ominus \otimes \bullet$ | \oplus_A | \oplus 15-20 ϕ |
| 3064 | P | $\odot \cup \ominus \otimes \bullet$ $\Pi \Sigma$ | \oplus_A \llcorner | \oplus 15-20 ϕ |
| | P | $\Sigma \circ \Pi \otimes$ | \oplus_A ⚡_A | Π |
| 3066 | P_d | O | $\oplus_A \oplus_A$ | \oplus 10-15 ϕ |
| 3068 | P_d | O | \oplus_A | \oplus 10-15 ϕ |
| 3070 | P_d | O | \oplus_A | \oplus 5-10 ϕ |
| 3072 | | | | |
| 3074 | | | | |

PETROGRAPHIC DESCRIPTION

WELL NAME: Anderson # 2-24 (# 11889)

LOCATION: SWSE 24-163-79

| DEPTH | TEXTURE | PARTICLES | STRUCTURES | RESERVIOR |
|-------|----------------|-----------|---------------------------------|-----------|
| 3164 | A | mas | ∞ ~ | π |
| 3166 | | | | |
| 3168 | | | | |
| 3170 | | | | |
| 3172 | | | | |
| 3174 | M _D | mas | ⊕ _A ≡ | ⊕ 5-10 ∅ |
| | SS | qtz grns | ∞ | △ 10-15 ∅ |
| 3176 | | | | |
| 3178 | | | | |
| 3180 | | | | |
| 3182 | P _d | ○ | ⊕ _A ⊕ _{Qtz} | π |
| 3184 | | | | |
| 3186 | | | | |

PETROGRAPHIC DESCRIPTION

WELL NAME: Anderson # 2-24 (# 11889)

LOCATION: SWSE 24-163-79

| DEPTH | TEXTURE | PARTICLES | STRUCTURES | RESERVIOR |
|-------|----------------|-----------|----------------|-----------|
| 3188 | | | | |
| 3190 | P | ○ ⊙ Λ | | ⊕ 10-15 φ |
| 3192 | W | Λ ∩ ⊙ ⊙ | ⊕ _A | ⊕ 5-10 φ |
| 3194 | | | | |
| 3196 | | | | |
| 3198 | | | | |
| 3200 | | | | |
| 3202 | P _d | ○ | ⊕ _A | ⊕ 5-10 φ |
| 3204 | | | | |
| 3206 | | | | |
| 3208 | W | Λ ∩ ⊙ | ⊕ _A | ⊕ 1-5 φ |
| 3210 | | | | |

PETROGRAPHIC DESCRIPTION

WELL NAME: Lavone # 29 (#12357)

LOCATION: NENW 29-163-78

| DEPTH | TEXTURE | PARTICLES | STRUCTURES | RESERVIOR |
|-------|----------------|-----------|--------------------|-------------|
| 3102 | | | | |
| 3104 | | | | |
| 3106 | | | | |
| 3108 | | | | |
| 3110 | P _d | ○ | ✚ _A | π |
| 3112 | P _d | ○ | ✚ _A | π |
| 3114 | P _D | ○ | ✚ _A | π |
| 3116 | P _D | ○ | ✚ _A | ✚ XL 5-10 φ |
| 3118 | P _D | ○ / | ✚ _{delay} | ✚ XL 5-10 φ |
| 3120 | P _D | ○ ⊕ | ✚ _A | ✚ XL 5-10 φ |
| 3122 | | | | |
| 3124 | P _D | ○ ⊕ | ✚ _A | ✚ XL 1-5 φ |

PETROGRAPHIC DESCRIPTION

WELL NAME: Lavone # 29 (#12357)

LOCATION: NENW 29-163-78

| DEPTH | TEXTURE | PARTICLES | STRUCTURES | RESERVIOR |
|-------|----------------|-----------|------------------|-------------|
| 3126 | P _d | ○ | ✚ _{C+A} | ✚ XL 5-10 ∅ |
| | P | ◎ | ✚ _A | ✚ L 10-15 ∅ |
| 3128 | | ◎ | ✚ _A | ✚ △ 1-5 ∅ |
| 3130 | | | | |
| 3132 | | | | |
| 3134 | P | ◎ ⊕ ◡ | ✚ _A ≡ | ✚ 15-20 ∅ |
| 3136 | | | | |
| 3138 | | | | |
| 3140 | M | ○ ◎ ⊕ | ✚ _A ● | ✚ 5-10 ∅ |
| 3142 | | | | |
| 3144 | P | ◎ | ✚ _A ● | ✚ 10-15 ∅ |
| 3146 | M | ○ ◡ ⊕ ◎ | ✚ _A ● | ✚ 10-15 ∅ |
| 3148 | | | ~~~~~ | ✚ 10-15 ∅ |

PETROGRAPHIC DESCRIPTION

WELL NAME: Brandjord # 2-20 (#12358)

LOCATION: NESE 20-163-78

| DEPTH | TEXTURE | PARTICLES | STRUCTURES | RESERVIOR |
|-------|----------------|-----------|--------------------|-------------|
| 3116 | P _d | ○ | ✚ _A | ✚ 5-10 φ |
| 3118 | P | ⊙ | ✚ _A | ✚ 10-15 φ |
| 3120 | | | | |
| 3122 | P | ⊙ | ✚ _A | ✚ 10-15 φ |
| 3124 | | | | |
| 3126 | W _d | Σ ○ ⊖ ⊕ | | ✚ 5-10 φ |
| 3128 | | | | |
| 3130 | P | ⊙ ⊕ ⊖ | ✚ _A 4-⊕ | ✚ Δ 15-20 φ |
| | W _d | ≡ ⊕ ⊖ | ✚ _A ≡ | ✚ 5-10 φ |
| 3132 | | | | |
| | W _d | ≡ | ✚ _A ≡ | ✚ 5-10 φ |
| 3134 | | | | |
| 3136 | | | | |
| 3138 | W _d | Σ ○ ⊕ ≡ | ✚ _A ≡ | ✚ 5-10 φ |

PETROGRAPHIC DESCRIPTION

WELL NAME: Brandjord # 2-20 (#12358)

LOCATION: NESE 20-163-78

| DEPTH | TEXTURE | PARTICLES | STRUCTURES | RESERVIOR |
|-------|----------------|-----------|---------------------------------|-----------|
| 3140 | | | | |
| 3142 | | | | |
| 3144 | P | ○ ⊗ | ⊕ _{ctA} ⊕ _A | ⊕ 10-15 φ |
| 3146 | | | | |
| 3148 | | | | |
| 3150 | W _d | π ⊗ ⊕ ∪ | ⊕ _A | ⊕ 5-10 φ |
| 3152 | P | ⊗ ⊕ ⊗ ⊙ | ⊕ _A | π |
| | P | π ⊗ ⊕ ⊙ | ⊕ _A | π |
| 3154 | | | | |
| 3156 | | | | |
| 3158 | W | ∪ ⊗ ⊗ π ⊙ | ∪ ∪ | ⊕ 5-10 φ |
| | W | ∪ π ⊗ | ⊕ _A ⊕ _A ∪ | ⊕ 10-15 φ |
| 3160 | | | | |
| | P | ⊙ π ⊗ | | ⊕ 10-15 φ |
| 3162 | W | π ⊗ ∪ | ⊕ _A ≡ | ⊕ 10-15 φ |

REFERENCES

- Adams, J. E., and Rhodes, M. L., 1960, Dolomitization by seepage refluxion: American Association of Petroleum Geologists Bulletin, v. 44, p. 1912-1920.
- Ahmed, M., and Last, W. M., 1991, Deposition and diagenesis of the MC-3 member of the Mission Canyon Formation, Pierson field, Manitoba, in J. E. Christopher and F. M. Haidl, eds., Sixth International Williston Basin Symposium: Saskatchewan Geological Society Special Publication no. 11, p. 123-129.
- Alexandersson, T., 1974, Carbonate cementation in coralline algal nodules in the Skagerrak, North Sea: biochemical precipitation in undersaturated waters: Journal of Sedimentary Petrology, v. 44, p. 7-26.
- Allan, J. R., and Matthews, R. K., 1977, Carbon and oxygen isotopes as diagenetic and stratigraphic tools: surface and subsurface data, Barbados, West Indies: Geology, v. 5, p. 16-20.
- Allan, J. R., and Matthews, R. K., 1982, Isotope signatures associated with early meteoric diagenesis: Sedimentology, v. 29, p. 797-817.
- Amthor, J. E., and Friedman, G. M., 1992, Early to late diagenetic dolomitization of platform carbonates: lower Ordovician Ellenburger Group, Permian Basin, Texas: Journal of Sedimentary Petrology, v. 62, p. 131-144.
- Anderson, S. B., and Hunt, J. B., 1964, Devonian salt solution in north central North Dakota, in Third International Williston Basin Symposium: Billings Geological Society, North Dakota Geological Society, and Saskatchewan Geological Society, p. 93-104.
- Ault, W. U., and Kulp, J. L., 1959, Isotopic geochemistry of sulphur: Geochimica et Cosmochimica Acta, v. 16, p. 201-235.

- Baillie, A. D., 1953, Devonian system of the Williston Basin area: Manitoba Mines Branch Publication no. 52-5.
- Bayliss, P., Smith, D. K., Mrose, M. E., and Berry, L. G., 1980, Mineral powder diffraction file data book: JCPDS International Centre for Diffraction Data, Swarthmore, Pennsylvania, 1168 pp.
- Beach, D. K., and Schumacher, A., 1982, Stanley field, North Dakota: a new model for a new exploration play, in J. E. Christopher and J. Kaldi, eds., Fourth International Williston Basin Symposium: Saskatchewan Geological Society Special Publication no. 6, p. 235-243.
- Behrens, E. W., and Land, L. S., 1972, Subtidal Holocene dolomite, Baffin Bay, Texas: Journal of Sedimentary Petrology, v. 42, p. 155-161.
- Bein, A., and Land, L. S., 1982, San Andres carbonates in the Texas Panhandle: sedimentation and diagenesis associated with magnesium-calcium-chloride brines: Bureau of Economic Geology, University of Texas, Report of Investigation 121, 48 pp.
- Bluemle, J. P., Anderson, S. B., and Carlson, C. G., 1981, Williston Basin stratigraphic nomenclature chart: North Dakota Geological Survey, Miscellaneous Series no. 61, sheet 1.
- Bluemle, J. P., Anderson, S. B., Andrew, J. A., Fischer, D. W., and LeFever, J. A., 1986, North Dakota Stratigraphic Column: North Dakota Geological Survey, Miscellaneous Series no. 66, sheet 1.
- Budd, D. A., and Land, L. S., 1990, Geochemical imprint of meteoric diagenesis in Holocene ooid sands, Schooner Cays, Bahamas: correlation of calcite cement geochemistry with extant groundwaters: Journal of Sedimentary Petrology, v. 60, p. 361-378.
- Budd, D. A., and Vacher, H. L., 1991, Predicting the thickness of fresh-water lenses in carbonate paleo-islands: Journal of Sedimentary Petrology, v. 61, p. 43-53.
- Butler, G. P., 1969, Modern evaporite deposition and geochemistry of coexisting brines, the sabkha, Trucial Coast, Arabian Gulf: Journal of Sedimentary Petrology, v. 39, p. 70-89.

- Butler, G. P., Krouse, R. H., and Mitchell, R., 1973, Sulphur-isotope geochemistry of an arid, supratidal evaporitic environment, Trucial Coast, in B. H. Purser, ed., The Persian Gulf, Holocene carbonate sedimentation and diagenesis in a shallow epicontinental sea: Springer-Verlag, New York, p. 453-471.
- Carver, R. E., 1971, Procedures in sedimentary petrology: Wiley-Interscience, New York, 653 pp.
- Choquette, P. W., and Pray, L. C., 1970, Geologic nomenclature and classification of porosity in sedimentary carbonates: American Association of Petroleum Geologists Bulletin, v. 54, p. 207-250.
- Christiansen, E. A., 1967, Collapse structures near Saskatoon, Saskatchewan, Canada: Canadian Journal of Earth Sciences, v. 4, p. 757-767.
- Claypool, G. E., Holser, W. T., Kaplan, I. R., Sakai, H., and Zak, I., 1980, The age curves of sulfur and oxygen isotopes in marine sulfate and their mutual interpretation: Chemical Geology, v. 28, p. 199-260.
- Clayton, R. N., Jones, B. F., and Berner, R. A., 1968, Isotope studies of dolomite formation under sedimentary conditions: Geochimica et Cosmochimica Acta, v. 32, p. 415-432.
- Coogan, A. H., 1970, Measurements of compaction in oolitic grainstone: Journal of Sedimentary Petrology, v. 40, p. 921-929.
- Crabtree, H. T., 1982, Lithologic types, depositional environment, and reservoir properties of the Mississippian Frobisher beds, Innes field, southeastern Saskatchewan, in J. E. Christopher and J. Kaldi, eds., Fourth International Williston Basin Symposium: Saskatchewan Geological Society Special Publication no. 6, p. 203-210.
- Craig, H., 1957, Isotopic standards for carbon and oxygen and correction factors for mass-spectrometric analysis of carbon dioxide: Geochimica et Cosmochimica Acta, v. 12, p. 133-149.
- Degens, E. T., and Epstein, S., 1964, Oxygen and carbon isotope ratios in coexisting calcites and dolomites from recent and ancient sediments: Geochimica et Cosmochimica Acta, v. 28, p. 23-44.

- De Mille, G., Shouldice, J. R., and Nelson, H. W., 1964, Collapse structures related to evaporites of the Prairie Formation, Saskatchewan: Geological Society of America Bulletin, v. 75, p. 307-316.
- Dunham, R. J., 1962, The classification of carbonate rocks according to depositional texture, *in* W. E. Ham, ed., Classification of carbonate rocks: American Association of Petroleum Geologists Memoir 1, p. 108-121.
- Elliot, T. L., 1982, Carbonate facies, depositional cycles, and the development of secondary porosity during burial diagenesis: Mission Canyon Formation, Haas field, North Dakota, *in* J. E. Christopher and J. Kaldi, eds., Fourth International Williston Basin Symposium: Saskatchewan Geological Society Special Publication no. 6, p. 131-151.
- Emiliani, C., and Shackleton, N. J., 1974, The Brunhes Epoch: isotopic paleotemperatures and geochronology: Science, v. 83, p. 511-514.
- Faure, G., 1986, Principles of isotope geology, second edition: John Wiley and Sons, New York, 589 pp.
- Friedman, G. M., 1964, Early diagenesis and lithification in carbonate sediments: Journal of Sedimentary Petrology, v. 34, p. 777-813.
- Gao, G., 1990, Geochemical and isotopic constraints on the diagenetic history of a massive stratal, late Cambrian (Royer) dolomite, lower Arbuckle Group, Slick Hills, SW Oklahoma, USA: Geochimica et Cosmochimica Acta, v. 54, p. 1979-1989.
- Given, R. K., and Lohmann, K. C., 1986, Isotopic evidence for the early meteoric diagenesis of the reef facies, Permian reef complex of west Texas and New Mexico: Journal of Sedimentary Petrology, v. 56, p. 183-193.
- Gregg, J. M., and Shelton, K. L., 1990, Dolomitization and dolomite neomorphism in the back reef facies of the Bonneterre and Davis Formations (Cambrian), southeastern Missouri: Journal of Sedimentary Petrology, v. 60, p. 549-562.
- Gregg, J. M., and Sibley, D. F., 1984, Epigenetic dolomitization and the origin of xenotopic dolomitic texture: Journal of Sedimentary Petrology, v. 54, p. 908-931.

- Gross, M. G., 1964, Variations in the O^{18}/O^{16} and C^{13}/C^{12} ratios of diagenetically altered limestones in the Bermuda Islands: *Journal of Geology*, v. 72, p. 170-194.
- Gross, M. G., and Tracey, J. I. Jr., 1966, Oxygen and carbon isotopic composition of limestones and dolomites, Bikini and Eniwetok Atolls: *Science*, v. 151, p. 1082-1084.
- Halley, R. B., and Harris, P. M., 1979, Fresh-water cementation of a 1,000-year-old oolite: *Journal of Sedimentary Petrology*, v. 49, p. 969-988.
- Hardie, L. A., 1967, The gypsum-anhydrite equilibrium at one atmosphere pressure: *American Mineralogist*, v. 52, p. 171-200.
- Harris, S. H., Land, C. B. Jr., and McKeever, J. H., 1966, Relation of Mission Canyon stratigraphy to oil production in north-central North Dakota: *American Association of Petroleum Geologists Bulletin*, v. 50, p. 2269-2276.
- Hays, P. D., and Grossman, E. L., 1991, Oxygen isotopes in meteoric calcite cements as indicators of continental paleoclimate: *Geology*, v. 19, p. 441-444.
- Holland, H. D., 1973, Systematics of the isotopic composition of sulfur in the oceans during the Phanerozoic and its implications for atmospheric oxygen: *Geochimica et Cosmochimica Acta*, v. 37, p. 2605-2616.
- Holser, W. T., 1979, Mineralogy of evaporites, *in* R. G. Burns, ed., *Marine Minerals: Mineralogical Society of America Short Course Notes 6*, p. 211-235.
- Holser, W. T., and Kaplan, I. R., 1966, Isotope geochemistry of sedimentary sulfates: *Chemical Geology*, v. 1, p. 93-135.
- Jennings, A. H., 1987, A geologic and economic appraisal of the oil potential of the Williston Basin (abstract), *in* C. G. Carlson and J. E. Christopher, eds., *Fifth International Williston Basin Symposium: Saskatchewan Geological Society Special Publication no. 9*, p. 196.
- Kaufman, J., Meyers, W. J., and Hanson, G. N., 1990, Burial cementation in the Swan Hills Formation (Devonian), Rosevear field, Alberta, Canada: *Journal of Sedimentary Petrology*, v. 60, p. 918-939.

- Keith, M. L., and Weber, J. N., 1964, Carbon and oxygen isotopic composition of selected limestones and fossils: *Geochimica et Cosmochimica Acta*, v. 28, p. 1787-1816.
- Kinard, J. C., 1964, Recent Mission Canyon discoveries in the Roth - N.E. Landa area, Bottineau County, North Dakota, in Third International Williston Basin Symposium: Billings Geological Society, North Dakota Geological Society, and Saskatchewan Geological Society, p. 241-246.
- Kinsman, D. J. J., 1969, Modes of formation, sedimentary associations, and diagenetic features of shallow-water and supratidal evaporites: *American Association of Petroleum Geologists Bulletin*, v. 53, p. 830-840.
- Kobluk, D. R., and Risk, M. J., 1977, Micritization and carbonate-grain binding by endolithic algae: *American Association of Petroleum Geologists Bulletin*, v. 61, p. 1069-1082.
- Kupsch, W. O., 1958, Surface structures in southern Saskatchewan, in Second International Williston Basin Symposium: Saskatchewan Geological Society and North Dakota Geological Society, p. 118-126.
- Laird, W. M., 1956, The Williston Basin-a backward look with a view to the future, in First International Williston Basin Symposium: North Dakota Geological Society and Saskatchewan Geological Society, p. 14-22.
- Land, L. S., 1970, Phreatic versus vadose meteoric diagenesis of limestones: evidence from a fossil water table: *Sedimentology*, v. 14, p. 175-185.
- Land, L. S., and Epstein, S., 1970, Late Pleistocene diagenesis and dolomitization, north Jamaica: *Sedimentology*, v. 14, p. 187-200.
- Land, L. S., and Goreau, T. F., 1970, Submarine lithification of Jamaican reefs: *Journal of Sedimentary Petrology*, v. 40, p. 457-462.
- Lee, Y. I., and Friedman, G. M., 1987, Deep-burial dolomitization in the Ordovician Ellenburger Group carbonates, west Texas and southeastern New Mexico: *Journal of Sedimentary Petrology*, v. 57, p. 544-557.

- Lindsay, R. F., and Roth, M. S., 1982, Carbonate and evaporite facies, dolomitization and reservoir distribution of the Mission Canyon Formation, Little Knife field, North Dakota, in J. E. Christopher and J. Kaldi, eds., Fourth International Williston Basin Symposium: Saskatchewan Geological Society Special Publication no. 6, p. 153-179.
- Longman, M. W., 1980, Carbonate diagenetic textures from nearsurface diagenetic environments: American Association of Petroleum Geologists Bulletin, v. 64, p. 461-487.
- Luther, M. R., 1988, Deposition and diagenesis of a portion of the Frobisher-Alida interval (Mississippian Madison Group), Wiley field, North Dakota: Unpublished Master of Arts Thesis, University of North Dakota, 313 pp.
- Machel, H. G., and Burton, E. A., 1991, Burial-diagenetic sabkha-like gypsum and anhydrite nodules: Journal of Sedimentary Petrology, v. 61, p. 394-405.
- MacNamara, J., and Thode, H. G., 1950, Comparison of the isotopic constitution of terrestrial and meteoritic sulphur: Physical Review, v. 78, p. 307-308.
- Maiklem, W. R., Bebout, D. G., and Glaister, R. P., 1969, Classification of anhydrite—a practical approach: Bulletin of Canadian Petroleum Geologists, v. 17, p. 194-233.
- Margolis, S., and Rex, R. W., 1971, Endolithic algae and micrite envelope formation in Bahamian oolites as revealed by scanning electron microscopy: Geological Society of America Bulletin, v. 82, p. 843-852.
- Matthews, R. K., 1967, Diagenetic fabrics in biosparites from the Pleistocene of Barbados, West Indies: Journal of Sedimentary Petrology, v. 37, p. 1147-1153.
- Matthews, R. K., 1968, Carbonate diagenesis: equilibration of sedimentary mineralogy to the subaerial environment; coral cap of Barbados, West Indies: Journal of Sedimentary Petrology, v. 38, p. 1110-1119.
- McCrea, J. M., 1950, On the isotopic chemistry of carbonates and a paleotemperature scale: Journal of Chemical Physics, v. 18, p. 849-857.

- McKenzie, J. A., 1981, Holocene dolomitization of calcium carbonate sediments from the coastal sabkhas of Abu Dhabi, U.A.E.: a stable isotope study: *Journal of Geology*, v. 89, p. 185-198.
- McTavish, G. J., 1991, Role of salt dissolution in controlling outcrop distribution in south-central Saskatchewan, *in* J. E. Christopher and F. Haidl, eds., Sixth International Williston Basin Symposium: Saskatchewan Geological Society Special Publication no. 11, p. 244-249.
- McTavish, G. J., and Vigrass, L. W., 1987, Salt dissolution and tectonics, south-central Saskatchewan, *in* C. G. Carlson and J. E. Christopher, eds., Fifth International Williston Basin Symposium: Saskatchewan Geological Society Special Publication no. 9, p. 157-168.
- Milner, R. L., 1956, Effects of salt solution in Saskatchewan, *in* First International Williston Basin Symposium: North Dakota Geological Survey and Saskatchewan Geological Survey, p. 111.
- Montana Oil Journal, 1991, Mission Canyon shoreline play sets pace for early '91 North Dakota drilling: *Montana Oil Journal*, v. 71, no. 4, p. 4-5.
- Montana Oil Journal, 1992, Madison fields production numbers impressive McLean, Ward, and Mountrail Counties, North Dakota: *Montana Oil Journal*, v. 72, no. 1, p.1.
- Murray, R. C., 1964, Origin and diagenesis of gypsum and anhydrite: *Journal of Sedimentary Petrology*, v. 34, p. 512-523.
- Obelenus, T. J., 1985, Depositional environments and diagenesis of carbonates and associated evaporites, Frobisher-Alida interval, Madison Group (Mississippian), Williston Basin, northwestern North Dakota: Unpublished Master of Science Thesis, University of North Dakota, 313 pp.
- Oglesby, C. A., 1987, Distinguishing between depositional and dissolution thinning: Devonian Prairie Formation, Williston Basin, North America, *in* C. G. Carlson and J. E. Christopher, eds., Fifth International Williston Basin Symposium: Saskatchewan Geological Society Special Publication no. 9, p. 47-52.

- Patterson, R. J., and Kinsman, D. J. J., 1981, Hydrologic framework of a sabkha along Arabian Gulf: American Association of Petroleum Geologists Bulletin, v. 65, p. 1457-1475.
- Patterson, R. J., and Kinsman, D. J. J., 1982, Formation of diagenetic dolomite in coastal sabkha along Arabian (Persian) Gulf: American Association of Petroleum Geologists Bulletin, v. 66, p. 28-43.
- Pierre, C., Ortlieb, L., and Person, A., 1984, Supratidal evaporitic dolomite at Ojo De Liebre lagoon: mineralogical and isotopic arguments for primary crystallization: Journal of Sedimentary Petrology, v. 54, p. 1049-1061.
- Pierre, C., and Rouchy, J-M., 1986, Oxygen and sulfur isotopes in anhydrites from Givetian and Visean evaporites of northern France and Belgium: Chemical Geology (Isotope Geoscience Section), v. 58, p. 245-252.
- Qing, H., and Mountjoy, E. W., 1989, Multistage dolomitization in Rainbow buildups, middle Devonian Keg River Formation, Alberta, Canada: Journal of Sedimentary Petrology, v. 59, p. 114-126.
- Quinn, C. F., 1986, Depositional history and diagenesis of the Sherwood and Bluell beds (Mississippian) southwestern Renville County, North Dakota: Unpublished Master of Arts Thesis, University of North Dakota, 254 pp.
- Rees, C. E., 1970, The sulphur isotope balance of the ocean: an improved model: Earth and Planetary Science Letters, v. 7, p. 366-370.
- Rooney, W. S. Jr., and Perkins, R. D., 1972, Distribution and geologic significance of microboring organisms within sediments of the Arlington Reef Complex, Australia: Geological Society of America Bulletin, v. 83, p. 1139-1150.
- Rothe, P., Hoefs, J., and Sonne, V., 1974, The isotopic composition of Tertiary carbonates from the Mainz Basin: an example of isotopic fractionations in 'closed basins': Sedimentology, v. 21, p. 373-395.
- Rush, P. F., and Chafetz, H. S., 1990, Fabric-retentive, non-luminescent brachiopods as indicators of original $^{13}\text{C}/^{12}\text{C}$ and $^{18}\text{O}/^{16}\text{O}$ compositions: a test: Journal of Sedimentary Petrology, v. 60, p. 968-981.

- Saller, A. H., 1984, Petrologic and geochemical constraints on the origin of subsurface dolomite, Enewetak Atoll: an example of dolomitization by normal seawater: *Geology*, v. 12, p. 217-220.
- Saskatchewan Geological Society, 1956, Report of the Mississippian names and correlations committee: Regina, Saskatchewan, 4 pp.
- Schidlowski, M., Junge, C. E., and Pietrek, H., 1977, Sulfur isotope variations in marine sulfate evaporites and the Phanerozoic oxygen budget: *Journal of Geophysical Research*, v. 82, p. 2557-2565.
- Schwartz, D. A., 1987, The deposition and diagenesis of the Bluell zone, upper Mission Canyon Formation (Mississippian), Flaxton field, Burke County, North Dakota: Unpublished Master of Science Thesis, University of North Dakota, 246 pp.
- Shanley, K. W., 1983, Stratigraphy and depositional model, upper Mission Canyon Formation (Mississippian) northeast Williston Basin, North Dakota: Unpublished Master of Science Thesis, Colorado School of Mines, 172 pp.
- Shinn, E. A., Ginsburg, R. N., and Lloyd, R. M., 1965, Recent supratidal dolomite from Andros Island, Bahamas, in L. C. Pray and R. C. Murray, eds., *Dolomitization and Limestone Diagenesis, a Symposium*: Society of Economic Paleontologists and Mineralogists Special Publication no. 13, p. 112-123.
- Shinn, E. A., and Robbin, D. M., 1983, Mechanical and chemical compaction in fine-grained shallow-water limestones: *Journal of Sedimentary Petrology*, v. 53, p. 595-618.
- Sloss, L. L., 1956, Geologic comparisons of Williston and other productive basins, in First International Williston Basin Symposium: North Dakota Geological Society and Saskatchewan Geological Society, p. 6-13.
- Sloss, L. L., 1969, Evaporite deposition from layered solutions: *American Association of Petroleum Geologists Bulletin*, v. 53, p. 776-789.
- Sloss, L. L., and Moritz, C. A., 1951, Paleozoic stratigraphy of southwestern Montana: *American Association of Petroleum Geologists Bulletin*, v. 35, p. 2135-2169.

- Smith, M. H., 1956, Types of oil fields in Bottineau County, North Dakota, in First International Williston Basin Symposium: North Dakota Geological Society and Saskatchewan Geological Society, p. 101-110.
- Steinen, R. P., and Matthews, R. K., 1973, Phreatic vs. vadose diagenesis: stratigraphy and mineralogy of a cored borehole on Barbados, W. I.: Journal of Sedimentary Petrology, v. 43, p. 1012-1020.
- Stephens, R. A., 1986, Depositional history and diagenesis of the upper Mission Canyon and lower Charles Formations (Mississippian), Billings County, North Dakota: Unpublished Master of Science Thesis, University of North Dakota, 236 pp.
- Supko, P. R., 1977, Subsurface dolomites, San Salvador, Bahamas: Journal of Sedimentary Petrology, v. 47, p. 1063-1077.
- Taylor, T. R., and Sibley, D. F., 1986, Petrographic and geochemical characteristics of dolomite types and the origin of ferroan dolomite in the Trenton Formation, Ordovician, Michigan Basin, U.S.A.: Sedimentology, v. 33, p. 61-86.
- Thomas, G. E., 1954, The Mississippian of the northeastern Williston Basin: Canadian Mining and Metallurgical Bulletin, v. 57, p. 136-142.
- Thomas, R. T., and Sibley, D. F., 1986, Petrographic and geochemical characteristics of dolomite types and the origin of ferroan dolomite in the Trenton Formation, Ordovician, Michigan Basin, U.S.A.: Sedimentology, v. 33, p. 61-86.
- Thompson, R. F., and Wright, I. D., 1983, Oil property evaluation: Penwell Publishers, Tulsa, Oklahoma, 200 pp.
- Thorstenson, D. C., MacKenzie, F. T., and Ristvet, B. L., 1972, Experimental vadose and phreatic cementation of skeletal carbonate sand: Journal of Sedimentary Petrology, v. 42, p. 162-167.
- Urey, H. C., 1951, Measurement of paleotemperatures and temperatures of the upper Cretaceous of England, Denmark, and the southeastern United States: Geological Society of America Bulletin, v. 62, p. 399-416.

- Vai, G. B., and Lucchi, F. R., 1977, Algal crusts, autochthonous and clastic gypsum in a cannibalistic evaporitic basin: a case history from the Messinian of northern Apennines: *Sedimentology*, v. 24, p. 211-244.
- Veizer, J., and Hoefs, J., 1976, The nature of O^{18}/O^{16} and C^{13}/C^{12} secular trends in sedimentary carbonate rocks: *Geochimica et Cosmochimica Acta*, v. 40, p. 1387-1395.
- Veizer, J., Holser, W. T., and Wilgus, C. K., 1980, Correlation of $^{13}C/^{12}C$ and $^{34}S/^{32}S$ secular variations: *Geochimica et Cosmochimica Acta*, v. 44, p. 579-587.
- Vogt, R. R., 1956, Alida field, southeast Saskatchewan, in First International Williston Basin Symposium: North Dakota Geological Society and Saskatchewan Geological Society, p. 94-100.
- Wagner, P. D., and Matthews, R. K., 1982, Porosity preservation in the upper Smackover (Jurassic) carbonate grapestone, Walker Creek field, Arkansas: response of paleophreatic lenses to burial processes: *Journal of Sedimentary Petrology*, v. 52, p. 3-18.
- Warren, J. K., 1989, *Evaporite sedimentology*: Prentice Hall, Englewood Cliffs, New Jersey, 285 pp.
- Wilson, J. F., 1975, *Carbonate facies in geologic history*: Springer-Verlag, New York, 471 pp.